STUDY OF HARMONIC GENERATION INDUCED BY HIGH POWER LASER BEAM PROFILES IN PLASMA

Thesis Submitted for the Award of the Degree of

DOCTOR OF PHILOSOPHY

in

Physics

By

Danish Nazir

Registration Number: 12020397

Supervised by

Dr. Vishal Thakur (17014)

Department of Physics (Professor)

Lovely Professional University

LOVELY PROFESSIONAL UNIVERSITY

Transforming Education Transforming India

LOVELY PROFESSIONAL UNIVERSITY, PUNJAB

2026

DECLARATION

I, hereby declared that the presented work in the thesis entitled "STUDY OF HARMONIC GENERATION INDUCED BY HIGH POWER LASER BEAM PROFILES IN PLASMA" in fulfilment of degree of **Doctor of Philosophy (Ph. D.)** is outcome of research work carried out by me under the supervision of Dr. Vishal Thakur, working as Professor, in the School of Chemical Engineering and Physical Sciences of Lovely Professional University, Punjab, India. This work has not been submitted in part or full to any other University or Institute for the award of any degree.

(Signature of Scholar)

Name of the scholar: Danish Nazir

Registration No.: 12020397

Department /school: Physics, School of Chemical Engineering and Physical Sciences

Lovely Professional University

Phagwara, (Punjab)

Date:

CERTIFICATE

This is to certify that the work reported in the Ph. D. thesis entitled “STUDY OF HARMONIC GENERATION INDUCED BY HIGH POWER LASER BEAM PROFILES IN PLASMA” submitted in fulfillment of the requirement for the award of degree of **Doctor of Philosophy (Ph.D.)** in Physics, is a research work carried out by Danish Nazir, 12020397 is bonafide record of his original work carried out under my supervision and that no part of thesis has been submitted for any other degree, diploma or equivalent course.

(Signature of Supervisor)

Name of supervisor: Vishal Thakur

Designation: Professor

Department/school: Department of Physics

University: Lovely Professional University

Phagwara, (Punjab)

Date:

ABSTRACT

This study investigates the second harmonic generation (SHG) and third harmonic generation (THG) using various laser beam profiles, including q-Gaussian, cosh-Gaussian (ChG), and Hermite-cosh-Gaussian (HchG) beams, under optimized laser and plasma parameters. Employing the paraxial approximation, we derived coupled equations for the beam width parameter and normalized amplitude for SHG and THG. These equations were numerically solved, and the results were interpreted graphically. When a high-intensity laser beam propagates through plasma, it exerts a ponderomotive force on electrons, displacing them from the axis and creating density perturbations. The electrostatic force from positive ions induces quiver velocity in electrons, which, when coupled with density perturbations, produces SHG and THG at frequencies $2\omega_1$ and $3\omega_1$ respectively, where $\omega_1$is the laser's fundamental frequency. Variations in plasma density alter its dielectric properties, changing the refractive index and causing self-focusing along the axis. This phenomenon, influenced by both the ponderomotive force and relativistic mass effects, is termed ponderomotive and relativistic self-focusing. We studied the impact of density ripples on the pulse slippage of THG for Gaussian and cosh-Gaussian beams, under optimal laser and plasma parameters. Our findings reveal that a higher density ripple factor significantly enhances efficiency and shifts the peak normalized amplitude of the THG pulse to greater normalized distances.

For cosh-Gaussian beams, efficiency gains were notably higher compared to Gaussian beams, with the former exhibiting oscillatory behaviour at shorter Rayleigh lengths, whereas the latter sustained self-focusing over longer distances. Additionally, self-focusing of Gaussian beams under relativistic effects and an exponential density ramp was analyzed. The density ramp enhanced Rayleigh length, reduced spot size, and strengthened self-focusing. For SHG, efficiency gains were assessed for Hermite-Gaussian and cosh-Gaussian beams under varying parameters, showing that cosh-Gaussian beams exhibited stronger and more sustained self-focusing than Hermite-Gaussian beams. The effect of linear absorption on Hermite-Gaussian beams was also explored. It was observed that linear absorption significantly intensified self-focusing

and reduced spot size, particularly at higher laser intensities and normalized plasma frequencies. The oscillatory behaviour of Hermite-Gaussian beams diminished with increasing values of these parameters. For Hermite-cosh-Gaussian beams, the beam width parameter was examined across different mode indices. The results showed sharp spot size reduction and sustained self-focusing over longer Rayleigh lengths compared to cosh-Gaussian beams, which displayed oscillations at shorter Rayleigh lengths. Overall, higher efficiency in SHG and THG was observed at increased laser intensities and with the inclusion of a density ripple or wiggler magnetic field, which helped satisfy the phase-matching condition and enhanced harmonic generation. In comparison, the efficiency gain was more pronounced for cosh-Gaussian and Hermite-cosh-Gaussian beams, making them advantageous for applications requiring high-intensity harmonics.

The study further demonstrated that variations in the decentred parameter could significantly impact SHG and THG intensity, emphasizing its sensitivity. This research provides valuable insights into the optimization of SHG and THG for diverse applications in medical diagnostics, microscopy, biomedical sensing, optical imaging, and other advanced technologies, highlighting the superior performance of cosh-Gaussian and Hermite-cosh-Gaussian laser beams.

PREFACE

The interaction of high-power laser beams with plasma has become a pivotal area of research in nonlinear optics due to its considerable scientific and technological implications. When an intense laser beam propagates through plasma, nonlinear interactions arise as a consequence of the ponderomotive force and relativistic effects. These interactions lead to density perturbations within the plasma, which couple with the incident laser field and result in higher harmonic generation. Among the various nonlinear processes, second harmonic generation (SHG) and third harmonic generation (THG) have garnered significant attention because of their extensive applications in medical diagnostics, microscopic imaging, biological sensing, optical communications, terahertz technology, laser industries, ultrafast photonics, and optoelectronic devices.

In this thesis, the effects of various laser and plasma parameters on SHG and THG have been investigated using different structured laser beam profiles, such as q-Gaussian, cosh-Gaussian, and Hermite–cosh Gaussian beams in plasma. Key parameters including laser intensity, plasma density, density ripple, decentered parameter, wiggler magnetic field, and plasma density ramp have been studied in detail to analyze their impact on harmonic generation efficiency. The results demonstrate that structured laser beam profiles can significantly enhance harmonic generation under suitable plasma conditions compared to conventional Gaussian beams.

The theoretical analysis presented herein has been conducted using nonlinear plasma theory under the Paraxial approximation and WKB approximation. The findings provide valuable insights into nonlinear laser–plasma interactions and may contribute to the development of efficient harmonic sources for advanced scientific and technological applications.

I express my sincere gratitude to my research supervisor, Prof. Vishal Thakur, for his constant guidance, encouragement, valuable suggestions, and unwavering support throughout this research. His insightful discussions and motivation were instrumental in the successful completion of this thesis. I am also grateful to all my teachers and colleagues for their cooperation and support during my research journey.

Finally, I extend my heartfelt thanks to my parents and family members for their unconditional love, patience, encouragement, and immense support throughout my research. Their blessings and sacrifices have been a constant source of strength and inspiration.

ACKNOWLEDGEMENTS

In the name of Allah, the Most Gracious, the Most Merciful— All praise is due to the One who is beyond time, beyond form, beyond comprehension. To Almighty Allah (SWT), the Eternal Source of knowledge and wisdom, the Light of the heavens and the earth, I offer my deepest and most humble gratitude. It is He who placed within me the breath of endurance and lit the lamp of curiosity in the dark alleys of uncertainty. Through seasons of ease and storms of hardship, His mercy has been my shelter, His decree my compass, and His remembrance my solace. This journey, like all journeys of meaning, began with His Name and ends in His praise. Without His will, not a single word of this thesis would have been written, not a single moment of clarity attained.

*At the heart of my gratitude stand my beloved parents, **Mr. Nazir Ahmed Wani** and **Mrs. Sanjeeda Anjum**—my first teachers, my lifelong guides. Their sacrifices were silent, their prayers unceasing, their love unconditional. They carried my dreams before I could walk and believed in me long before I ever believed in myself. Their strength has been my foundation, and their affection, the shade under which I grew. No expression of thanks could ever encompass what I owe them; I can only pray that my success brings joy to their hearts as their unwavering love has brought peace to mine.*

*To the memory of my late grandfather, **Mr. Rustum Wani**—a man of gentle strength and principled silence—your legacy lives in the values I strive to uphold. Though you departed this world, your presence echoes in every act of honesty, in every step I took toward purpose. And to my grandmother, **Hajra Begum**, whose prayers are as enduring as the morning sun and whose faith in me has never wavered—your love has been the spiritual thread binding my soul through this academic pilgrimage.*

*To someone, who was not part of my life during the long and demanding journey of my PhD, yet has now become the very reason I live with purpose and hope. Fate chose its own time, and when you entered my world, everything found meaning. **Assia Arshid**, your love is my peace after years of struggle, my strength in moments of*

silence, and my home in a life once shaped only by ambition. What began as a solitary journey found its true destination the day you became my forever.

To my maternal grandparents, ***Ali Mohd Sehrai*** *and* ***Bibi Khatoon****—thank you for imparting lessons of resilience, compassion, and humility. Your wisdom, kindness, and unwavering prayers have been vital pillars of my life. The values you instilled, and the stories you shared, have profoundly shaped my character and perspective. Your love and blessings continue to guide me in all I do.*

To my uncles, ***Dr. Mashkoor Wani*** *and* ***Shamim Ahmed****—your encouragement, wisdom, and steadfast support have been instrumental throughout my journey. Your guidance and belief in my abilities gave me strength during moments of doubt, and I remain deeply grateful for your constant presence and counsel.*

*To my sisters—****Aarina, Dr. Aasima, Kehkashan, and Darakshan****—you are not merely my family but my refuge, my laughter in sorrow, and my joy in victory. You saw me not just as I was, but as I could be. Your words—gentle, fierce, encouraging—were the music that played when the world grew too quiet. In your eyes, I have always found strength; in your hearts, a place I belong.*

To my precious nephew, ***Mohd Arhab,*** *and my beloved niece,* ***Anam Fatima****—your innocent smiles and boundless curiosity have been a light in my life. You remind me of hope, wonder, and the joy of simple moments. May your journeys be blessed, and may the fruits of this work one day inspire you to seek knowledge, kindness, and truth.*

*To my dear cousins—****Mohd Suhair, Zainab Fatima, Mohd Aly Sayam, and Fatima****—your camaraderie, encouragement, and cheerful presence have been an ongoing source of happiness and inspiration. The bond we share and the warmth of our relationship have uplifted me during challenging times and added treasured memories to this journey. I am grateful for your support and the joy you bring into my life.*

To my mentor and research supervisor, ***Professor Vishal Thakur****—thank you for being more than a guide; thank you for being a true intellectual companion. Your*

unwavering support, your incisive questions, and your generosity with time and thought have deeply shaped the fabric of this thesis. You taught me that knowledge must not only be sought, but questioned; not merely understood, but transformed. It has been a privilege to learn under your thoughtful supervision. What sets Professor Thakur apart is not just his command over the subject, but the genuine care he extends to his students. Even during the most demanding phases of research, he remained approachable, kind, and encouraging. He believed in my work even at times when I struggled to, and that quiet confidence gave me the courage to persevere. His unwavering commitment to my development as a researcher—and more importantly, as a thinker—is a gift I will carry with me throughout my life. It has been one of the greatest privileges of my academic journey to have been mentored by him.

To ***Dr. Vinay Sharma****—your quiet strength and kind presence made a difference when I needed it most. Thank you for being a voice of calm in moments of uncertainty and for believing in me without condition. Your sincerity will not be forgotten.*

*To my friends—****Amit Kumar, Vaseem Akram, Mashahid Hussain Choudhary, Sachit Gupta, and Dr. Shah Imtiaz,*** *—thank you for standing beside me not just as companions in academia but as comrades in life. You filled this journey with light, with laughter, with perspective. You reminded me that even the heaviest burdens can be lightened by a shared moment of joy, or a simple "you've got this."*

This thesis is not just an academic manuscript—it is a reflection of questions long wrestled with, of late nights filled with equations and prayer, of moments when the lines between science and wonder blurred. It delves into the rich dynamics of second and third harmonic generation as intense laser pulses travel through the ocean of plasma—a realm where the invisible becomes radiant. Through the nonlinear interaction of light and matter, driven by the ponderomotive force and shaped by delicate density variations, the fundamental laser beam gives birth to harmonic echoes of itself. These echoes resonate far beyond the plasma—they speak to advancements in imaging, sensing, communication, and the limitless potential of light harnessed through understanding. This research, while grounded in theory and

physics, is ultimately an offering—to the community of knowledge, and to the future that awaits its fruits.

Every page of this work carries the fingerprints of those who guided me, prayed for me, questioned me, or simply sat beside me in silence. You may not see your names on the cover, but your presence is felt in every word.

And so, I end as I began—with gratitude to Allah (SWT), the Knower of what is hidden in hearts, the Turner of destinies, the Granter of light in darkness. May He accept this work, flawed though it may be, as a humble contribution in the pursuit of beneficial knowledge. May He bless those who walked with me, and may He guide us all toward truth, mercy, and meaning.

TABLE OF CONTENTS

LIST OF FIGURES

Appendix

List of papers published/communicated

1. D. Nazir, V. Sharma, V. Thakur, Magnetically enhanced third harmonic generation using q-Gaussian laser beam in plasma, *Journal of Optics*. (2023) 1–7.
2. A.A. Butt, D. Nazir, N. Kant, V. Sharma, V. Thakur, The effect of density ramp on self-focusing of q-Gaussian laser beam in magnetized plasma, *Journal of Optics* 1–9 (2023).
3. D. Nazir, V. Sharma, V. Thakur, Third Harmonic Generation Of Cosh-Gaussian Laser Beam In Magnetized Plasma, *Journal of Optics* 1–6 (2025).
4. Danish Nazir, Vishal Thakur, Second Harmonic Generation of Circularly Polarized Hermite-cosh Gaussian laser beam in Magnetized plasma. *Applied Physics B* (2025) (SCOPUS) (Published).
5. Danish Nazir, Vishal Thakur, Optimized Third Harmonic Generation in Plasma Using a Cosh-Gaussian Beam with an Exponential Density Ramp. *Iranian Journal of Physics Research.* (2025) (SCOPUS) (Accepted).
6. Danish Nazir, Vishal Thakur, Nonlinear Cherenkov Terahertz Radiation from a Cosh-Gaussian Beam in Magnetized Plasma. *Journal of the Korean Physical Society*. (2026) SCOPUS (Communicated).

Conference Papers.

7. Danish Nazir, Anees Akber Butt, Vinay Sharma, Vishal Thakur, Self-focusing of a q-Gaussian Laser Beam in Magnetized Plasma under Relativistic Conditions. *Nonlinear Optics Quantum Optics journal* (Accepted).

Book Chapter

8. A.A. Butt, D. Nazir, V. Thakur. The Role of Relativistic Nonlinearity in Self-Focusing and Second Harmonic Generation of q-Gaussian Beams in Plasma.

Chapter-1

Introduction and Review

1.1 Introduction

The advent of lasers as revolutionary light source in 1960 by Theodore H. Maiman marked a revolutionary milestone in modern science, unlocking unprecedented capabilities in precision measurement, communication, and energy delivery. This coherent light source, capable of extreme intensities and ultrashort pulses, catalysed advancements across disciplines, from quantum optics to materials engineering. Parallel to this, the discovery and understanding of plasma the fourth state of matter, ionized gas comprising free electrons and ions traces back to Irving Langmuir's pioneering work in the 1920s. Plasma, ubiquitous in astrophysical phenomena and fusion research, has since emerged as a dynamic medium for exploring nonlinear optical responses of materials to light. The confluence of high-power lasers and plasma physics has birthed a vibrant field of study, where extreme laser fields drive exotic phenomena such as particle acceleration, Wakefield generation, and higher order harmonic generation (HHG). Frequency of plasma is the most important parameter while studying plasmas and some rapid oscillations of electrons occur which we call Langmuir waves. An electromagnetic wave's phase velocity in plasma is determined by $v_\varphi = \omega_1/k_1$, where ω_1 being the electromagnetic wave frequency and k_1 is wave number and phase velocity $v_\varphi = c(1-\omega_p^2/\omega_1^2)^{-1/2}$, here ω_p is frequency of plasma and is shown by $\omega_p = (4\pi n_0 e^2/m)^{1/2}$, c represents the speed of light, and m denotes the mass of the electron.$e,$ being electric charge and n_0, equilibrium density of the plasma. Electromagnetic oscillations characterise plasma density, and laser plasma interactions depend on plasma frequency. When $\omega_1 > \omega_p$, electrons cannot protect the electromagnetic field, and the plasma is said to as under-dense. When $\omega_1 < \omega_p$, plasma electrons react quickly and the electromagnetic wave gets reflected, indicating that the plasma exhibits high density.

Exposure of plasma to a powerful laser pulse results in the relativistic jittering motion of its electrons and the resulting nonlinear plasma currents can convert the incident laser frequency into its integer multiples, producing coherent harmonics. This process, distinct from atomic HHG [1,2] in gaseous media, offers a pathway to generate intense, ultrashort XUV [3], ICF [4,5], ultrafast spectroscopy [6,7], compact particle acceleration [8,9] X-ray pulses [10,11] with applications spanning, chirped pulse amplification (CPA) [12,13], attosecond science [14], advanced imaging, and inertial confinement fusion diagnostics. Yet the spatiotemporal behaviour of the driving laser beam has a profound impact on both the efficiency and spectral organization of plasma-based harmonics. Although earlier work has widely investigated harmonic generation under theoretical Gaussian beam profiles, most high-power laser systems used in practice operate with structured beams, e.g., Laguerre-Gaussian, Bessel-Gaussian, or flattened profiles, for increased energy delivery or to reduce propagation losses. The effect of such non-uniform beam geometries on harmonic yield, phase matching, and angular distribution is still poorly understood. Extremely high SHG and THG amplitudes can aid in a more thorough examination of the many areas of study that are crucial to daily living. To investigate the various laser parameters influencing the efficiency of SHG and THG, we are encouraged to investigate many laser profiles, including q-Gaussian, cosh-Gaussian (chG), and Hermite-cosh-Gaussian (HchG) beams. Through rigorous theoretical and empirical analysis, the thesis aims to establish a framework for harnessing structured light to unlock new frontiers in nonlinear optics and high-energy-density science, contributing to the next generation of laser-driven technologies.

1.2 Nonlinear Phenomena

The way a medium (such as a crystal or plasma) reacts to an electric field (such as that produced by a laser) is exactly proportional to the field itself in linear optics. Nevertheless, nonlinear optics addresses circumstances in which this response deviates from linearity, usually when strong laser light is employed. This indicates that the medium's polarisation (P) now incorporates higher-order factors rather than a linear relationship with the electric field (E). In year 1961,Peter Franken [15], and his colleagues used a ruby laser on a quartz crystal to make the first observation of SHG, which laid the groundwork for nonlinear optics. THG came soon after, in the early 1960s, when scientists expanded nonlinear study into third-order processes in gases and solids. The SHG takes places due to atomic vibrations which vary quadratically with the intensity of optical field. Electric field provided by the intense laser is strong enough for Kerr effect to occur and is known as Optical Kerr Effect (OKE) [16]. SHG intensity varies with the squared electric field strength, reflecting its nonlinear optical nature. Therefore, intensity-modulated refractive index is provided as

$$\mathrm{n} = \mathrm{n}_0 + \mathrm{n}_2 \mathrm{I} \tag{1.2.1}$$

n_0 is linear refractive index at low intensities, n_2, refractive index influenced by optical nonlinearity coefficient (Kerr coefficient), I denotes intensity of light beam. Polarization density is given as

$$P(t) = \varepsilon_0 \sum_{n=1}^{\infty} \chi^{(n)} E^n(t) \tag{1.2.2}$$

Here $\chi^{(1)}$ is linear susceptibility, $\chi^{(2)}$ accounts for second order nonlinearities like second harmonic generation, $\chi^{(3)}$ [17], accounts for third order nonlinearities like third harmonic generation.

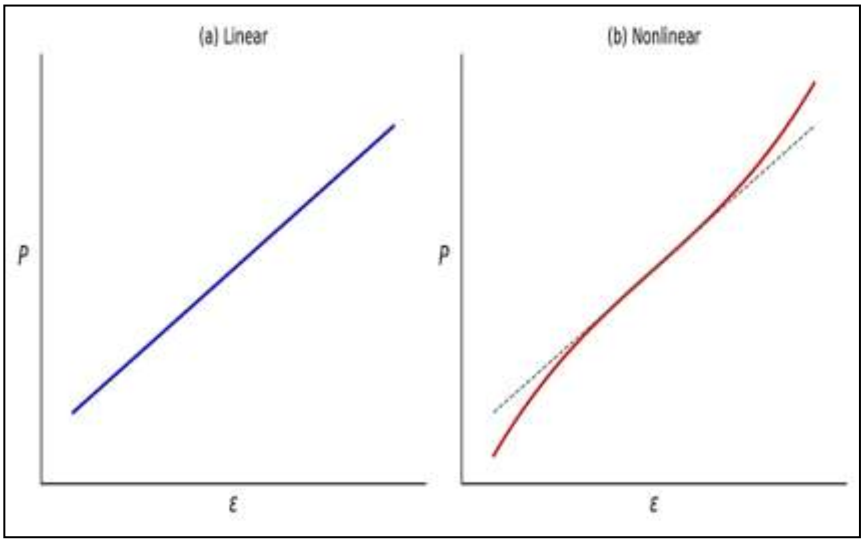

Fig. 1.1 The response of a nonlinear dielectric medium is represented through a nonlinear relationship between its polarization P and the electric field E.

1.2.1 Second harmonic generation

It is another important nonlinear phenomenon that takes place during transmission of intense laser beam through plasma as the investigation of frequency multiplication process in plasmas has a rich history, dating back to the early experiments on plasma physics and nonlinear optics. Early theoretical work laid the foundation for understanding the basic mechanisms of harmonic generation, particularly in the context of gas-phase media. However, as laser technology advanced, enabling the generation of high-intensity pulses, researchers began to explore harmonic generation in more complex media, including plasmas.

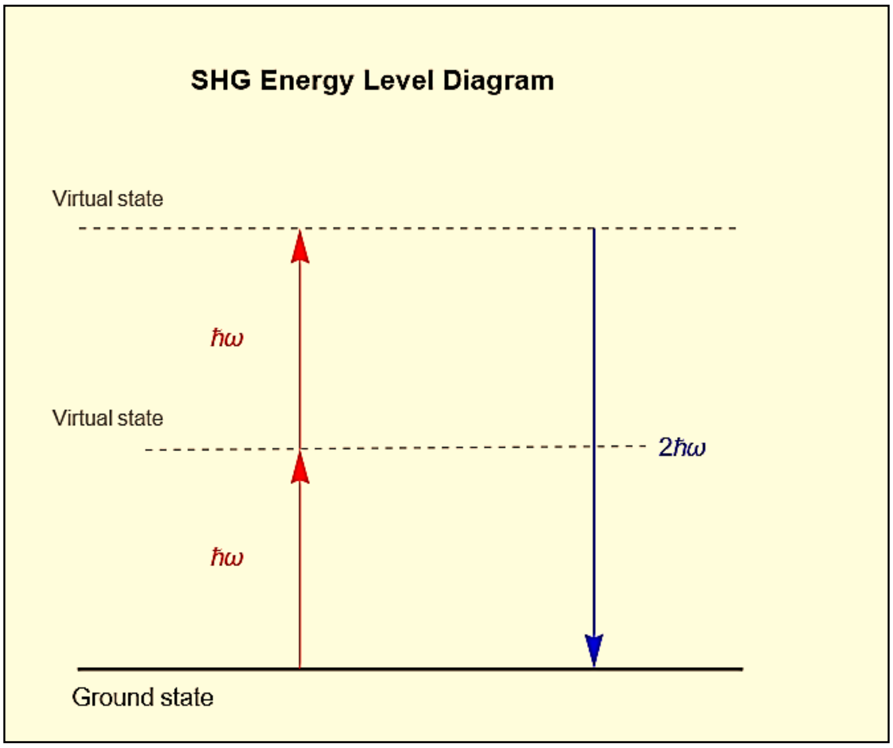

Fig .1.2 Representation of Second harmonic generations

The SHG energy level diagram illustrates the quantum mechanical representation of Second harmonic generation, an effect in nonlinear optics where two photons of frequency ω interact within a non-centrosymmetric medium to produce a single photon of frequency 2ω. As shown in the diagram, the system absorbs two photons sequentially, each with energy $\hbar\omega$, promoting it to a higher-energy virtual state an intermediate state that does not correspond to a real electronic level. From this virtual state, the system emits a single photon of energy $2\hbar\omega$, corresponding to the second harmonics. This process is determined by the material's second-order nonlinear susceptibility $\chi^{(2)}$, and efficient SHG requires phase matching to conserve momentum and ensure constructive interference of the generated harmonic wave.

Second Harmonic Generation (SHG) makes path for the conversion of invisible laser light into the visible range. For instance, radiation of $10{,}600$ Å can be converted to light of around $5{,}200$ Å wavelength, which falls almost within visible range. This process may be understood as an interaction involving photon exchange between various frequency components of the laser field, thereby doubling its frequency and reducing the wavelength by half of the original light

1.2.2 Third harmonic Generation

The third harmonic generation (THG) mechanism is depicted in the picture. Three photons with frequency ω are simultaneously absorbed by a nonlinear medium, like plasma, via virtual energy states, which are intermediate, non-resonant levels that are distinct from actual atomic or molecular states. Without sacrificing overall energy conservation, the system can momentarily access higher energy configurations thanks to these virtual transitions. The system releases one photon with energy $3\hbar\omega$ to return to the ground state after the three photons $(\hbar\omega + \hbar\omega + \hbar\omega)$ have been absorbed. This process is mediated by the material's cubic susceptibility $\chi^{(3)}$.

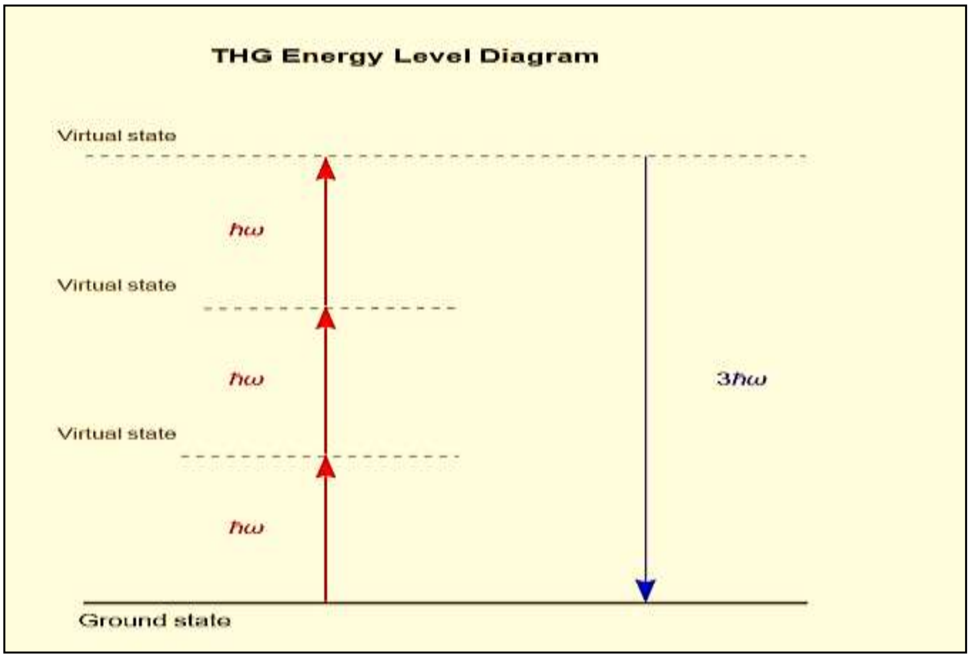

Fig. 1.3 Representation of Third harmonic generations

1.3 Wiggler magnetic field

Wigglers are a linear array of magnets placed such that each subsequent magnet has an opposite polarity, producing a spatially alternating magnetic field. When electrons or other charged particles move through this field, they are repeatedly deflected from side to side, which makes them accelerate and produce radiation with high energy and frequency [18]. These cyclic oscillations cause the production of intense electromagnetic radiation, which is very useful in experimental and diagnostic applications. Wigglers in the case of harmonic generation also have a major role to play by facilitating conditions of phase matching—providing the added momentum necessary for electrons to couple effectively with an incoming laser beam. Further, the wiggler field tends to maintain electrons localized in the plasma medium and assists the conditions of resonance through stabilization of cyclotron frequency so that the process of nonlinear optics is more efficiently enhanced.

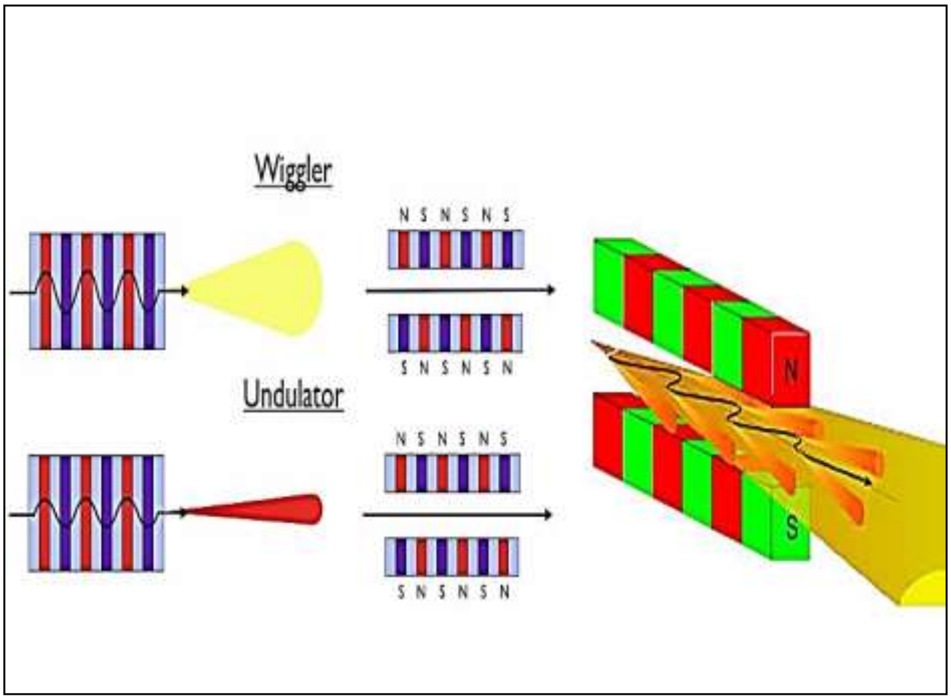

Fig. 1.4 Wiggler magnetic field and Undulator

https://www.google.com/imgres?q=wiggler%20magnetic%20field&imgurl=https%3A%2F%2Fwww.hsmagnets.com%2Fwpcontent%2Fuploads%2F2020%2F04%2FWiggler .

1.4 Plasma Density Ramp

A plasma density ramp, in laser–plasma interactions, is a spatially graded electron density profile, in which the electron number density ramps up or down along the direction of laser propagation instead of being constant. These ramps may be introduced naturally in expanding plasmas or designed on purpose by utilizing tailored gas jets or foil targets. One of the most commonly investigated types is the exponential density ramp, given by $n_e(z) = n_0 e^{\alpha z}$, where n_0 is the base density and α determines the ramp steepness. The exponential profile better simulates realistic plasma generation conditions than step or linear ramps and has a significant role. It adds a spatially varying refractive index because the plasma frequency varies gradually, modulating the phase-matching conditions and dispersion relation essential for effective frequency conversion, resulting in a position-dependent phase mismatch

$\Delta k(z)$ between the harmonic and fundamental waves. While usual phase mismatch is known to reduce harmonic efficiency, a gradient in an exponential ramp can enable quasi-phase matching with periodic resetting of the phase relation and increased harmonic build-up along large interaction lengths. The influence of the ramp is particularly notable when its density scale length equals or is on the order of the Rayleigh range of the laser or plasma skin depth since it allows strong localization of the field and ongoing nonlinear coupling. In addition, in the relativistic regime or with the conditions of tight focusing, the exponential ramp will cause self-focusing or refractive guiding, further increasing the field intensity seen by the plasma. This enhances the nonlinear source terms that are accountable for higher harmonic generation. When laser beams with structured beam shapes, like q-Gaussian, cosh-Gaussian, or Hermite–cosh Gaussian beams, are incident on such a ramp, the interaction between the spatial structure of the beam intensity and changing plasma density results in complex coupling patterns. These can lead to spatially selective harmonic emission regions, angular redistribution of the harmonic radiation, and even off-axis lobe enhancement in emission. Moreover, the ramp also changes the group velocity dispersion of the group and can change the effective wave breaking threshold, affecting the coherence and spectral sharpness of the produced harmonics. In summary, the exponential plasma density ramp proves to be an effective tool for the design and improvement of harmonic generation via spatial phase-matching control, field localization, and nonlinear coupling mechanisms. However, less attention has been paid to the influence of laser beam profiles on these processes, particularly in plasma environments.

Research has shown that different laser beam profiles can significantly affect the interaction dynamics. Gaussian beams, which have a symmetric intensity distribution, are the most commonly studied and utilized in laser-plasma experiments. However, recent studies suggest that other beam profiles, such as Laguerre-Gaussian beams with their characteristic orbital angular momentum, and Bessel beams, known for their non-diffracting nature, can introduce unique nonlinear effects in plasma. These effects can alter the phase matching conditions, electron trajectories, and other critical parameters that influence harmonic generation.

The influence of beam profiles on harmonic generation has also been explored in other nonlinear media, such as gases and solids, providing valuable insights that can be extrapolated to plasma studies. However, the complex nature of plasma, with its dynamic ionization and recombination processes, introduces additional challenges that require dedicated investigation. This thesis seeks to fill this gap by systematically studying the influence of different high-power laser beam profiles on harmonic generation in plasma, using theoretical models.

1.5 Literature Review

Erokhin et al. (1969) [2] discovered that nonlinear dispersion creates second harmonics, with a possible energy transition coefficient of unity. They considered ion location and density perturbation, leading to nonlinear effects and SHG, and found that this process can produce a coefficient of energy of unity.

Basov et al. (1979) [19] conducted theoretical and experimental research on the SHG, focusing on laser plasma contact at critical density levels using solid targets and the Kalmar laser. They discovered laser plasma contact at the crucial plasma density zone for the first time using a Kalmar laser.

Sodha et al. (1979) [20] investigated SHG in the context of strong laser plasma contact, where ponderomotive self-focusing is the cause of nonlinearity. They investigated how the strength of the incident laser pulse and the plasma's non-uniformity affected the beam width parameter. They noticed that when the beam traverses farther inside the plasma, the density of electrons drops, causing amplification of beam parameter. However, the beam parameter greatly decreases as the input laser's strength rises.

Thakur and Sharma (1981) [21] examined the SHG electrostatic pulse in heated plasma using a Gaussian electromagnetic pulse. Electrostatic pulses are created at two times the carrier frequency of approaching pulse due to the force $\left(\vec{v} \times \vec{B}\right)$. They found that when an electromagnetic pulse with a same intensity distribution is created along its wavefront, the resulting Gaussian electrostatic pulse has a pulse width $\left(1/\sqrt{2}\right)$ of times the original phase width. A third harmonic signal is created when the produced pulse and the incident electromagnetic pulse contacts once again with one another.

Heinz and Loy (1988) [22] examined the nonlinear process of SHG, in order to better understand surfaces and interfaces in cases when the medium is centrosymmetric. They gathered the information necessary for the advancement and utilisation of the semiconductor method. In their controlled investigation, they noticed the sensitivity of

SHG to various electronic characteristics and the reliance of nonlinearity on the semiconductor surfaces' chemical composition.

Liu et al. (1993) [23] studied the harmonic production utilising interactions between picosecond and a microsecond, laser pulses in neutral and ionised gases. They looked at how the effectiveness of THG varied experimentally. They found that the only way the gain increases is if distinct plasma effects are combined with phase matching requirements. They investigated the requirement of incoming lasers with increasing intensities for relativistic harmonic production**.**

Krylov et al.'s (1995) [24] observed that second harmonic generation (SHG) becomes less efficient at higher intensities, likely due to the onset of continuum generation. The reported gain remains below 50%, which may be attributed to phase modulation effects in the incoming pulse, underscoring the critical role of phase modulation in influencing SHG efficiency.

Birulin et al. (1996) [25] proposed a theoretical model for high-harmonic production in homogeneous or inhomogeneous dispersive mediums. They experimentally demonstrated that interference of two waves leads to harmonic generations, and as contact length increases, the efficiency of generating harmonics increases.

Malka et al (1996) [26] studied the relationship between relativistic plasma and second harmonic production. They observed a second harmonic pulse spreading across a Rayleigh length, revealing that ionisation and ponderomotive force produce radial electron density, giving (SHG) its power. Their research supports the effectiveness of second harmonic pulses and the impact of incoming laser intensity on SHG efficiency, aligning with theoretical research.

Ramachandran (1996) [27] investigated side scattering above the one-fourth critical density and found the maximum increase for second harmonic Raman scattering via laser plasma contact. The Raman effect is more prominent than SHG when the plasma is underdense. Both the SHG and the Raman become irrelevant for collisional plasma**.**

Brandi and Neto's 1997 [28] study examined THG through laser-plasma interaction, analyzing its oscillatory behaviour considering various electron plasma density values. They found that decreased THG behaviours was due to fine spectral linewidth, and only modest levels of incoming laser intensity were used to analyse the THG, going beyond the low-density approximation.

Parashar and Sharma (1998) [29] had studied the SHG under the action of an obliquely impinging laser at the vacuum–plasma boundary. A laser pulse with elevated field strength when incident on plasma at some angle results SHG in reflected component. They observed that second harmonic power gets vanishes at normal and grazing angle. Their study showed that second harmonic power is sensitive to the angle at which the wave strikes. The power yield increases with electron density is optimum at critical density and again decreases with increase in density.

Kim and Lee (1999) [30] conducted an in-depth comparison of Hermite–Gaussian (HG) and Laguerre–Gaussian (LG) beam profiles and demonstrated that, despite diffraction effects, the total beam power remains invariant along the propagation axis. By applying Lommel's lemma, they derived a power-series solution that agrees closely with Lax's formalism. Their approach involved representing the transverse electric-field components and solving the Helmholtz equation in the half-space $z > 0$, which confirmed that beam power is conserved during propagation. Their analysis also showed that, under the paraxial approximation, the dominant contributions to the field arise from the lowest-order terms in the series. Finally, they obtained an explicit vectorial expression for the field traveling via the z-axis, verifying its consistency with Lax's equations for paraxial wave behaviour.

Singh et al. (2002) [31] studied phase-matched relativistic second harmonic generation in plasma. Their research focused on the mechanism by which the interaction between an intense laser beam and plasma results in the creation of density perturbations. When these perturbations are combined with the fluctuating electron velocity at the fundamental frequency, they lead to second harmonic generation. The research emphasized that these density modulations, or ripples, may be caused by acoustic waves, which can be internally or externally driven. One of their major findings was that the second harmonic signal's conversion efficiency is sensitive to the angle of the incident laser beam and the density ripple orientation.

Banerjee et al. (2002) [32] explored how plasma electrons react when irradiated by an ultra-intense laser under relativistic conditions. Their experimental observations pointed out that, at these extremely high intensities of lasers, electron density plays a vital role in the production of harmonics. They noted that VUV radiation is produced mainly through relativistic Thomson scattering with energetic electrons. The study also reported an estimated efficiency for high-order harmonic generation to be about 10^{-7} , with a size of the laser beam having been reported at about 3 mm.

Kant and Sharma (2004) [33] investigated resonant harmonic generation initiated by a highly energetic electromagnetic wave propagating in an ionized medium influenced by a spatially varying magnetic structure. They identified that a gradient in particle density along the propagation axis plays a central role in driving second harmonic generation. Their analysis focused on conditions where the wave undergoes self-contraction within the magnetically perturbed plasma environment. This self-contraction was shown to enhance the output of the second harmonic component. Furthermore, the study revealed that the contracted wave exhibits a periodic modulation in amplitude, reaching maximum values at deeper locations within the medium.

Upadhyay and Tripathi (2005) [34] have explored second harmonic generation (SHG) in a laser-created plasma channel. They studied how the influence exerted by a short-duration laser excitation in a rarefied plasma environment results in SHG happening in denser areas, with the resulting harmonic traveling at a minor angle with respect to the channel axis. Their work reported that through ponderomotive self-focusing, the second harmonic had an pulsating character correlated with the channel density profile. They reported significantly improved conversion efficiency at increased plasma densities and a linear dependence of peak efficiency on the channel radius. Their research was limited to self-guided laser beams and did not cover converging beams.

Sandhu et al. (2005) [35] examined second harmonic generation (SHG) and hard X-ray emission due to the engagement from the interaction between an ultra-powerful optical field and a low-density ionized medium" already formed on a solid target. They aimed to determine a relationship between SHG and high frequency X-ray production regarding plasma scale length. They determined a particular scale length at which SHG was minimized and hard X-ray emission was maximized. The experimental results indicated excellent conformity with theoretical predictions. They also found that SHG efficiency improved dramatically at increased incident laser frequencies.

Carrasco et al. (2006) [36] explored the generation of harmonics—both second and third order using a vector-Gaussian beam interacting with a nonlinear optical crystal. Their analysis, based on the first Born approximation, yielded formulations involving the nonlinear susceptibility tensor. A key aspect of their research was the role of the Gouy phase shift, particularly in third-order harmonic generation within centrosymmetric materials. The results demonstrated that the efficiency of both harmonic processes is strongly influenced by the system's geometry and diminishes as the crystal dimensions are reduced.

Dhaiyaa et al. (2007) [37] performed a theoretical and simulation study of second and third order harmonic generation in plasma with imposed ripples to density of plasma, which allowed for phase matching. They showed that these density modulations could be used to allow both even and odd harmonic generation, as evidenced from particle-in-cell simulations. For relativistic regimes, they saw that harmonic generation efficiency increased strongly when phase matching was facilitated using these ripples compared to the absence of phase matching.

Gupta et al. (2007) [38] studied THG due to the interplay caused by a Gaussian beam of elevated intensity and hot, colliosionless plasma. Following the paraxial approximation, they obtained the expressions that explained relativistic as well as ponderomotive nonlinearities of the incident laser. Their study explained that the second harmonic component gets induced in the plasma due to the Lorentz force and then couples with the fundamental oscillatory velocity in order to generate THG. The study concluded that the highest THG power achieved was on the order of 10^{-6}.

Pallavi et al. (2007) [39] analyzed second harmonic generation (SHG) due to the interplay between a elevated-intensity, linearly polarized laser beam and magnetized plasma. They established that a second-order nonlinear current density is produced in the transverse direction, which leads to SHG. An analytical result for the normalized second harmonic amplitude was obtained, which was oscillatory in nature. Their findings revealed that both the magnetic field intensity and the incident laser intensity positively affect the SHG efficiency.

Kaur and Sharma (2008) [40] gave an analytical investigation of third harmonics in the course of propagation of a powerful laser via plasma produced from a thin metal film. When the laser reflects at the critical density surface in the plasma, it causes ripples in the density that meet the condition of phase matching, hence improving THG efficiency. They ascribed the THG to the superposition of the back-reflected wave from the critical layer and saw that efficiency improved with increased density scale.

Verma & Sharma (2009) [41] examined SHG in magnetized plasma with periodic density modulations. A high external magnetic field combined with ripples in density ensured the phase matching necessary for efficient harmonic generation. The research emphasized that SHG efficiency increases as a result of the combined effect of the ponderomotive force, magnetic field, and density modulation. Also, they noted that an increase in electron density further increased SHG efficiency because of increased coupling between the laser and the magnetic field.

Rajput et al. (2009) [42] investigated resonant THG when a very high-intensity laser is propagated across the plasma. The wiggler field was employed to accomplish the phase matching condition, which significantly enhanced THG efficiency. However, pulse slippage happened because of mismatch of the velocity between the third harmonics and the basic pulses. They pointed out that the third harmonic pulse travelled for larger distances, and the THG efficiency grew tremendously with the increase in the strength of the wiggler field.

Prashar (2009) [43] examined the second harmonic creation when plasma is filled with parallel plane wave guides, while also taking into account the density ripple that provided the phase matching. The plasma frequency must be more than 0.5 times the incidence pulse frequency in order to achieve increased efficiency. They claimed that the sixth power of the incident pulse frequency has an inverse relationship with the efficiency loss.

Patil et al. (2009) [44] In their study of the Hermite-Gaussian (HG) laser beam examined the oscillatory behaviour of laser beams travelling through collisionless plasma. In order to determine the beam width parameter expressions and investigate how the beam width parameter behaves with linear distance of propagation at various decentred parameter and linear absorption coefficient values, they employed the W.K.B. and paraxial approximation. They found that there is nonlinearity in their study under ponderomotive force, and that both odd and even p-values defocus, causing the beam width parameter to oscillate.

Kaur et al. (2010) [45] used the short pulse laser propagating through rippled density plasma to study the THG. Where density ripple provides additional momentum to electrons and this satisfied the phase matching condition results increase in self-focusing that enhanced the efficiency of THG. They observed that, at high intensity of incident laser, the plasma density decreases along axis and, resonance condition for THG reduces, result decrease in efficiency. Nonlinearity depends upon the intensity of incident laser, and is independent of the frequency of incident laser. In their study, at very high intensity of incident laser the relativistic nonlinearity is dominant.

Askari and Norzooi (2010) [46] investigated the SHG, where nonlinearity caused by the field induced force resulted in the creation of harmonics. Phase matching is achieved through the influence exerted by the wiggler magnetic field, which raises the

SHG efficiency to a suitable level. They demonstrated how the laser and plasma frequencies affect the second harmonic pulse's efficiency.

Kant et al. (2011) [47] investigated the Gaussian laser beam for second harmonic production with density transition. They noted the increased second harmonic pulse intensity, the rise in self-focusing, and the beam's extension to multiple Rayleigh lengths by implementing plasma density ramp. They saw a noticeable increase in the second harmonic pulse's efficiency when an exponential density ramp was present.

Kant et al. (2012) [48] examined Hermit-Gaussian laser beam interaction they also examined the results of plasma density ramp on laser self-focusing. They noticed that when plasma density gradient was introduced, the beam showed more self-focusing. In their investigation of the beam width parameter change at optimal values of various laser parameters, they found that the laser pulse propagates across multiple Rayleigh lengths without exhibiting diffraction.

Kant et al. (2012) [49] investigated the resonant THG that occurs when a strong laser travels through electron-hole plasma, a semiconductor. The wiggler field findings showed a high efficiency of the third harmonic pulse, satisfying the phase matching criteria. They looked at several laser parameter optimal settings to determine the third harmonic pulse's highest efficiency.

Sharma and Sharma (2012) [50] examined laser-plasma interaction and evaluated the SHG in the relativistic and ponderomotive regimes while an intense short pulse laser was traveling through magnetised plasma. Using the paraxial approximation, they were able to establish the linked equations of spatial beam parameter and oscillation frequency of the second harmonic pulse. They found that when varying magnetic field values are used, the power of the plasma wave varies. Their research showed that the wiggler magnetic field's fluctuation in strength has a significant impact on the SHG's output.

Sharma et al. (2013) [51] examined the THG when a strong Gaussian laser pulse travelled through plasma at various magnetic field strengths. When the wiggler magnetic field gave plasma electrons enough velocity to meet the phase matching requirement, there was a noticeable increase in efficiency. They discovered in cases where a wiggler magnetic field is applied, the Rayleigh length increases.

Mihailescu et al. (2013) [52] investigated the influence of various laser settings on the power output of harmonic production and the higher harmonic generations through strong laser plasma contact. In their work, scientists used a femtosecond Ti-Sapphire terawatt laser to reflect harmonics, and they examined how the efficiency of harmonic creation was affected by various laser characteristics.

Jha et al. (2014) [53] examined chirp - modulated laser pulses in a magnetised plasma waveguide. By using a variational method, they were able to derive equations that explain the incident laser's spot size, pulse duration, and chirp parameter. They also investigated the influence exerted by an external magnetic field on the chirping, spot size, and pulse duration of both chirped and unchirped lasers. Their important finding is that the unchirped laser pulse achieves both a positive and negative chirp in an external magnetic field.

Chen et al. (2014) [54] used chirped nonlinear photonic crystals to investigate SHG and THG. For phase matching with finite bandwidth, they created a manufactured chirped poled lithium niobate (CPPLN) nonlinear photonic crystal that produced second and third harmonic generations. They demonstrated how the bandwidth and efficiency are impacted by the chirped rate. They demonstrated how CPPLN produces many primary-coloured lasers that may be utilised in large-screen laser displays.

Thakur and Kant (2015) [55] used density transition to study laser beam self-focusing and investigated THG during high intensity laser plasma contact. In their work, the wiggler-induced field is used to ensure the phase matching criteria, which results in an efficiency boost. They demonstrated pulse slippage as a result of the fundamental and third harmonic pulses' different velocities.

Aggarwal et al. (2015) [56] investigated wiggler aided SHG, which occurs when atomic clusters are present and a very strong laser beam travels through plasma. The wiggler field is in charge of the phase matching condition, which raises SHG efficiency. They investigated the impact of cluster size and fundamental laser intensity on second harmonic pulse efficiency. There is an increase in SHG efficiency, and pulse slippage is shown.

Singh et al. (2015) [57] examined the SHG and THG when a strong laser beam passes through a magnetised plasma when relativistic self-focusing is in effect. Nonlinearity results from self-focusing plasma channels caused by relativistic mass fluctuation under effect of a magnetic field. At fundamental frequency, the density perturbation occurs, which, when combined with the electrons' quiver velocity, results in THG. Their research showed that the plasma's magnetic field significantly affects THG's efficiency.

Verma et al. (2015) [58] investigated the strong laser plasma interaction when an electric field was dispersed transversely. SHG occurs when the density perturbation combines with the electrons' fundamental vibrational speed. The second harmonic pulse's efficiency is greatly increased by the phase matching condition, which is caused by the induced electric field's duration.

Gupta et al. (2015) [59] investigated the SHG using an powerful q-Gaussian laser beam, taking into account the parabolic ionized channel and the fact that nonlinear absorption is caused by collisions. Non-uniform irradiance causes the plasma electrons to heat unevenly, which leads to self-focusing and density gradients that excite the plasma wave at its fundamental frequency and interact with the incoming laser to produce SHG.

Rathore and Kumar (2016) [60] had given the study of THG using quantum hydrodynamic model. Third harmonic current is produced when Gaussian beam propagates through plasma in normal wiggler field that produce transverse current and provided the phase matching. They observed the maximum efficiency when phase matching condition is satisfied. Quantum effects in harmonic generation were also studied in their work.

Purohit et al. (2016) [61] examined how second harmonic signals can be generated within a collisionless plasma when driven by a self-focused hollow Gaussian laser beam. Adopting the paraxial approximation, they derived coupled equations that track beam width evolution during propagation. Their analysis revealed that both relativistic mass variation and radiation pressure contribute significantly to harmonic generation through nonlinear interactions. The study concluded that key interaction parameters play a decisive role in determining the overall SHG efficiency.

Ganeev et al. (2016) [62] studied the augmentation of a single harmonic by resonance and the amplification across multiple harmonic orders by quasi-phase matching in mid-infrared femtosecond pulses propagating through indium plasma. They found that the enhancement achieved through the quasi-phase-matching macroprocess is similar to the enhancement achieved through the resonantly enhanced harmonic microprocess. The study suggests that combining these techniques would be a helpful tool for producing powerful short wavelength radiations.

Vij et al. (2016) [63] studied the occurrence of third harmonic generation in plasma with short-pulse laser propagation when subjected to clusters with density ripple. The ripples in plasma provided the Phase matching and higher density of electrons outside the cluster region enhance the amplitude of THG. With the rise in collisional frequency of electrons, the absorption decreases and efficiency of THG decreases. The efficiency of THG is maximum at low collisional frequency. They reported the group velocity mismatch of THG and fundamental laser, due to which pulse slippage is observed.

Kant and Thakur (2016) [64] conducted a detailed investigation into SHG) resulting from a chirped pulse in plasma, taking into account the effects of relativistic self-focusing. Their study systematically examined how the chirp parameter and the normalized plasma frequency influence the conversion efficiency of the second harmonic signal. A key finding of their work was the role of cyclotron frequency in enhancing SHG efficiency. This enhancement was attributed to the facilitation of phase matching, which was achieved through the presence of a periodic magnetic structure, commonly referred to as a wiggler field.

Kumar et al. (2016) [65] explored the production of harmonic frequencies resulting from laser–plasma interactions in magnetized quantum plasma using a quantum hydrodynamic framework. Their focus was on (SHG) induced by a laser emitting light with linear polarization, beam propagating via dense plasma through the influence of a uniform magnetic field. They noticed that including quantum effects such as Fermi pressure and electron spin significantly reduced wave dispersion. Additionally, their findings highlighted a disparity in propagation speeds between the incident wave and its generated second harmonics, resulting in pulse slippage. The study concluded that the amplitude of the SHG reaches its peak so its fundamental frequency ω_1 and its second harmonic $2\omega_1$ are resonant with the cyclotron frequency.

Leblanc et al. (2017) [66] studied the production of high-order harmonics from plasma mirrors, paying particular attention to phase and spatial amplitude profiles that are impacted by laser beam properties. They investigated Relativistic Oscillating Mirror and Coherent Wake Emission processes, confirming models and improving knowledge of laser-plasma interactions.

Varaki and Jafari (2018) [67] analyzed harmonic generation resulting from polarized Gaussian laser and magnetised plasma when exposed to a planar magnetostatic wiggler field. By applying perturbative techniques, they observed that incorporating the wiggler field helped fulfil the resonance condition, leading to a noticeable enhancement in SHG efficiency. Their analysis also demonstrated that the efficiency of the second harmonic pulse increased with higher plasma frequencies.

Sharma and Jha (2019) [68] studied circularly polarised laser beam in obliquely magnetised plasma to generate second harmonics, demonstrating the impact of magnetic field direction on radiation amplitude. As magnetic field intensity and obliqueness rise, so does amplitude.

Maity et al. (2021) [69] used cell-based particle simulations to study harmonic generation in magnetised plasma. They found that efficiency relies on the strength of the magnetic field and rises with laser intensity. They also found the ideal magnetic field for optimising harmonic generation efficiency in an O-mode configuration. The proper magnetic field strength and laser intensity both boost efficiency.

Yang et al. (2022) [70] the study investigates high-order harmonic generation (HHG) induced by a high-power laser beam on plasma surfaces, specifically focusing on the effects of plasma surface profiles. The research reveals that a convex plasma surface, formed by a pre-pulse, leads to a saddle-shaped divergence of harmonics. This divergence is influenced by the oblique incidence of the laser and is supported by 2D particle in cell (PIC) simulations, highlighting the importance of plasma surface shape in controlling harmonic generation characteristics.

Walia et al. (2022) [71] studied that the ponderomotive force of the Cosh-Gaussian beam causes a redistribution of charge carriers, leading to the generation of density values in the radial direction. The gradients of density arisen by the ponderomotive force led to the creation of electron plasma waves (EPWs), and these EPWs interact with the input beam to produce second harmonic waves. The focusing behaviour of the beam and the SHG yield are improved by increasing the plasma density, beam radius, and decentred parameter, while decreasing the beam intensity.

Mathijssen et al. (2023) [72] presented a setup to produce high order harmonics in laser induced plasma, which can generate coherent VUV and EUV light and characterisation via harmonic analysis. High order harmonics in the plasmas of aluminium, nickel, tin, silver and indium were achieved with high variation in yields and harmonic distributions. It is possible that charge density increases with the use of tin plasmas used to detect harmonic orders of up to 25 at wavelength $62.4\,nm$ and energy of 19.9 eV. The optimal laser settings and time intervals must be set, which can also serve to enhance yields of harmonics to monitor temporal dynamics.

Fu et al. (2023) [73] observed a 100-fold increase in SHG from an air plasma using an orthogonal pump-probe laser configuration, highlighting polarization effects and sub-picosecond dynamics in frequency conversion.. The increased efficiency of second harmonic production is detected in a sub-picosecond time frame and is consistent for fundamental pulse lengths ranging from $0.1\,ps$ to over $2\,ps$. The polarisation of the field is complicated relying on the polarisation of both input fundamental beams with the proposed orthogonal pump-probe configuration.

Antipov et al. (2024) [74] examined the process of high-harmonic generation resulting from laser interactions with plasma, highlighting how laser-modified electron beams can emit coherent radiation at harmonic frequencies—approximately one hundred times shorter than the driving laser wavelength. Their study underscores the critical role of maintaining energy stability and carefully adjusting parameters such as the momentum compaction factor (R56) to achieve effective electron bunching at higher harmonics. This technique is intended to produce narrow-band, tunable, and stable radiation, offering advancements for next-generation plasma-based radiation sources.

Mitrofanov et al. (2024) [75] explored the production of harmonics triggered by powerful laser radiation interacting with dense material surfaces. They explored two primary approaches: optical amplification in the longer-wavelength range (mid-infrared) and amplification of pulses with varying frequency components (chirped pulses) in the shorter-wavelength range (near-infrared). Their research also included the detection of high-order harmonics, with experimental data extending down to $35\,nm$, providing a potential source for structured optical output in the deep UV range.

Singh and Walia (2024) [76] analyzed how relativistic and ponderomotive nonlinear effects responsible for modifying electron mass and generating density inhomogeneities enhance self-focusing and boost second harmonic generation (SHG) efficiency. Their study focused on high-intensity Cosh-Gaussian laser beams interacting with thermally excited, quantum-degenerate plasma. They concluded that the efficiency of SHG and the degree of self-focusing are strongly influenced by the specific laser and plasma conditions.

Hazanov et al. (2025) [77] revealed nonharmonic Mollow-type triplets while discussing high harmonic generation (HHG) in systems with isolated bound states. In relation to high-power laser interactions in plasma, it highlights the significant nonlinear response and offers possible experimental setups for investigating these events. Nonharmonic Mollow-type triplets in HHG are produced by isolated bound states. Results improve knowledge of ultrafast dynamics and HHG.

1.6 Research Gap

Many studies have focused on self-focusing and harmonic generation (SHG and THG) using conventional Gaussian laser beams. However, investigations into how alternative beam shapes—such as q-Gaussian, cosh-Gaussian, and Hermite–cosh Gaussian profiles—affect SHG and THG remain scarce. Early work has demonstrated that non-Gaussian profiles can produce stronger self-focusing and potentially higher harmonic conversion efficiencies, yet systematic comparisons across different beam families are lacking. Moreover, while laser–plasma interactions involve complex phenomena like ionization, particle acceleration, and collisional damping, their combined influence on harmonic yields for non-Gaussian beams is not well understood. To address this gap, our research examines SHG and THG in various plasma environments using different laser profiles, aiming to identify beam parameters that maximize harmonic output and clarify the underlying physical mechanisms.

1.7 Objectives

The primary goal of this thesis is to optimise several laser and plasma parameters in order to increase the efficiency of second and third order harmonic production of laser beams in plasma. To accomplish high –efficiency we choose to use several laser profiles in our study for increased second and third harmonic production for high power lasers. To accomplish these goals, the three issues listed below were examined.

1. Third harmonic generation of q- Gaussian laser beam in magnetized plasma.
2. Second harmonic generation of circularly polarized Hermite-cosh Gaussian laser beam in plasma.
3. Third harmonic generation of cosh-Gaussian laser beam in magnetized plasma.

1.8 Thesis Outline

In this thesis, we have undertaken a comprehensive theoretical investigation into second order and third order harmonic generation (SHG and THG) from intense laser beams interacting with plasma, with a particular focus on how different laser beam profiles influence nonlinear optical processes. While Gaussian beams have traditionally dominated such studies, we recognize that real high-power laser systems often exhibit structured profiles such as q-Gaussian, cosh-Gaussian (chG), and Hermite–cosh Gaussian (HchG) beams. These structured beams are known to exhibit enhanced focusing, field localization, and phase matching characteristics that can significantly improve harmonic generation efficiency. The thesis begins with a detailed introduction to the fundamental principles of laser-plasma interaction, nonlinear optics, and harmonic generation mechanisms. The literature review outlines the historical development of SHG and THG, highlighting key theoretical advances while identifying the research gap related to the limited study of structured beam profiles in plasma environments. Following this, we present the governing equations derived from Maxwell's laws, the equation of continuity, and the nonlinear wave equations tailored for plasmas. A comparative description of q-Gaussian, chG, and HchG beams is provided, discussing their electric field structures, propagation behaviour, and relevance to nonlinear coupling in plasma. The core contributions of this thesis are then organized into three main chapters, each dealing with a specific beam profile. In the first case, we examine the third harmonic generation using a q-Gaussian beam in magnetized plasma. Analytical expressions third harmonic amplitude were derived under relativistic and ponderomotive nonlinearities, with a wiggler magnetic field enabling phase matching. The second major study explores second harmonic generation with a circularly polarized Hermite–cosh Gaussian beam in plasma, emphasizing the spatial beam shaping effect on SHG yield. In the third part, we analyze third harmonic generation from a cosh-Gaussian beam, deriving beam width evolution and harmonic amplitude under similar nonlinear conditions. Each of these studies includes a rigorous mathematical formulation, numerical analysis using Mathematica, and graphical visualization of results using Origin. By solving coupled differential equations for beam width and harmonic amplitude, the role of key parameters namely intensity, beam waist, magnetic field strength, and plasma density ramp is systematically evaluated. The results clearly demonstrate that structured beams offer superior self-focusing, stronger nonlinear coupling, and improved harmonic conversion efficiency compared to Gaussian beams. In conclusion, this thesis presents a unified and comparative framework for understanding and optimizing SHG and THG using various laser beams. The findings contribute toward advancing structured light applications in plasma diagnostics, ultrafast optics, and high-energy-density science.

References

[1] M.S. Sodha, M. Faisal, M. Verma, Effect of self-focusing on third harmonic generation by a Gaussian beam in a collisional plasma, *Physics of Plasmas,* **16** (2009) 082304.

[2] N. Erokhin, S. MOISEEV, V. ZAKHAROV, Second harmonic generation by an electromagnetic wave incident on an inhomogeneous plasma (Second harmonic generation by electromagnetic wave incident on inhomogeneous plasma, determining power output), *ZHURNAL EKSPERIMENTAL’NOI I TEORETICHESKOI FIZIKI* ,**56** (1969) 179.

[3] P. Salieres, M. Lewenstein, Generation of ultrashort coherent XUV pulses by harmonic conversion ofintense laser pulses in gases: towards attosecond pulses, *Measurement Science and Technology* ,**12** (2001) 1818.

[4] R.L. McCrory, Laser-driven ICF experiments, in: Nuclear Fusion by Inertial Confinement, *CRC Press*,**13** (2020) 555.

[5] E. Lindman, Laser-induced magnetic fields in ICF capsules, *High Energy Density Physics*, **6** (2010) 227.

[6] R. Ganeev, C. Hutchison, T. Witting, F. Frank, W. Okell, A. Zaïr, S. Weber, P. Redkin, D. Lei, T. Roschuk, others, High-order harmonic generation in graphite plasma plumes using ultrashort laser pulses: a systematic analysis of harmonic radiation and plasma conditions, *Journal of Physics B: Atomic, Molecular and Optical Physics* ,**45** (2012) 165402.

[7] G.D. Reid, K. Wynne, Ultrafast laser technology and spectroscopy, *Encyclopaedia of Analytical Chemistry* ,**35** (2000) 13644.

[8] T. Tajima, High energy laser plasma accelerators, *Laser and Particle Beams* ,**3** *(1985) 351.*

[9] T. Tajima, J.M. Dawson, Laser electron accelerator, *Physical Review Letters*,**43** (1979) 267.

[10] A.S. Johnson, D.R. Austin, D.A. Wood, C. Brahms, A. Gregory, K.B. Holzner, S. Jarosch, E.W. Larsen, S. Parker, C.S. Strüber, others, High-flux soft x-ray harmonic generation from ionization-shaped few-cycle laser pulses, *Science Advances* ,**4** (2018) 3761.

[11] G. Lambert, J. Gautier, C. Hauri, P. Zeitoun, C. Valentin, T. Marchenko, F. Tissandier, J.P. Goddet, M. Ribière, G. Rey, others, An optimized kHz two-colour high harmonic source for seeding free-electron lasers and plasma-based soft x-ray lasers, *New Journal of Physics* ,**11** (2009) 083033.

[12] Y.-H. Chuang, L. Zheng, D. Meyerhofer, Propagation of light pulses in a chirped-pulse-amplification laser, *IEEE Journal of Quantum Electronics* ,**29** (1993) 270.

[13] X. Lavocat-Dubuis, F. Vidal, J.-P. Matte, C. Popovici, T. Ozaki, J.-C. Kieffer, Effects of chirp and pulse shape on high harmonic generation and absorption in overdense plasmas, *Laser and Particle Beams,* **29** (2011) 95.

[14] C. Thaury, F. Quéré, High-order harmonic and attosecond pulse generation on plasma mirrors: basic mechanisms, Journal of Physics B: Atomic, Molecular and *Optical Physics*, **43** (2010) 213001.

[15] P.A. Franken, A.E. Hill, C.W. Peters, G. Weinreich, Generation of Optical Harmonics, *Phys. Rev. Lett.* **7** (1961) 118.

[16] J.K. Ll.D, XL. A new relation between electricity and light: Dielectrified media birefringent, *Philosophical Magazine Series*, **1** 50 (1875) 337.

[17] J.F. WARD, Calculation of Nonlinear Optical Susceptibilities Using Diagrammatic Perturbation Theory, *Rev. Mod. Phys,* **37** (1965) 18.

[18] K.W. Robinson, Radiation Effects in Circular Electron Accelerators, *Phys. Rev*, **111** (1958) 373.

[19] N.G. Basov, V.Y. Bychenkov, O.N. Krokhin, M. Osipov, A.A. Rupasov, V.P. Silin, G.V. Sklizkov, A.N. Starodub, V.T. Tikhonchuk, A.S. Shikanov, Second harmonic generation in a laser plasma, *Soviet Journal of Quantum Electronics,* **9** (1979) 1081.

[20] D. Subbarao, M. Sodha, Theory of paraxial self-focusing, *Journal of Applied Physics*, **50** (1979) 4604.

[21] R. Sharma, Generation of a second harmonic electrostatic pulse by an EM pulse and third harmonic generation in a plasma, *Proc. Indian Natl. Sci. Acad., Part A;(India)* **47** (1981) 448.

[18] T. Heinz, M. Loy, Optical second-harmonic generation from semiconductor surfaces, *Advances in Laser Science III, Edited by AC Tam, JL Cole and WC Stwalley (American Institute of Physics, New York*, **19** (1988) 452 .

[23] E. Esarey, A. Ting, P. Sprangle, D. Umstadter, X. Liu, Nonlinear analysis of relativistic harmonic generation by intense lasers in plasmas, *IEEE Transactions on Plasma Science*, **21** (1993) 95.

[24] A. Birulin, V. Platonenko, V. Strelkov, High-harmonic generation in interfering waves, *Journal of Experimental and Theoretical Physics*, **83** (1996) 33.

[25] V. Malka, A. Modena, Z. Najmudin, A. Dangor, C. Clayton, K. Marsh, C. Joshi, C. Danson, D. Neely, F. Walsh, Second harmonic generation and its interaction with relativistic plasma waves driven by forward Raman instability in underdense plasmas, *Physics of Plasmas,* **4** (1997) 1127.

[26] K. Ramachandran, Second harmonic stimulated Raman scattering of laser radiation in a plasma, *IEEE Transactions on Plasma Science*, **24** (1996) 487.

[27] H. Brandi, P. Maia Neto, Third-harmonic generation via laser-plasma interaction: Beyond the low-density approximation, *Journal of Modern Optics*, **45** (1998) 573.

[28] J. Parashar, A. Sharma, Second-harmonic generation by an obliquely incident laser on a vacuum-plasma interface, *Europhysics Letters*, **41** (1998) 389.

[29] H.-C. Kim, Y.H. Lee, Hermite–Gaussian and Laguerre–Gaussian beams beyond the paraxial approximation, *Optics Communications*, **169** (1999) 9.

[30] M. Singh, A.P. Jain, J. Parashar, Phase-matched relativistic second harmonic generation in a plasma., *Journal of the Indian Institute of Science*, **82** (2002) 183.

[31] S. Banerjee, A. Valenzuela, R. Shah, A. Maksimchuk, D. Umstadter, High harmonic generation in relativistic laser–plasma interaction, *Physics of Plasmas* ,**9** (2002) 2393.

[32] A. Sharma, others, Resonant second-harmonic generation of a short pulse laser in a plasma channel, *Journal of Physics D: Applied Physics*, **37** (2004) 2395.

[33] A. Upadhyay, V. Tripathi, Second harmonic generation in a laser channel, *Journal of Plasma Physics* ,**71** (2005) 359.

[34] A. Sandhu, G. Kumar, S. Sengupta, A. Das, P. Kaw, Laser-Pulse-Induced Second-Harmonic and Hard X-Ray Emission Role of Plasma-Wave Breaking, *Physical Review Letters*, **95** (2005) 025005.

[35] S. Carrasco, B.E. Saleh, M.C. Teich, J.T. Fourkas, Second-and third-harmonic generation with vector Gaussian beams, *Journal of the Optical Society of America B* ,**23** (2006) 2134.

[36] D. Dahiya, V. Sajal, A. Sharma, Phase-matched second-and third-harmonic generation in plasmas with density ripple, *Physics of Plasmas*, **14** (2007) 123104.

[37] D.N. Gupta, M.S. Hur, I. Hwang, H. Suk, A.K. Sharma, Plasma density ramp for relativistic self-focusing of an intense laser, *JOSA B* ,**24** (2007) 1155.

[38] P. Jha, R.K. Mishra, G. Raj, A.K. Upadhyay, Second harmonic generation in laser magnetized–plasma interaction, *Physics of Plasmas* ,**14** (2007) 053107.

[39] S. Kaur, A. Sharma, Resonant third harmonic generation in a laser produced thin foil plasma, *Physics of Plasmas* ,**15** (2008) 102705.

[40] U. Verma, A. Sharma, Laser second harmonic generation in a rippled density plasma in the presence of azimuthal magnetic field, *Laser and Particle Beams* ,**27** (2009) 719.

[41] J. Rajput, N. Kant, H. Singh, V. Nanda, Resonant third harmonic generation of a short pulse laser in plasma by applying a wiggler magnetic field, *Optics Communications*, **282** (2009) 4614.

[42] J. Parashar, Resonant second harmonic generation in a plasma filled parallel plane waveguide, *Indian journal of Pure and applied Physics*, **47** (2009) 103.

[43] S. Patil, S. Navare, M. Takale, M. Dongare, Self-focusing of cosh-Gaussian laser beams in a parabolic medium with linear absorption, *Optics and Lasers in Engineering* ,**47** (2009) 604.

[44] S. Kaur, S. Yadav, A. Sharma, Effect of self-focusing on resonant third harmonic generation of laser in a rippled density plasma, *Physics of Plasmas* ,**17** (2010) 053101.

[45] H.R. ASKARI, M. NOROOZI, Effect of a wiggler magnetic field and the ponderomotive force on the second harmonic generation in laser-plasma interactions, *Turkish Journal of Physics* ,**33** (2009) 299.

[46] N. Kant, D.N. Gupta, H. Suk, Generation of second-harmonic radiations of a self-focusing laser from a plasma with density-transition, *Physics Letters A*, **375** (2011) 3134.

[47] N. Kant, M.A. Wani, A. Kumar, Self-focusing of Hermite–Gaussian laser beams in plasma under plasma density ramp, *Optics Communications,* **285** (2012) 4483.

[48] V. Nanda, N. Kant, M.A. Wani, Self-focusing of a Hermite-cosh Gaussian laser beam in a magnetoplasma with ramp density profile, *Physics of Plasmas*, **20** (2013) 113109.

[49] P. Sharma, R. Sharma, Study of second harmonic generation by high power laser beam in magneto plasma, *Physics of Plasmas* ,**19** (2012) 12.

[50] H. Sharma, H. Jaloree, J. Parashar, Magnetic wiggler-assisted third-harmonic generation of a Gaussian laser pulse in plasma, *Turkish Journal of Physics,* **37** (2013) 368.

[51] A. Mihailescu, V. Stancalie, V. Pais, High harmonics generation at the interaction of an intense fs laser pulse with an overdense plasma layer, in: *Journal of Physics: Conference Series, IOP Publishing,***508** (2014) 012019.

[52] P. Jha, H. Hemlata, R.K. Mishra, Evolution of chirped laser pulses in a magnetized plasma channel, *Physics of Plasmas,* **21** (2014) 123106.

[53] B.-Q. Chen, M.-L. Ren, R.-J. Liu, C. Zhang, Y. Sheng, B.-Q. Ma, Z.-Y. Li, Simultaneous broadband generation of second and third harmonics from chirped nonlinear photonic crystals, *Light: Science & Applications*, **3** (2014) 189.

[54] V. Thakur, N. Kant, Effect of pulse slippage on density transition-based resonant third-harmonic generation of short-pulse laser in plasma, *Frontiers of Physics,* **11** (2016) 1.

[55] M. Aggarwal, S. Vij, N. Kant, Wiggler magnetic field assisted second harmonic generation in clusters, *The European Physical Journal D,* **69** (2015) 1.

[56] M. Singh, D.N. Gupta, Relativistic third-harmonic generation of a laser in a self-sustained magnetized plasma channel, *IEEE Journal of Quantum Electronics,* **50** (2014) 491.

[57] A. Singh, N. Gupta, Second-harmonic generation by relativistic self-focusing of cosh-Gaussian laser beam in underdense plasma, *Laser and Particle Beams,* **34** (2016) 1.

[58] N. Gupta, N. Singh, A. Singh, Second harmonic generation of q-Gaussian laser beam in preformed collisional plasma channel with nonlinear absorption, *Physics of Plasmas*, **22** (2015) 113106.

[59] N.S. Rathore, P. Kumar, Phase matched third harmonic generation of a Gaussian Laser pulse in high-density quantum plasma, *American Journal of Modern Physics*, **5** (2016) 154.

[60] G. Purohit, P. Rawat, R. Gauniyal, Second harmonic generation by self-focusing of intense hollow Gaussian laser beam in collisionless plasma, P*hysics of Plasmas*, **23** (2016) 013103.

[61] R.A. Ganeev, Frequency Conversion of Ultrashort Pulses in Extended Laser-Produced Plasmas, *Springer Singapore* ,**89** (2016) 51.

[62] S. Vij, N. Kant, M. Aggarwal, Resonant third harmonic generation in clusters with density ripple: effect of pulse slippage, *Laser and Particle Beams,* **34** (2016) 171.

[63] N. Kant, V. Thakur, Second harmonic generation by a chirped laser pulse in magnetized-plasma, *Optik* ,**127** (2016) 4167.

[64] P. Kumar, S. Singh, A.K. Singh, Harmonic generation in magnetized quantum plasma, in: *AIP Conference Proceedings, AIP Publishing*,**1728** (2016) 020173.

[65] A. Leblanc, S. Monchocé, H. Vincenti, S. Kahaly, J.-L. Vay, F. Quéré, Spatial properties of high-order harmonic beams from plasma mirrors: a ptychographic study, *Physical Review Letters*, **119** (2017) 155001.

[66] M. Abedi-Varaki, S. Jafari, Second-harmonic generation of a linearly polarized laser pulse propagating through magnetized plasma in the presence of a planar magnetostatic wiggler, *The European Physical Journal Plus*, **133** (2018) 1.

[67] P. Sharma, P. Jha, Second harmonic generation by circularly polarized laser beam propagating in obliquely magnetized plasma, *The European Physical Journal D*, **73** (2019) 1.

[68] S. Maity, D. Mandal, A. Vashistha, L.P. Goswami, A. Das, Harmonic generation in the interaction of laser with a magnetized overdense plasma, *Journal of Plasma Physics*, **87** (2021) 905870509.

[69] C. Yang, C. Zhou, Y. Zheng, D. Zhang, J. Gao, Y. Bai, R. Qi, J. Qian, J. Gui, Z. Zhang, others, Divergence of High-Order Harmonic Generation by a Convex Plasma Surface, *Applied Sciences,* **12** (2022) 5745.

[70] K. Walia, K. Singh, D. Tripathi, Second harmonic generation of high power Cosh-Gaussian beam in cold collisionless plasma, *Communications in Theoretical Physics*, **74** (2022) 105502.

[71] J. Mathijssen, Z. Mazzotta, A.M. Heinzerling, K.S.E. Eikema, S. Witte, Material-specific high-order harmonic generation in laser-produced plasmas for varying plasma dynamics, *Applied Physics B* ,**129** (2023) 11.

[72] S.Y. Fu, K.J.G. Francis, M.L.P. Chong, E. Yiwen, X.-C. Zhang, Enhanced second harmonic generation in laser-induced air plasma, *Optics Letters,* **48** (2023) 3199.

[73] S. Antipov, I. Agapov, R. Brinkmann, Á. Ferran Pousa, A. Martinez de la Ossa, E.A. Schneidmiller, M. Thévenet, Coherent high-harmonic generation with laser-plasma beams, *Physical Review Accelerators and Beams,* **27** (2024) 100704.

[74] A. Mitrofanov, M. Rozhko, M. Nazarov, N. Yakushkin, Y.O. Romanovskii, A. Voronin, A. Fedotov, D. Sidorov-Biryukov, Generation and Registration of High Harmonics at Surface Plasma in Coherent Wake Emission and Relativistic Oscillating Mirror Modes by High-Power Laser Pulses, *Moscow University Physics Bulletin* **79** (2024) 353.

[75] K. Singh, K. Walia, Second Harmonic Generation of High Power Cosh-Gaussian Beam in Thermal Quantum Plasma: Effect of Relativistic and Ponderomotive Nonlinearity, *Journal of Contemporary Physics (Armenian Academy of Sciences),* **59** (2024) 244.

[76] S. Hazanov, A. Gorlach, R. Ruimy, D. Yakushevskiy, M. Even Tzur, M.F. Ciappina, I. Kaminer, High Interharmonic Generation from Isolated Bound States, *ACS Photonics* ,**12** (2025) 2440.

Chapter -2

Method and Materials

2.1 Governing Equations and Techniques

In our work we have used following equations,

$$\vec{\nabla}.\vec{B} = 0 \tag{2.1}$$

$$\vec{\nabla}.\vec{D} = 4\pi\rho \tag{2.2}$$

$$\vec{\nabla} \times \vec{E} = -\frac{1}{c}\frac{\partial \vec{B}}{\partial t} \tag{2.3}$$

$$\vec{\nabla} \times \vec{H} = \frac{4\pi}{c}\vec{J} + \frac{1}{c}\frac{\partial \vec{D}}{\partial t} \tag{2.4}$$

$\vec{D} = \in_0 \vec{E} + 4\pi \vec{P}$ and $\vec{B} = \mu_0 \vec{H} + 4\pi \vec{M}$

In this context vectors $\vec{E}$ and $\vec{H}$ denote electromagnetic filed components of electromagnetic radiation. The polarization vector $\vec{P}$ and the magnetization vector $\vec{M}$ characterize the electric dipole moment and magnetic moment per unit volume, respectively arising due to the displacement and orientation of bound electrons in neutral atoms and molecules. Additionally, ρ and $\vec{J}$ refer to the charge density and current density parameters of free charges, which are linked through the continuity equation as under

$$\frac{\partial \rho}{\partial t} + \vec{\nabla}.\vec{D} = 0 \tag{2.5}$$

When plasma is fully ionized $\vec{P} = \vec{M} = 0$

By employing the governing relation ensuring local conservation of density, one can derive the expressions for the nonlinear current density .This relationship connects the time-varying charge density to the divergence of current density, enabling the formulation of nonlinear source terms responsible for harmonic generation in a plasma or nonlinear medium. To derive the wave equation that governs electromagnetic wave propagation in plasmas, one begins by taking the curl of Maxwell's third equation. By subsequently applying Maxwell's fourth equation, the resulting expression can be formulated as.

$$\nabla^2 \vec{E}_2 = \frac{4\pi}{c^2}\frac{\partial \vec{J}_2}{\partial t} + \frac{1}{c^2}\frac{\partial^2 \vec{E}_2}{\partial t^2} \tag{2.6}$$

When we consider plasma the above equation can be written as

$$\nabla^2 \vec{E}_2 - \frac{\epsilon}{c^2}\frac{\partial^2 \vec{E}}{\partial t^2} = \frac{\omega_p^2}{c^2}\vec{E} \tag{2.7}$$

2.2 Physical relevance of some important laser beams related to our study

2.2.1 q-Gaussian

The q-Gaussian beam represents a flexible adaptation of the traditional Gaussian beam, where the parameter q determines the extent to which its intensity profile diverges from the classical Gaussian shape. By tuning q, the beam's spatial characteristics can be tailored, enabling controlled deviations from the symmetric, bell-shaped distribution typical of standard Gaussian beams. The beam profile is represented by:

$$I(r) = I_0 \left[1 - (1-q)\frac{r^2}{\omega_0^2}\right]^{\frac{1}{1-q}}$$

- $I(r)$: Laser beams intensity at a radial distance r from the center of the beam (i.e., off-axis intensity).
- I_0: Maximum intensity at the centre $(r = 0)$.
- q: being the parameter, which controls the shape of the beam
  When $q \to 1$, the beam becomes a standard Gaussian.
  When $q < 1$,the profile becomes more super-Gaussian or flat-topped.
  When $q > 1$,the profile becomes more peaked or long tailed
- r: radial distance from beam axis.

- ω_0: The beam waist radius, which defines the distance from the axis where the intensity significantly drops. For Gaussian beams, it's the radius at which the intensity falls to $1/e^2$ of I_0.

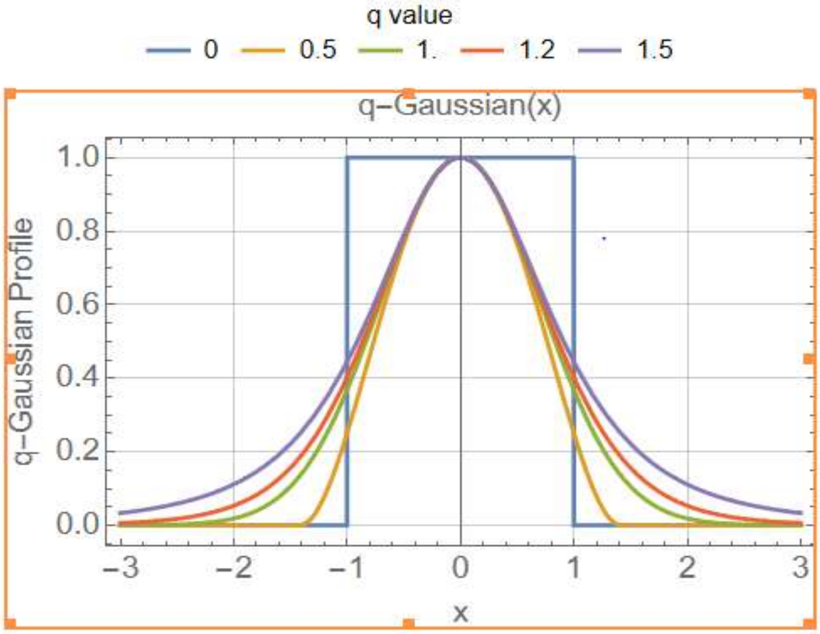

Fig. 2.1 Dependence of the q-Gaussian profile shape on the parameter q, illustrating the transition from a rectangular ($q = 0$) to a standard Gaussian ($q = 1$), and broader-tailed distributions for $q > 1$.

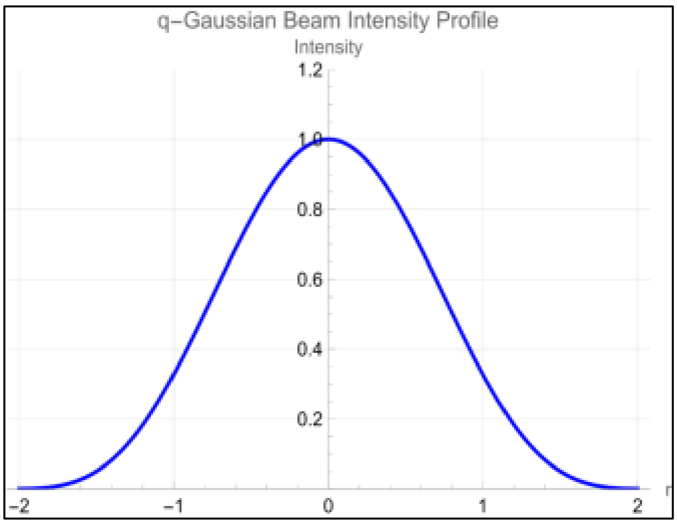

Fig. 2.2 Intensity profile of a q- Gaussian laser beam

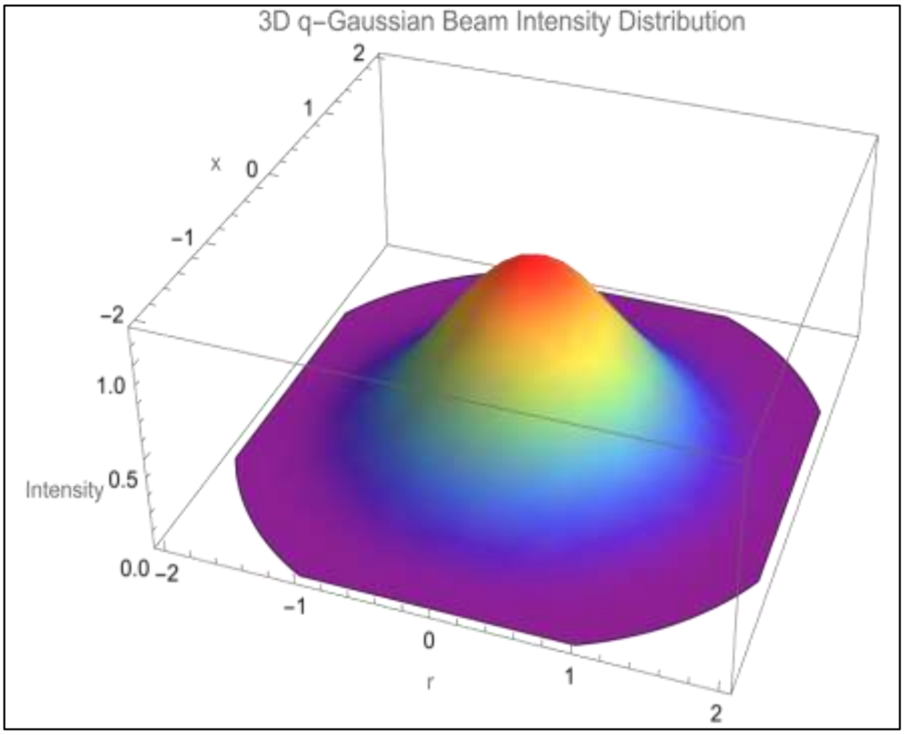

Fig. 2.3 Intensity profile of a q Gaussian laser beam in 3 -D

Where I_0 the peak intensity is r is radial coordinate, ω_0 is beam waist, q is the shape parameter. It has been investigated and recommended therein to duplicate the behaviour using a q-Gaussian distribution function. The use of a non-paraxial theory takes nonlinearity into account by accounting for the relativistic reduction in plasma frequency. Using the WKB and paraxial approximations, equations governing normalised amplitude evolution were derived and solved numerically. Key findings reveal that adjusting the laser intensity parameter, q-values, and plasma density ramp significantly influences the beam’s self-focusing dynamics. Specifically, higher laser intensities enhance self-focusing, while optimized density ramps enable efficient focusing of beams with lower q-values.

Comparisons between q-Gaussian and conventional Gaussian beams highlight distinct advantages of the former. Numerical simulations demonstrate that q-Gaussian beams exhibit stronger self-focusing in plasmas, leading to extended interaction lengths. This prolonged confinement enhances the generation of large-amplitude plasma waves, critical for applications such as electron acceleration. The non-Gaussian intensity profile of q-beams redistributes plasma density more effectively, creating favourable conditions for sustained self-focusing. The study concludes that tailoring q-parameters, intensity, and density gradients offers precise control over laser-plasma interactions, paving the way for optimized particle acceleration and wave-driven phenomena.

2.2.2 cosh-Gaussian (chG)

Under suitable conditions, the chG beam profile closely resembles flat-top field distributions. When two coherent decentred Gaussian beams of equal waist width are superimposed, we get the chG beam, which has centres at $\left(\frac{b}{2},0\right)$ and $\left(-\frac{b}{2},0\right)$. Cosh-Gaussian laser beams electric field is given by

$$\vec{E}_1 = \hat{x}A(z)\exp[-i(\omega_1 t - k_1 z)].$$

$$A(z) = A_0(z,r)\exp[-iks(r,z)].$$

$$A_{0p}^2 = \frac{E_0^2}{f^2(z)}\mathrm{Exp}\left[\frac{b^2}{2}\right]\left\{\begin{array}{l}\mathrm{Exp}\left[-2\left(\frac{r}{r_0 f(z)}+\frac{b}{2}\right)^2\right]+\mathrm{Exp}\left[-2\left(\frac{r}{r_0 f(z)}-\frac{b}{2}\right)^2\right]\\ +2\mathrm{Exp}\left[-\left(\frac{2r^2}{r_0^2 f^2(z)}+\frac{b^2}{2}\right)\right]\end{array}\right\}.$$

$$\vec{E}_1 = \hat{x}\frac{E_0}{f(z)}\mathrm{Exp}\left[\frac{b^2}{4}\right]\left\{\begin{array}{l}\mathrm{Exp}\left[-2\left(\frac{r}{r_0 f(z)}+\frac{b}{2}\right)^2\right]+\mathrm{Exp}\left[-2\left(\frac{r}{r_0 f(z)}-\frac{b}{2}\right)^2\right]\\ +2\mathrm{Exp}\left[-\left(\frac{2r^2}{r_0^2 f^2(z)}+\frac{b^2}{2}\right)\right]\end{array}\right\}^{1/2}\exp^{[-ikS(r,z)](z)\exp[-i(\omega_1 t-k_1 z)].}$$

- $\vec{E}$: Field vector representing the beam's electric component
- $\hat{x}$: Polarization direction (beam is linearly polarized along x-axis).
- E_0: Field amplitude.

- $f(z)$: Beam evolution function along the propagation direction (often includes diffraction effects; e.g., $f(z) = \sqrt{1 + \left(\frac{z}{z_R}\right)^2}$
- b: Beam shaping parameter that controls the "cosh" component spread.
- r: Radial distance from the beam axis.
- r_0: Beam waist (spot size at the focus).
- $S(r, z)$: Eikonal or phase function (includes diffraction phase, Gouy phase, etc.).
- ω_1: Angular frequency of the fundamental wave.
- k_1: Wave number corresponding to ω_1, typically $k_1 = \omega_1/c$.
- k: Generic wave number used in phase function.
- $\exp[-i(\omega_1 t - k_1 z)]$: Plane wave factor representing temporal and spatial oscillations.
- $\exp[-iks(r, z)]$: Additional phase contribution from beam curvature or nonlinear phase.

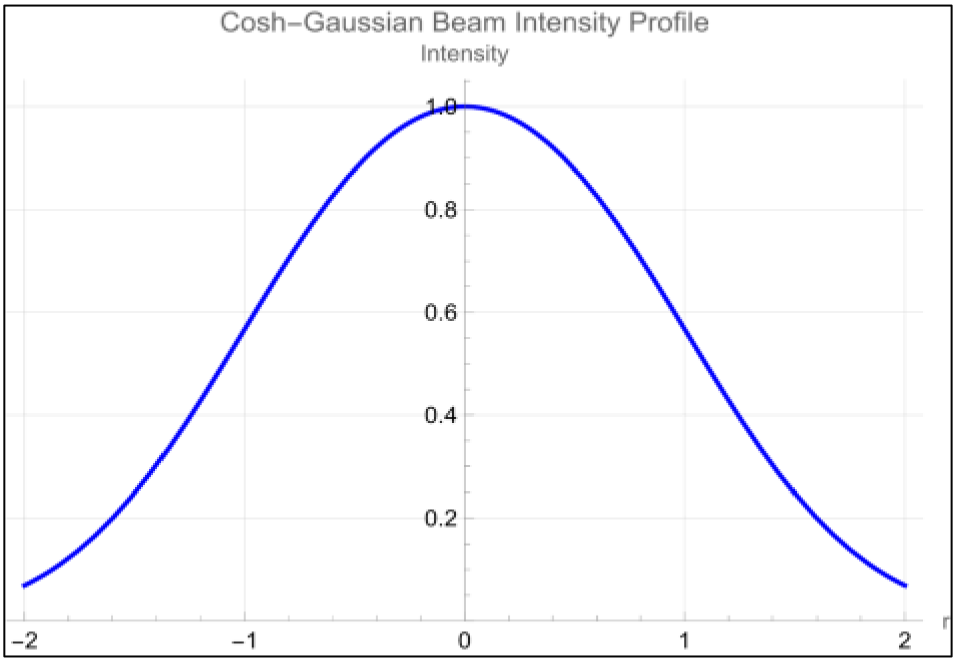

Fig. (2.4) Intensity distribution of a Cosh-Gaussian beam

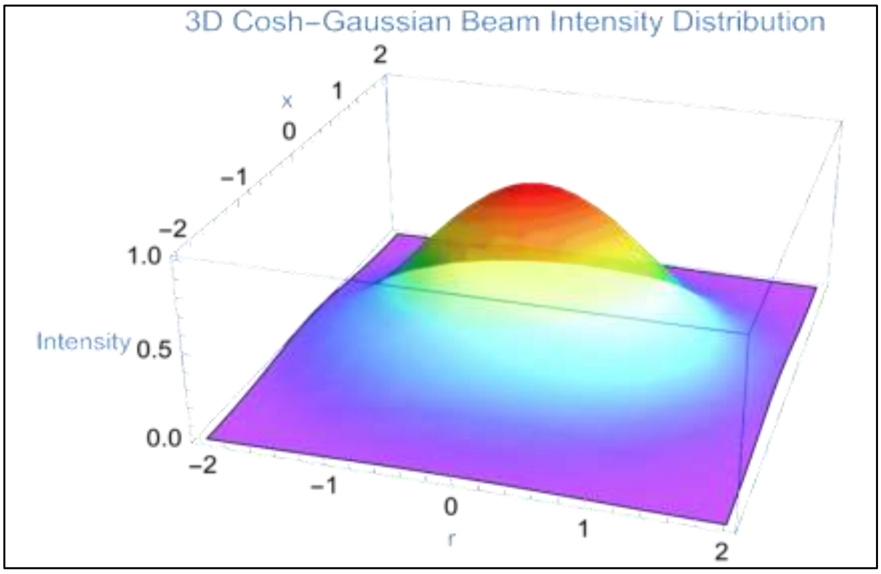

Fig. (2.5) Cosh-Gaussian beam intensity distribution in 3 –D

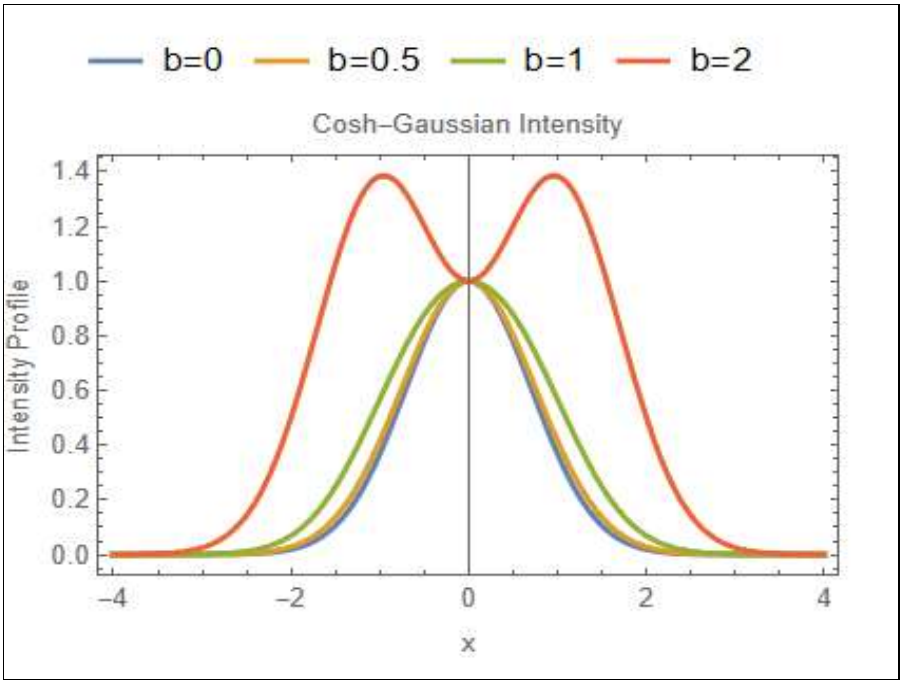

Fig (2.6) Intensity profiles of the cosh-Gaussian beam for different values of the parameter b. The curves demonstrate the transition from a standard Gaussian ($b = 0$) to broadened, double-peaked profiles as b increases.

2.2.3 Hermite-cosh-Gaussian (HchG)

The solution of Helmholtz equations with paraxial approximations yields Hermite-Gaussian beams. The field is expressed in the rectangular coordinate system for these beams. This is the generalized form of the complex argument's Hermite-Gaussian and sinusoidal functions. The Gaussian field can be written as a multiple of Hermite polynomial, sinusoidal, and Gaussian complex argument functions.

When distributed at $z = 0$, Hermite-sinusoidal Gaussian beams are known as Hermite-cosh-Gaussian (HchG) laser beams.

$$E_3 = A_3 e^{i(\omega t - kz)}$$

$$A_3 = A_{30}(r, z) e^{-ikS_{(r,z)}}$$

$$E_3 = A_{30}^2 = \frac{E_{30}^2}{f^2(z)}\left[H_m\left(\frac{\sqrt{2}r}{r_0 f(z)}\right)\right] e^{\left(\frac{b^2}{4}\right)}\left\{\exp\left[-2\left(\frac{r}{r_0 f(z)}+\frac{b}{2}\right)^2\right]\right]^{1/2}$$

$$+\exp-2\left(\frac{r}{r_0 f(z)}-\frac{b}{2}\right)^2\Bigg]\Bigg\}$$

$$+2\exp\left[-\left(\frac{2r^2}{r_0^2 f(z)^2}+\frac{b^2}{2}\right)\right] e^{-ikS(r,z)} e^{i(\omega t-kz)}$$

The mode index associated with the Hermite polynomial function is denoted by m. Accordingly we developed the formulas for the beam width parameter and the normalised amplitude of SHG and THG for various laser profiles using the paraxial approximation and the aforementioned laser profiles. Mathematica software has been utilised to solve these expressions numerically. ORIGIN software has been used to plot graphs in order to analyse the results.

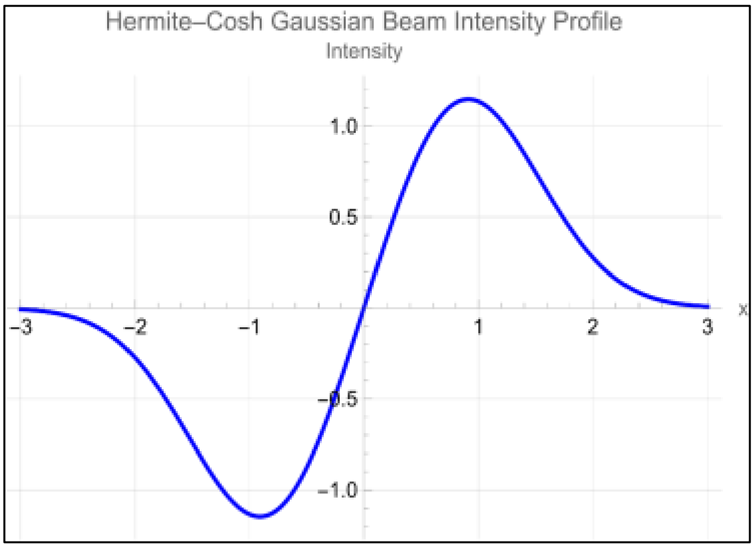

Fig. (2.7) Intensity contour arising from a Hermite–Cosh Gaussian beam structure.

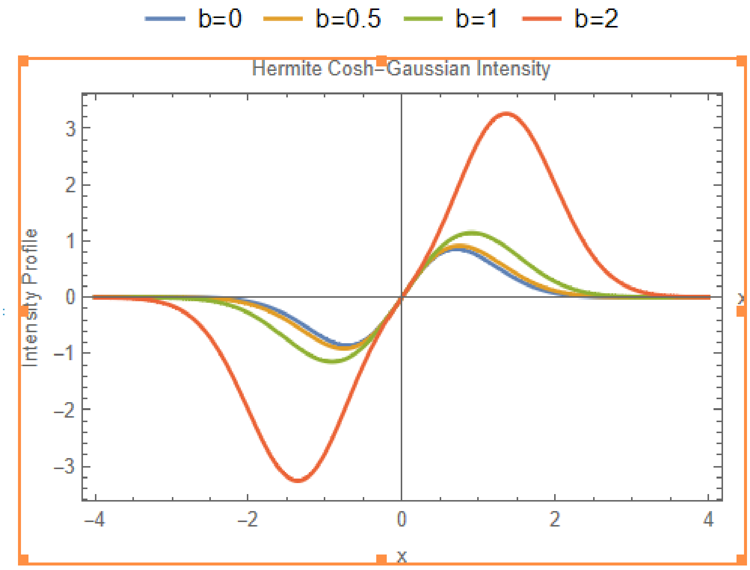

Fig (2.8) Intensity profiles of the Hermite cosh-Gaussian beam for various values of the parameter bb. The plot illustrates how increasing bb modifies the beam's asymmetry and peak structure.

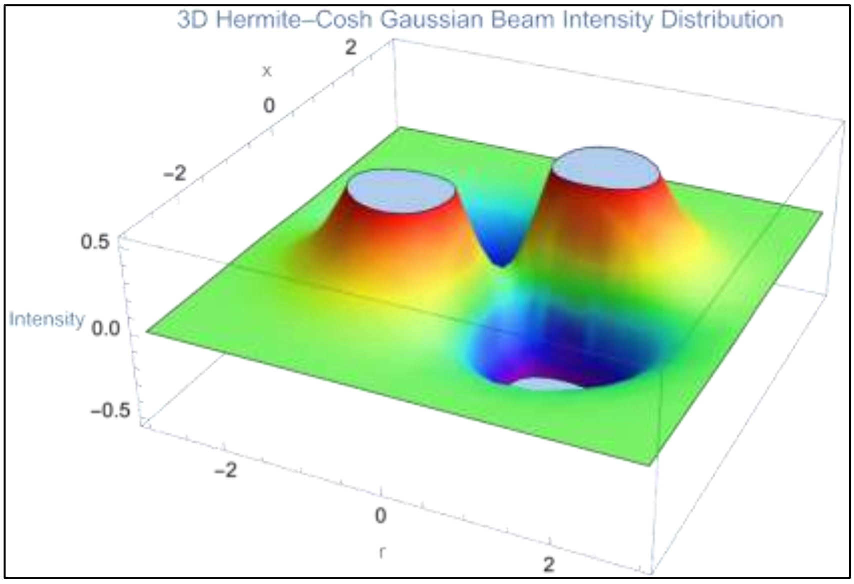

Fig. (2.9) Hermite–Cosh Gaussian beam intensity distribution in 3-D

Methodology used

The present work adopts a rigorous theoretical and computational methodology to analyze nonlinear laser–plasma interactions and associated harmonic generation processes. The formulation is based on the paraxial approximation combined with the Wentzel–Kramers–Brillouin (WKB) approximation, which are well-established and widely used in modeling the propagation of high-intensity laser beams in plasma under slowly varying envelope conditions. These approximations allow systematic derivation of the governing wave equations while retaining the essential physics of diffraction, nonlinear coupling, and plasma response.

Using this framework, the nonlinear current densities and evolution equations for second and third harmonic fields are derived for different structured laser beam profiles. The resulting coupled equations are then solved numerically using Mathematica over a physically relevant range of laser and plasma parameters to examine the influence of beam shaping, external magnetic fields, and plasma nonlinearity. The numerical outcomes are subsequently represented through graphical plots generated using Origin software, enabling clear visualization and comparative analysis of parameter-dependent trends. This integrated analytical–numerical approach ensures consistency, reliability, and clarity in interpreting the nonlinear dynamics investigated in the thesis.

Chapter- 3

Magnetically Enhanced Third Harmonic Generation using q-Gaussian Laser Beam in Plasma

3.1 Introduction

In recent years, a captivating and dynamic field of research has blossomed at the confluence of laser technology and plasma physics, driven by the development of short-pulse lasers. This enthralling interplay between laser beams and plasma has garnered significant attention as non-linearity has come to existence due to its remarkable versatility and profound potential applications. Within this vibrant landscape, we bear witness to remarkable milestones, encompassing particle acceleration through laser-driven plasmas [1–3], creation of laser plasma channels [4–7], production of super-continuum light [8,9], advancements in inertial confinement fusion [10–12], generation of higher harmonic frequencies [13–16], probing into nonlinear effects [17,18] within the extreme ultraviolet spectrum [19], precise performance of photoelectron spectroscopy [20] and the meticulous measurement of high-density materials [21,22].

Plasma electrons are driven by the powerful ponderomotive force of an intense laser into rapid oscillations at relativistic speeds, which result in the generation of high-order harmonics. The third harmonic generation plays a crucial role in the field of laser-plasma interaction. Esarey et al.'s [23] in-depth studies of harmonic generation in plasma under the impact of extraordinarily strong lasers working in a relativistic environment their novel work includes the creation of a nonlinear model using cold fluid assumptions that can accommodate the extremes of high laser intensity. The evaluation of the current-modulated harmonic generation process has been greatly aided by their study. The process known as current-modulated harmonic generation occurs when a current usually an electron current is present in the plasma and influences or modulates the harmonics produced in it as a result of contact with high-intensity lasers.

In a detailed investigation of the generation of second-order resonant harmonics in a plasma channel, Kant et al. [24] used a strong laser pulse their thorough investigation led to a notable improvement in the production of second-order harmonics, highlighting the enormous potential in this field. Surprisingly, their research revealed an intriguing phenomenon plasma electron accelerated into motion at relativistic speeds as the laser beam intensity surpassed a critical threshold. This remarkable discovery underscores the pivotal role of relativistic effects within the realm of laser-plasma interactions. A thorough investigation into the nonlinear optical self-focusing phenomenon in third harmonic-generating lasers operating in a clustered gas environment was carried out by Parashar et al. [25] Their research showed that the focusing of the pump laser, which results in a remarkable tenfold increase in efficiency, is intricately linked to the efficiency of harmonic generation. Simultaneously, Singh et al. [26] thoroughly accounted for relativistic effects while delving into the complex world of third harmonic generation within a laser interacting with a self-sustained magnetised plasma. Their ground breaking research showed that the presence of a self-sustaining magnetised plasma channel significantly increased the yield of the third harmonic generation. Regarding third-harmonic production in electron-hole plasma exposed to a brief pulse laser in the presence of a wiggler magnetic field, Kant et al. [27] made an important discovery according to their conclusions, the phase matching condition was satisfied when a particular wiggler wave number was used. The effectiveness of energy conversion was noticeably improved as a result of their study.

Various methods can be employed to generate harmonics in laser beams within plasmas. These methods encompass leveraging density gradients within the plasma or employing external magnetic fields. Furthermore, optical second and third harmonics can be generated using a planar waveguide. Interestingly this waveguide approach doesn't rely on short-duration pulses or resonant amplification, making it a compelling means to double the frequency of light at lower power levels. A key advantage of utilising a waveguide is its ability to maintain a small mode area over a more extended distance compared to what's achievable in a linear medium, where diffraction limits the interaction length, typically to the Rayleigh length.

A third harmonic pulse emerges as a result of the complex interaction between second harmonic density oscillations brought on by the ponderomotive force and the quiver velocity of electrons at the fundamental frequency. An intense laser beam creates a strong electric field that gives the electrons in the plasma a ponderomotive force as it passes through the plasma medium. An intense laser beam is actually a wave that oscillates as a result it carries a powerful electric field within it. When this laser beam passes through materials, like plasma it induces an oscillating field in its surrounding area. Therefore, when the laser beam travels through the plasma medium it generates a field. Due to the electrons being forced to oscillate at relativistic speeds, a large number of high-order harmonics are generated. There are areas of localised fluctuations in the charge density due to the relativistic oscillation motion of the electrons in the plasma. Moving off from the positively charged ions in the plasma, electrons produce electron-rich regions, which are places with an excess of negative charge, and electron-poor regions, which are areas with a deficiency of electrons. We call these changes in localised charge densities plasma density perturbations. Due to its wide range of uses, the third harmonic among these holds a crucial position in the field of laser-plasma interaction. Using a wiggler magnetic field to help with phase matching conditions, we analyse in depth the effects of plasma density and magnetic field strength on the production of third harmonics in this manuscript. The derived formulas for the beam width parameter and the normalised amplitude of the third harmonic pulse are presented in Section II. In Section III these concepts are elucidated through graphical representations, enhancing their comprehension. Section IV offers a concise summary of the findings as a whole.

3.2 Mathematical Formulation

We will be taking intense q-Gaussian laser beam having electric and magnetic fields given as under

$$\vec{E}_1(r,z,t) = \hat{x}E_{00}\left[1 - \frac{(1-q)r^2}{2r_0^2 f_1^2(\xi)}\right]^{\frac{1}{1-q}} \exp[i(k_1 z - \omega_1 t)] \tag{3.1}$$

$$\vec{B} = \frac{c\vec{k}_1 \times \vec{E}_1}{\omega_1} \qquad 3.1(a)$$

$$\vec{B}_w = \hat{y} B_0 \exp(ik_0 z) \qquad 3.1(b)$$

Where we know that $\hat{x}$ is a unit vector and indicates the direction of the electric field. ω_1 is the fundamental laser frequency, $\vec{k}_1$ is a unit vector, $\vec{B}_w$ is the wiggler magnetic field and k_0 be the wiggler wave number. Amplitude of the fundamental laser pulse is given by $A_1^2 = A_{10}^2 / f_1^2 \exp[-r^2/2{r_0}^2{f_1}^2]$. For q Gaussian the amplitude would be $\mathrm{A}_{10}(r,\xi) = A_{00}\left[1-(1-q)\frac{r^2}{2r_0^2 f_1^2(\xi)}\right]^{\frac{1}{1-q}}$. The wave vector $\overrightarrow{k}$ experiences a proportional growth alongside with frequency ω so $\vec{k}_3 > 3\vec{k}_1$ .The magnetic wiggler can give the third harmonic photon the difference in momentum.

Now the laser will impart an oscillatory velocity on the electrons which is given by

$$\vec{v}_1 = e\frac{\vec{E}_1}{mi(\omega_1 + iv)} \qquad (3.2)$$

The third harmonic current density J_3 is created by the density inhomogeneity beating with v, causing resonant third harmonic creation. Linear current density $\vec{J}_3^L$ and non-linear current density $\vec{J}_3^{NL}$ [28] are as under.

$$\vec{J}_3^L = \frac{n_0 e^2 \vec{E}_3}{m3i\omega_1} \qquad (3.3)$$

$$\vec{J}_3^{NL} = \frac{-n_0^0 e^5 B_w (\overrightarrow{E_1^{(q)}})^3\, k_1}{16cim^4\omega_1^4(\omega_1+iv)}\left[\frac{5k_1}{18\omega_1} + \frac{k_1+K_0}{\omega_1+iv}\right]\hat{x} \qquad (3.4)$$

$$A_3' = A_{30}'(z)\psi_3 \text{ Where } \psi_3 = \exp\left[\left[1-\frac{(1-q)r^2}{2r_0^2 f_1^2}\right]^{\frac{3}{1-q}}\right]\exp(-3ik_1S_1) \qquad (3.5)$$

$$A_3' = A_{30}'(z)\exp\left[\left[1-\frac{(1-q)r^2}{2r_0^2 f_1^2}\right]^{\frac{3}{1-q}}\right]\exp(-3ik_1S_1), \qquad (3.6)$$

$$\frac{\partial \vec{E}_3}{\partial z} = \hat{x}\exp[-i\{3\omega_1 t - (3k_1 + k_0)z\}]\frac{\partial A_3'}{\partial z} + A_3'\hat{x}\exp[-i\{3\omega_1 t - (3k_1 + k_0)z\}]\{i(3k_1 + k_0)\}, \tag{3.7}$$

$$\frac{\partial^2 \vec{E}_3}{\partial z^2} = \hat{x}\exp[-i\{3\omega_1 t - (3k_1 + k_0)z\}]\frac{\partial^2 A_3'}{\partial z^2} + \hat{x}\exp[-i\{3\omega_1 t - (3k_1 + k_0)z\}]\{i(3k_1 + k_0)\}\frac{\partial A_3'}{\partial z} + \exp\left[-i\{3\omega_1 t - (3k_1 + k_0)z\}\{i(3k_1 + k_0)\}\frac{\partial A_3'}{\partial z} + A_3'\exp[-i\{3\omega_1 t - (3k_1 + k_0)z\}]\{i(3k_1 + k_0)\}^2 \tag{3.8}$$

$\partial^2 A_3' / \partial z^2$ being small gets neglected

$$\frac{\partial^2 \vec{E}_3}{\partial z^2} = 2\hat{x}\exp\left[-i\{3\omega_1 t - (3k_1 + k_0)z\}\{i(3k_1 + k_0)\}\frac{\partial A_3'^{(q)}}{\partial z} + A_3'\hat{x}\exp[-i\{3\omega_1 t - (3k_1 + k_0)z\}]\{i(3k_1 + k_0)\}^2, \tag{3.9}$$

$$\frac{\partial A_3'}{\partial z} = \frac{A_3'}{A_{30}'}\frac{\partial A_{30}'}{\partial z} + A_3'(z)(-3ik_1)\frac{\partial S_1}{\partial z} + A_3'\left[\left[1 - \frac{(1-q)r^2}{2r_0^2 f_1^2}\right]^{\frac{3}{1-q}}\right]\frac{\partial f_1}{\partial z}, \tag{3.10}$$

$$\frac{\partial A_3'}{\partial z} = \exp\left[\frac{-3r^2}{2r_0^2 f_1^2}\right]\exp(-3ik_1 S_1)\frac{\partial A_{30}'}{\partial z} + A_{30}'(z)(-3ik_1)\exp\left[1 - \frac{(1-q)r^2}{2r_0^2 f_1^2}\right]^{\frac{3}{1-q}}\exp(-3ik_1)\frac{\partial S_1}{\partial z} + A_{30}'\left[1 - \frac{(1-q)r^2}{2r_0^2 f_1^2}\right]^{\frac{3}{1-q}}\exp\left[1 - \frac{(1-q)r^2}{2r_0^2 f_1^2}\right]^{\frac{3}{1-q}}\exp(-3ik_1 S_1)\frac{\partial f_1}{\partial z}, \tag{3.11}$$

The behaviour of the third harmonic field can be characterized using the equation below,

$$\nabla^2 \vec{E}_3 = \frac{4\pi}{c^2}\frac{\partial \vec{J}_3^L}{\partial t} + \frac{4\pi}{c^2}\frac{\partial \vec{J}_3^{NL}}{\partial t} + \frac{1}{c^2}\frac{\partial^2 \vec{E}_3}{\partial t^2}, \tag{3.12}$$

$$\frac{4\pi}{c^2}\vec{J}_3^L = \frac{\omega_p^2}{c^2}\vec{E}_3 \tag{3.13}$$

this equation can be further written as

$$\nabla^2 \vec{E}_3 = \left[\frac{\varepsilon_0+\varphi(E_1 E_1{}^*)}{c^2}\right]\frac{\partial^2 \vec{E}_3}{\partial t^2} + \frac{4\pi}{c^2}\frac{\partial \vec{J}_3^{NL}}{\partial t} + \frac{1}{c^2}\frac{\partial^2 \vec{E}_3}{\partial t^2} \tag{3.14}$$

the mass nonlinearity can be written as

$$\varepsilon_0 + \varphi(E_1 E_1{}^*) \tag{3.15}$$

Where $\varphi(E_1 E_1{}^*) = \varphi\left(\frac{(A_{10}^q)^2}{2f_1^2}\right) - \frac{(A_{10}^q)^2}{2r_0^2 f_1^4}\varphi'\left(\frac{(A_{10}^q)^2}{2f_1^2}\right)$ (3.16)

Also $\varepsilon_0 = 1 - \omega_p^2/\omega_1^2$ and $\varphi = \frac{\omega_p^2}{\omega_1^2}\left[1 - \frac{1}{1+\mathrm{a}^2/2}\right]$, a being laser field parameter is a measure of how strong a laser beam is. It is important because it determines how the laser beam interacts with matter. Plasma frequency is given by $\omega_p = (4\pi n_0 e^2/m)^{1/2}$, n_0 being density of electron e and m are the charge and mass of the electron respectively.

$\varphi'\left(\frac{A_{10}^2}{2f_1^2}\right) = \varepsilon_s \varepsilon_2/\varepsilon_0 exp - \frac{\varepsilon_2 A_{10}^2}{2\varepsilon_0 f_1^2} f_3$ [29].

Now using equations (3.1a), (3.3), (3.5) and (3.6) and applying paraxial approximation we obtained the expression,

$$\frac{\partial^2 f_3}{f_3\, \partial z} = -\frac{9}{2k_3^2 f_3^5 r_0^4} + \frac{1}{k_3^2}\left[\frac{9\omega_1^2}{c^2}\frac{(A_{10}^q)^2}{2r_0^2 f_1^4}\phi\left(\frac{(A_{10}^q)^2}{2f_1^2}\right)\right] = 0 \tag{3.17}$$

Which is the expression for beam width parameter of a q-Gaussian laser.

From the linear part of equation (3.6), the reformed equation comes out to be as follows

$$\nabla^2 \vec{E}_3 + \left[\left(\frac{9\omega_1^2 - 10\omega_p^2}{c^2}\right) + \frac{9\omega_1^2 \varphi\left(\overrightarrow{E_1 E_1}^*\right)}{c^2}\right]\vec{E}_3 = \frac{4\pi}{c^2}\frac{\partial \vec{J}_3^{NL}}{\partial t} \tag{3.18}$$

Now specific solution of equation (3.12) can be written as.

$$\vec{E}_3 = A_3' Exp[-i\{3\omega_1 t - (3k_1 + k_0)z\}] \tag{3.19}$$

$A_3' = A_{30}'(Z)\psi_3$, and $\psi_3 = \exp\left[\left[1-\frac{(1-q)r^2}{2r_0^2f_1^2}\right]^{\frac{3}{1-q}}\right]\exp(-3ik_1S_1)$ where A_3' being third harmonic pulse amplitude and A_{30}' being constant third harmonic pulse amplitude. Using equations (3.10) and (3.12) and multiplying by $r\psi_3^*$ and integrating with respect to 'r'it we got the equation as under.

$$\int \frac{r\psi_3^*\,\partial^2\psi_3}{\partial r^2} = \exp\left[1-\frac{(1-q)r^2}{2r_0^2f_1^2}\right]^{\frac{3}{1-q}} + 3\left[\left[1-\frac{(1-q)r^2}{2r_0^2f_1^2}\right]^{\frac{3}{1-q}}+1\right]\exp\left[1-\frac{(1-q)r^2}{2r_0^2f_1^2}\right]^{\frac{3}{1-q}} + \frac{4(ik_1)(r_0^2f_1^2)}{3}\left(\frac{\partial f_1}{f_3\,\partial z}\right)\left[\left[1-\frac{(1-q)r^2}{2r_0^2f_1^2}\right]^{\frac{3}{1-q}}\right]\exp\left[1-\frac{(1-q)r^2}{2r_0^2f_1^2}\right]^{\frac{3}{1-q}} - 6k_1^2(r_0^2f_1^2)^2\left[\left[1-\frac{(1-q)r^2}{2r_0^2f_1^2}\right]^{\frac{3}{1-q}}+1\right]\exp\left(\left[1-\frac{(1-q)r^2}{2r_0^2f_1^2}\right]^{\frac{3}{1-q}}\right)\left(\frac{\partial f_1}{f_3\,\partial z}\right)^2 \quad (3.20)$$

$$\int \frac{r\psi_3^*\,\partial\psi_3\,\partial r}{r\,\partial r} + \int \frac{r\psi_3^*\,\partial^2\psi_3}{\partial r^2} = \begin{bmatrix} \left[1+ik_1\left(\frac{\partial f_1}{f_{1\,\partial z}}\right)(r_0^2f_1^2)\right] \\ +1+\frac{3}{r_0^2f_1^2}\left[\left[1-\frac{(1-q)r^2}{2r_0^2f_1^2}\right]^{\frac{3}{1-q}}+1\right] \\ +\frac{4(ik_1)(r_0^2f_1^2)}{3}\left(\frac{\partial f_1}{f_3\,\partial z}\right)\left[\frac{3r^2}{r_0^2f_1^2}+1\right] \\ -6k_1^2(r_0^2f_1^2)^2\left[\left[1-\frac{(1-q)r^2}{2r_0^2f_1^2}\right]^{\frac{3}{1-q}}+1\right]\left(\frac{\partial f_1}{f_3\,\partial z}\right)^2 \end{bmatrix}\exp\left[\left[1-\frac{(1-q)r^2}{2r_0^2f_1^2}\right]^{\frac{3}{1-q}}\right], \quad (3.21)$$

$$\int \frac{r\psi_3^*\,\partial\psi_3\,\partial r}{r\,\partial r} = \int \left(\frac{-3r}{r_0^2f_1^2}\right)\exp\left[1-\frac{(1-q)r^2}{2r_0^2f_1^2}\right]^{\frac{3}{1-q}}\Bigg]\partial r - \int (3ik_1)\exp\left[1-\frac{(1-q)r^2}{2r_0^2f_1^2}\right]^{\frac{3}{1-q}}\Bigg]\left(\frac{r\,\partial f}{f\,\partial z}\right)\partial r,$$

$$\int \frac{r\psi_3^* \,\partial\psi_3 \,\partial r}{r\,\partial r} =$$

$$\left(\frac{-3}{r_0^2 f_1^2}\right) \int \ \frac{r\left(r_0^2 f_1^2\right)}{(-3r)} \exp\left[\left[1 - \frac{(1-q)r^2}{2r_0^2 f_1^2}\right]^{\frac{3}{1-q}}\right] \partial x \,(3ik_1) \left(\frac{\partial f}{f\,\partial z}\right) \int \ \left(r \frac{\left(r_0^2 f_1^2\right)}{(-3r)}\right) \exp\left[\left[1 - \frac{(1-q)r^2}{2r_0^2 f_1^2}\right]^{\frac{3}{1-q}}\right] \partial r,$$

$$\int \frac{r\psi_3^* \,\partial\psi_3 \,\partial r}{r\,\partial r} = \exp\left[\left[1 - \frac{(1-q)r^2}{2r_0^2 f_1^2}\right]^{\frac{3}{1-q}}\right] + ik_1 \left(\frac{\partial f}{f\,\partial z}\right) \left(\frac{\left(r_0^2 f_1^2\right)}{f_1}\right) \exp\left[\left[1 - \frac{(1-q)r^2}{2r_0^2 f_1^2}\right]^{\frac{3}{1-q}}\right],$$

$$\int \frac{r\psi_3^* \,\partial\psi_3 \,\partial r}{r\,\partial r} = \exp\left[\left[1 - \frac{(1-q)r^2}{2r_0^2 f_1^2}\right]^{\frac{3}{1-q}}\right] \left[1 + ik_1 \left(\frac{\partial f}{f\,\partial z}\right) \left(\frac{\left(r_0^2 f_1^2\right)}{f_1}\right)\right]. \tag{3.22}$$

Differentiate Eq. (3.19) with respect to ' r ', we obtain

$$\frac{\partial^2\psi_3}{\partial r^2} = -\frac{3}{r_0^2 f_1^2} \exp\left(\left[1 - \frac{(1-q)r^2}{2r_0^2 f_1^2}\right]^{\frac{3}{1-q}}\right) \exp(-3ik_1 S_1) + 9\left(\frac{r}{r_0^2 f_1^2}\right)^2 \exp\left(\left[1 - \frac{(1-q)r^2}{2r_0^2 f_1^2}\right]^{\frac{3}{1-q}}\right) \exp(-3ik_1 S_1) - \frac{3r}{r_0^2 f_1^2}(-3ik_1) \exp\left(\left[1 - \frac{(1-q)r^2}{2r_0^2 f_1^2}\right]^{\frac{3}{1-q}}\right) \exp(-3ik_1 S_1) \frac{\partial S_1}{\partial r} + (-3ik_1)\left(\left[1 - \frac{(1-q)r^2}{2r_0^2 f_1^2}\right]^{\frac{3}{1-q}}\right) \exp\left(\left[1 - \frac{(1-q)r^2}{2r_0^2 f_1^2}\right]^{\frac{3}{1-q}}\right) exp(-3ik_1 S_1) \frac{\partial S_1}{\partial r} + (-3ik_1)^2 \exp\left(\left[1 - \frac{(1-q)r^2}{2r_0^2 f_1^2}\right]^{\frac{3}{1-q}}\right) \exp(-3ik_1 S_1) \left(\frac{\partial S_1}{\partial r}\right)^2 + (-3ik_1) \exp\left(\left[1 - \frac{(1-q)r^2}{2r_0^2 f_1^2}\right]^{\frac{3}{1-q}}\right) \exp(-3ik_1 S_1) \frac{\partial^2 S_1}{\partial r^2},$$

$$\frac{\partial^2\psi_3}{\partial r^2} \quad = \frac{3}{r_0^2 f_1^2} \exp\left(\left[1 - \frac{(1-q)r^2}{2r_0^2 f_1^2}\right]^{\frac{3}{1-q}}\right) \exp(-3ik_1 S_1) + \frac{9r^2}{\left(r_0^2 f_1^2\right)^2} \exp\left(\left[1 - \frac{(1-q)r^2}{2r_0^2 f_1^2}\right]^{\frac{3}{1-q}}\right) \exp(-3ik_1 S_1) + \frac{12ik_1 r}{r_0^2 f_1^2} \exp\left(\left[1 - \frac{(1-q)r^2}{2r_0^2 f_1^2}\right]^{\frac{3}{1-q}}\right) \exp(-2ik_1 S_1) \left(\frac{\partial S_1}{\partial r}\right) -$$

$$9k_1^2 \exp\left(\left[1-\frac{(1-q)r^2}{2r_0^2f_1^2}\right]^{\frac{3}{1-q}}\right)\exp(-3ik_1S_1)\left(\frac{\partial S_1}{\partial r}\right)^2 +$$

$$(-3ik_1)\exp\left(\left[1-\frac{(1-q)r^2}{2r_0^2f_1^2}\right]^{\frac{3}{1-q}}\right)\exp(-3ik_1S_1)\frac{\partial^2 S_1}{\partial r^2} \tag{3.23}$$

On solving further we got

$$-\frac{2}{3}i\frac{\partial A'_{30}}{\partial \xi}+\left\{-\frac{2}{3}\left[\left(\frac{r_0\omega_1}{c}\right)^2-\left(9-\frac{10\omega_p^2}{\omega_1^2}\right)+\left(\frac{r_0\omega_1}{c}\right)^2\phi\left(\frac{\left(A_{10}^{(q)}\right)^2}{2f_1^2}\right)\right]-9\left(\frac{r_0\omega_1}{c}\right)\left(1-\frac{\omega_p^2}{9\omega_1^2}\right)\right\}^2 A'_{30}$$
$$+A'_{30}\left[5+\frac{i}{f_3}\frac{\partial f_1}{\partial \xi}+\frac{4i}{3f_3}\frac{\partial f_1}{\partial \xi}-6f_1^2\left(\frac{1}{f_3}\frac{\partial f_1}{\partial \xi}\right)^2\right]$$
$$=-\frac{1}{16}\left(\frac{\omega_p^2}{\omega_1^2}\right)\left(\frac{eB_w}{cm\omega_1}\right)\left(\frac{eA_{10}^{(q)}}{m\omega_1 c}\right)^2\left(\frac{r_0\omega_1}{c}\right)^2\left(1-\frac{\omega_p^2}{\omega_1^2}\right)^{1/2}$$
$$\times\left[1-(1-q)\frac{r^2}{r_0^2f_1^2}\right]^{\frac{2}{1-q}}\times\left[3\left(1-\frac{\omega_p^2}{9\omega_1^2}\right)^{1/2}-31\left(1-\frac{\omega_p^2}{\omega_1^2}\right)^{1/2}\right]$$

(3.24)

Where $A_{10}^{(q)}(r,\xi)=A_{00}\left[1-(1-q)\frac{r^2}{2r_0^2f_1^2(\xi)}\right]^{\frac{1}{1-q}}$

The parameter q in the above expression governs the shape of the transverse intensity distribution of the laser beam and allows a continuous transition from a standard Gaussian profile to more generalized beam forms.

For $q=1$, the expression reduces to the conventional Gaussian beam, while values $q<1$ produce flattened, super-Gaussian type profiles and $q>1$ lead to more sharply peaked distributions.

Thus, the q-parameter provides an additional degree of freedom to control the spatial localization and effective intensity of the beam, which directly influences nonlinear coupling and harmonic generation efficiency in plasma.

By varying q, the present model enables systematic investigation of how different beam shapes affect self-focusing behaviour and third harmonic yield, thereby generalizing earlier Gaussian-based analyses.

Now substituting the values of $k_1 = \frac{\omega_1}{c}\left(1-\frac{\omega_p^2}{\omega_1^2}\right)^{\frac{1}{2}}$ and $k_0 = \frac{3\omega_1}{c}\left[\left\{\left(1-\frac{\omega_p^2}{9\omega_1^2}\right)^{\frac{1}{2}}\right\}^{\frac{1}{2}} - \left(1-\frac{\omega_p^2}{\omega_1^2}\right)^{\frac{1}{2}}\right]$ so then normalising the equation we got the final equation of third harmonic amplitude of a q-Gaussian laser beam.

$$
\begin{aligned}
&-\frac{2}{3} i \frac{\partial \mathrm{A}_{30}}{\partial \xi} + \left[-\frac{2}{3}\left\{\left(\frac{r_0\omega_1}{c}\right)^2 - \left(9-\frac{10\omega_p^2}{\omega_1^2}\right) + \left(\frac{r_0\omega_1}{c}\right)^2 \phi\left(\frac{A_{00}^2}{2f_1^2}\left[1-\frac{(1-q)r^2}{2r_0^2 f_1^2}\right]^{\frac{2}{1-q}}\right)\right\}^2\right. \\
&\quad \left. -9\left(\frac{r_0\omega_1}{c}\right)\left(1-\frac{\omega_p^2}{9\omega_1^2}\right)^2\right]\mathrm{A}_{30} \\
&+\mathrm{A}_{30}\left[5+\frac{i}{f_3}\frac{\partial f_1}{\partial \xi}+\frac{4i}{3f_3}\frac{\partial f_1}{\partial \xi}-6f_1^2\left(\frac{1}{f_3}\frac{\partial f_1}{\partial \xi}\right)^2\right] \\
&= -\frac{1}{16}\left(\frac{\omega_p^2}{\omega_1^2}\right)\left(\frac{eB_w}{cm\omega_1}\right)\left(\frac{eA_{00}}{m\omega_1 c}\right)^2\left(\frac{r_0\omega_1}{c}\right)^2\left(1-\frac{\omega_p^2}{\omega_1^2}\right)^{1/2} \\
&\quad \times\left[1-\frac{(1-q)r^2}{2r_0^2 f_1^2}\right]^{\frac{3}{1-q}}\left[3\left(1-\frac{\omega_p^2}{9\omega_1^2}\right)^{1/2} - 31\left(1-\frac{\omega_p^2}{\omega_1^2}\right)^{1/2}\right]
\end{aligned}
\tag{3.25}
$$

3.3 Results and discussions

Two interconnected differential equations (3.17) and (3.25) are numerically solved to obtain the amplitude and beam width parameter for a q-Gaussian laser beam as a function of propagation distance. The plasma is irradiated by a Nd: YLF laser with wavelength $1053\,nm$ a pulse duration of $4.5\,ps$ and a spot size of $50\ \mu m$, under a wiggler magnetic field $B_w = 1.2\,MG$ and a wiggler period of approximately $0.028\,cm$. These equations were solved numerically for ideal values of different laser parameters as $\mathrm{eA}_{10}/\mathrm{m}\omega_1\mathrm{c} = 50$, $\omega_p/\omega_1 = 0.8$, $eB_w/m\omega_1 c = 0.7$, $d = 10$.

Figure.1 shows that the intensity of the third harmonic wave is significantly enhanced with increasing wiggler magnetic field strength at a normalized distance $\xi = 0.8$. The maximum value is seen in the graph when $B_w = 70\,MG$ this is because the wiggler magnetic field satisfies the phase matching criterion for third harmonic generation, which allows the amplitude of the third harmonic pulse to grow. Similar results have been reported by Jyoti et al. [28] they studied the third harmonic generation of a short pulse laser in plasma under the influence of a wiggler magnetic field. Sharma et al. [29] also showed that the self-focusing of a laser beam is stronger in the presence of an exponential plasma density ramp can further enhance the efficiency of third harmonic generation. The wiggler magnetic field adds additional momentum to the third harmonic photons, which results in a significant increase in the normalized amplitude of the third harmonic wave. The highest enhancement in the third harmonic amplitude is observed in the presence of an exponential density ramp for optimal values of the incident laser intensity, wiggler magnetic field strength, and plasma frequency.

Figure. 2 shows how the normalized third harmonic amplitude changes for different values of the ratio of plasma frequency to laser frequency, ω_p/ω_1. As it is obvious from the graph that peak value is at $\omega_p/\omega_1 = 0.8$ .The normalized amplitude of the third harmonic pulse increases significantly with increasingω_p/ω_1, as the plasma density increases. This is similar to the results reported by Aggarwal et al. [30] in which they studied that using a wiggler magnetic field the second harmonic production in a gas containing atomic clusters. The second harmonic photon received the appropriate momentum from the wiggler magnetic field .Singh et al.[26] also reported a significant increase in the amplitude of the second and third harmonic pulses with ω_p/ω_1, under the effect of relativistic self-focusing. In their case the density ripple provided the phase matching criterion for efficient harmonic generation.

Figure.3 shows the fluctuation of the Third harmonic amplitude normalized to the incident field amplitude with normalized distance for different values of the intensity of the incident laser beam. As it is seen in the graph that we have a peak value at $10.2 \times 10^{14}\ W/cm^2$.Increasing the value of the intensity of the incident laser results in an increase in the refractive index, which occurs where the laser beam reaches its minimum spot size. This is consistent with the results reported by Thakur and Kant [31] they disclosed the intensification of harmonic generation of third order with the increase in the intensity of the pump laser. Vij [32] studied that the efficiency of third harmonic generation is increased due to cluster plasmon resonance. Sharma et al.[33]

also studied that for the Hermite-cosh-Gaussian laser the normalised amplitude in THG shows fluctuation with normalised distance ξ for optimal normalised wiggler magnetic field values and variable fundamental laser intensity. As from their study it is quite evident that as the normalised wiggler field and intensity grows, so does the normalised amplitude of THG. Basiry et al. [34] studied that the third harmonic electric field gets larger when the deviation parameter from the centre and the external magnetic field are both increased. The third harmonic electric field, on the other hand, becomes weaker as the laser beam width is increased. Finally, the third harmonic electric field is also strengthened by raising the wavenumber and amplitude of the rippling electron density.

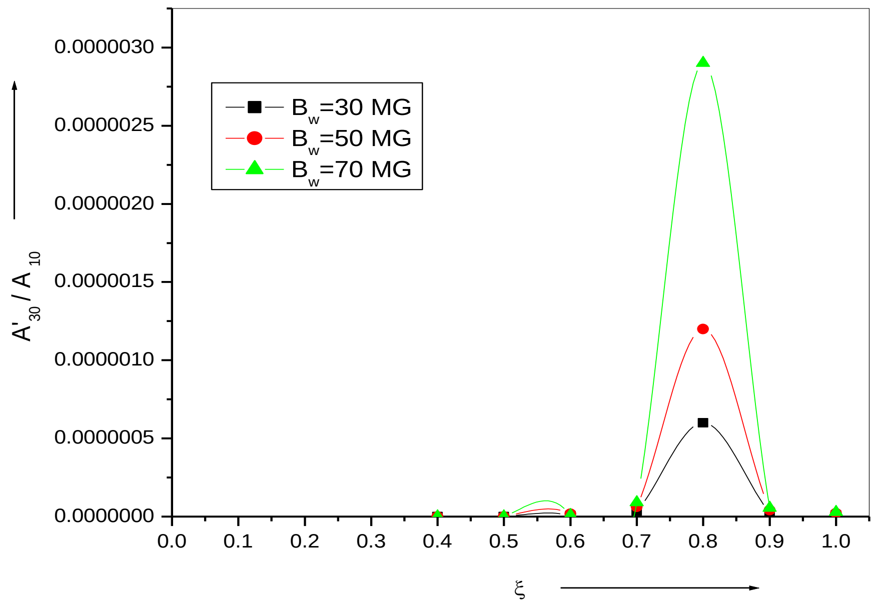

Fig. 3.1. Variation of normalized third harmonic amplitude with normalized propagation distance ξ for $eA_{10} / m\omega_1 c = 50$, $\omega_p/\omega_1 = 0.8$ and $d = 10$.

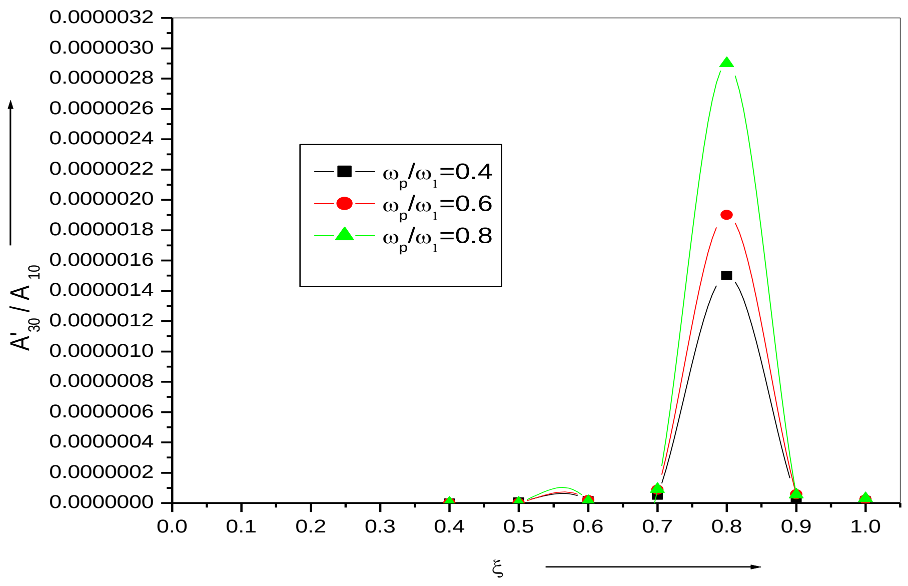

Fig. 3.2. Variation of normalized third harmonic amplitude with normalized propagation distance ξ for $eA_{10}\,/m\omega_1 c = 50$, $eB_w/m\omega_1 c = 0.7$and $d\ =\ 10$.

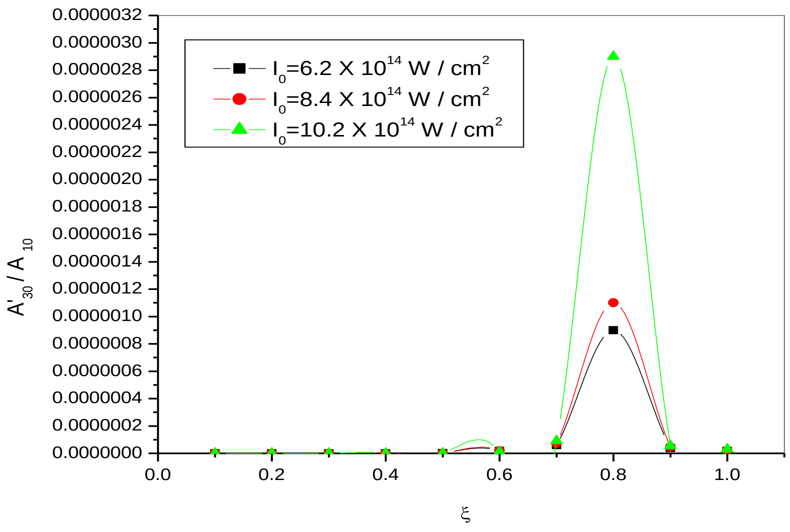

Fig. 3.3. Variation of normalized third harmonic amplitude with normalized propagation distance ξ for the values $\omega_p/\omega_1 = 0.8$, $eB_w/m\omega_1 c = 0.7$and $d\ =\ 10$.

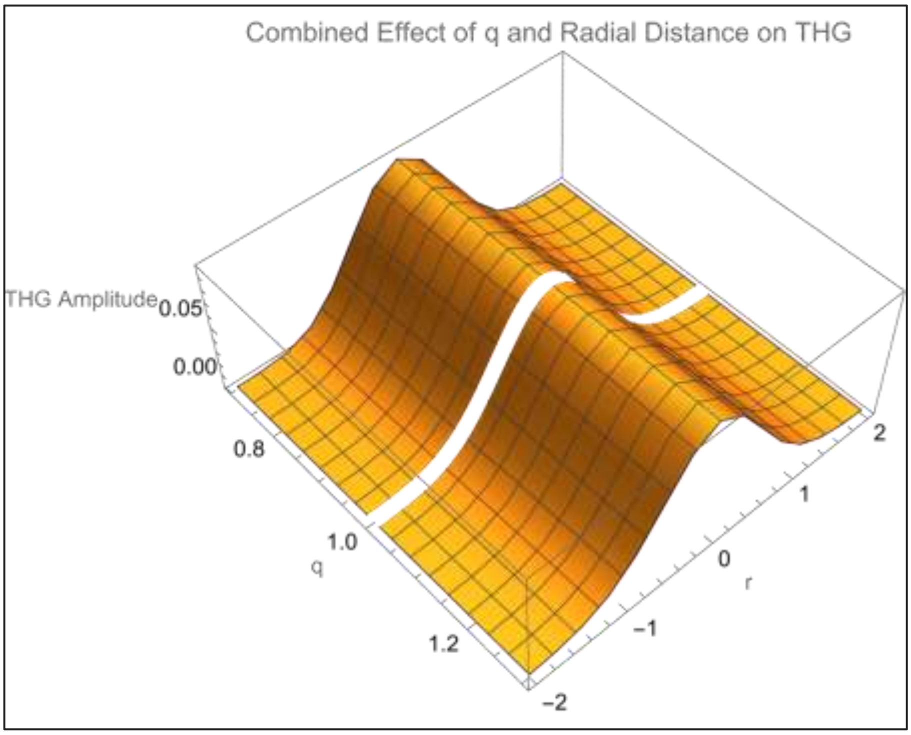

Fig 3.4 Influence of the q-parameter on the normalized third harmonic generation amplitude.

The figure confirms that the q-parameter significantly influences the magnitude of third harmonic generation. By adjusting q, the beam shape and effective intensity distribution are modified, leading to corresponding variations in THG amplitude.

3.4 Conclusion

It was concluded that the THG efficiency can be significantly enhanced by using a q-Gaussian beam with a small waist size and high laser intensity. The magnetic field also plays a role in enhancing the THG efficiency but its effect is less significant than the beam waist size and laser intensity. The normalized amplitude of third harmonic generation (THG) is maximized at a wiggler magnetic field parameter $B_w = 70MG$ of $\xi = 0.8$. This is because the wiggler field provides the additional momentum required for the THG photon to be resonant. The THG amplitude also increases significantly with the intensity of the incident laser pulse. The enhanced THG efficiency from using a q-Gaussian beam with a small waist size and a high laser intensity could lead to new and more powerful applications for THG in magnetized plasmas. For example, the enhanced THG efficiency could be used to generate high-power, coherent ultraviolet radiation for applications in microscopy, spectroscopy, and materials processing. The enhanced THG efficiency could also be used to generate high-energy electrons and positrons for applications in cancer therapy and particle accelerators.

References

[1] T. Tajima, J.M. Dawson 1979 Laser electron accelerator, *Physical Review Letters*. **43** 267.

[2] C. Geddes, C. Toth, J. Van Tilborg, E. Esarey, C. Schroeder, D. Bruhwiler, C. Nieter, J. Cary, W. Leemans 2004 High-quality electron beams from a laser Wakefield accelerator using plasma-channel guiding, *Nature.* **431** 538.

[3] R. Singh, A. Sharma, V. Tripathi 2010 Relativistic self-distortion of a laser pulse and ponderomotive acceleration of electrons in an axially inhomogeneous plasma, *Laser and Particle Beams.***28** 299.

[4] A. Chiron, G. Bonnaud, A. Dulieu, J. Miquel, G. Malka, M. Louis-Jacquet, G. Mainfray 1996 Experimental observations and simulations on relativistic self-guiding of an ultra-intense laser pulse in underdense plasmas, *Physics of Plasmas.* **3** 1373.

[5] P. Young, M. Foord, J. Hammer, W. Kruer, M. Tabak, S. Wilks 1995 Time-dependent channel formation in a laser-produced plasma, *Physical Review Letters.***75** 1082.

[6] P. Gibbon, P. Monot, T. Auguste, G. Mainfray1995Measurable signatures of relativistic self-focusing in underdense plasmas, *Physics of Plasmas*. **2** 305.

[7] A. Singh, K. Walia 2010 Relativistic self-focusing and self-channelling of Gaussian laser beam in plasma, *Applied Physics B.***101** 617.

[8] P. Corkum, C. Rolland, T. Srinivasan-Rao 1986 Supercontinuum generation in gases, *Physical Review Letters*. **57** 2268.

[9] A. Ting, K. Krushelnick, H. Burris, A. Fisher, C. Manka, C. Moore 1996 Backscattered supercontinuum emission from high-intensity laser–plasma interactions, *Optics Letters*. **21** 1096.

[10] M. Tabak, J. Hammer, M.E. Glinsky, W.L. Kruer, S.C. Wilks, J. Woodworth, E.M. Campbell, M.D. Perry, R.J. Mason 1994 Ignition and high gain with ultrapowerful lasers, *Physics of Plasmas*. **11** 626.

[11] H. Hora2007 New aspects for fusion energy using inertial confinement, *Laser and Particle Beams.***25** 37.

[12] C. Deutsch, H. Furukawa, K. Mima, M. Murakami, K. Nishihara 1996 Interaction physics of the fast ignitor concept, *Physical Review Letters.***77** 2483.

[13] A. Willes, P. Robinson, D. Melrose 1996 Second harmonic electromagnetic emission via Langmuir wave coalescence, *Physics of Plasmas.***3** 149.

[14] C. Grebogi, V.K. Tripathi, H.-H. Chen 1983 Harmonic generation of radiation in a steep density profile, *The Physics of Fluids.***26** 1904.

[15] R. Ondarza-Rovira, T. Boyd 2000 Plasma harmonic emission from laser interactions with dense plasma, *Physics of Plasmas.***7** 1520.

[16] A.S. Pirozhkov, S.V. Bulanov, T.Z. Esirkepov, M. Mori, A. Sagisaka, H. Daido 2006, Attosecond pulse generation in the relativistic regime of the laser-foil interaction: The sliding mirror model, Physics of Plasmas. **13**.

[17] A.A. Butt, N. Kant, V. Thakur 2023 Self-focusing of a q-gaussian laser beam under the influence of an exponential plasma density ramp in plasma, Physica Scripta. **98** 045621.

[18] A.A. Butt, V. Sharma, N. Kant, V. Thakur 2023 Combined effect of plasma density ramp and wiggler magnetic field on self-focusing of q-Gaussian laser beam in underdense plasma, Journal of Optics. 1.

[19] B. Bergues, D. Rivas, M. Weidman, A. Muschet, W. Helml, A. Guggenmos, V. Pervak, U. Kleineberg, G. Marcus, R. Kienberger 2018 Tabletop nonlinear optics in the 100-eV spectral region, *Optica.***5** 237.

[18] M. Drescher, M. Hentschel, R. Kienberger, M. Uiberacker, V. Yakovlev, A. Scrinzi, T. Westerwalbesloh, U. Kleineberg, U. Heinzmann, F. Krausz, 2002 Time-resolved atomic inner-shell spectroscopy, *Nature.***419** 803.

[19] Y. Xu, S. Wu, W. Zheng 2015 A scheme to produce high density and high temperature plasma for opacity measurement, *Physics of Plasmas.* **22** 4.

[20] J. Bailey, G. Rochau, R. Mancini, C. Iglesias, J. MacFarlane, I. Golovkin, C. Blancard, P. Cosse, G. Faussurier 2009 Experimental investigation of opacity models for stellar interior, inertial fusion, and high energy density plasmas, *Physics of Plasmas.***16** 5.

[21] E. Esarey, A. Ting, P. Sprangle, D. Umstadter, X. Liu 1993 Nonlinear analysis of relativistic harmonic generation by intense lasers in plasmas, *IEEE Transactions on Plasma Science.***21** 95.

[22] A. Sharma,2004 Resonant second-harmonic generation of a short pulse laser in a plasma channel, *Journal of Physics D: Applied Physics.***37** 2395.

[23] J. Parashar 2008 Effect of self-focusing on laser third harmonic generation in a clustered gas, *Physica Scripta.***79** 015501.

[24] M. Singh, D.N. Gupta 2014 Relativistic third-harmonic generation of a laser in a self-sustained magnetized plasma channel, *IEEE Journal of Quantum Electronics.***50** 491.

[25] V. Thakur, N. Kant 2016 Effect of pulse slippage on density transition-based resonant third-harmonic generation of short-pulse laser in plasma, *Frontiers of Physics.***11** 1.

[26] V. Sharma, V. Thakur, N. Kant 2020 Second harmonic generation of cosh-Gaussian laser beam in magnetized plasma, *Optical and Quantum Electronics*. **52** 444.

[27] V. Thakur, N. Kant 2018 Resonant second harmonic generation in plasma under exponential density ramp profile, *Optik.***168** 159.

[28] J. Rajput, N. Kant, H. Singh, V. Nanda 2009 Resonant third harmonic generation of a short pulse laser in plasma by applying a wiggler magnetic field, *Optics Communications.***282** 4614.

[29] V. Sharma, V. Thakur, N. Kant 2019 Third harmonic generation of a relativistic self-focusing laser in plasma in the presence of wiggler magnetic field, *High Energy Density Physics.***32** 51.

[30] M. Aggarwal, S. Vij, N. Kant 2015 Wiggler magnetic field assisted second harmonic generation in clusters, *The European Physical Journal D.* **69** 1.

[31] S. Vij2018 Wiggler magnetic field assisted third harmonic generation in expanding clusters, *Physica Scripta*. **93** 045602.

[32] V. Sharma, V. Thakur, N. Kant 2021 Hermite-cosh-Gaussian laser-induced third harmonic generation in plasma, *Optical and Quantum Electronics.***53** 281.

Chapter - 4

Third Harmonic Generation of Cosh- Gaussian Laser beam in magnetized plasma

4.1 Introduction

Short pulse lasers, traveling through plasma, always tend to produce harmonics. Due to the wide application domains where this phenomenon can be used, there is a lot of interest from researchers. Among these different kinds of harmonic generation techniques, THG is of importance due to applications such as in medicine ,telecommunications, and optoelectronics, [1–8] with laser profile significantly influencing efficiency and outcomes.

Aluminium nitride thin films have been studied using SHG techniques, with theoretical models closely aligning with experimental results, demonstrating the reliability of SHG in characterizing such materials [9]. Similarly, Marrucci et al.[10] applied SHG optical analysis to examine surface absorption phenomena in liquid-solid interfaces relevant to lubricants, showcasing the diverse utility of these nonlinear optical methods.

In plasma physics, the efficiency of THG has been seen to improve under relativistic self-focusing conditions enhanced by external magnetic fields such as the wiggler field, which provides resonance and increases photon velocity .Sharma et al.[11]. Banerjee et al.[12] experimentally investigated harmonic generation during relativistic laser-plasma interactions, highlighting the significant contribution of relativistic Thomson scattering to the generated harmonics.

Studies extending to complex systems have revealed that SHG can serve as a sensitive probe of phase transitions, such as the melting and freezing behaviours of binary organic powder mixtures, which differ markedly from those of pure substances ,Simon et al. [13]. In plasma environments, Liu et al [14], found that third harmonic generation is significantly influenced by density ripple structures, though its efficiency saturates under weakly relativistic intensities due to temporal fluctuations in laser intensity.

The role of laser parameters and plasma conditions on SHG efficiency has also been detailed, showing that modulation of these factors can optimize harmonic outputs, Askari et al. [15]. Phase matching of THG in plasma channels is dependent on background density perturbations meeting resonance requirements ,Shibhu et al.[16]. Furthermore, Varaki et al. demonstrated that in magnetized plasma, increased wiggler magnetic field strength and plasma frequency substantially enhance SHG conversion efficiency.

Other laser beam profiles, such as hollow Gaussian beams, have been analyzed for their sensitivity in generating SHG and electron plasma waves under ponderomotive nonlinearities ,Purohit et al.[17] . Singh et al.[18], investigated the effects of density ripples and incident angles on harmonic generation efficiency in relativistic laser-plasma interactions, noting improvement in second harmonic yield with optimized geometric configuration.

Magnetized plasma studies continue to provide valuable insights; for example, Jha et al. reported optimal SHG conversion when laser pulses interact with plasma under transverse magnetic fields. Material advancements have suggested potential for novel optical media designed to minimize group velocity mismatch between fundamental and harmonic waves, thus increasing conversion efficiency ,Trippenbach et al. [19].

The third harmonic generation process has also been shown to benefit from plasma density gradients and wiggler magnetic fields which aid phase matching and impart angular momentum to photons ,Thakur et al. [20]. Sharma et al. [23], showed how strong ponderomotive forces and electron heating through high-amplitude electromagnetic waves can drive efficient third harmonic generation. Similarly, Rajput et al[24]. found that a wiggler magnetic field notably boosts third harmonic efficiency in laser-plasma interactions.

Finally, investigations into Hermite-Gaussian laser beams under ponderomotive non-linearity emphasized the sensitivity of second harmonic yield to mode structure and plasma density ,Wadhwa and Singh [26]. Nazir et al.[27] further highlighted the critical role of wiggler magnetic fields and plasma parameters in enhancing THG in magnetized plasmas using q-Gaussian laser beams.

The propagation of an intense laser beam through plasma results in electrons moving away from the axial region due to ponderomotive force, static electric force, and density perturbation, leading to the third harmonic generation. We have chosen the ponderomotive nonlinearity and studied the THG of cosh-Gaussian laser beam in magnetised plasma, because of its larger efficiency gain.

The manuscript is divided into sections where section .2 provides the normalised amplitude expressions. Section .3 presents a visual discussion of the solutions we found by solving these equations numerically using the beam width parameter expressions that were determined by other researchers. Section .4 contains a discussion of the findings.

4.2 Mathematical formulation

We have considered a powerful cosh-Gaussian laser beam that is incident across a plasma in under the influence of a wiggler magnetic field.

The incident laser's electric field $\overrightarrow{E_1}$ and the wiggler field $\vec{B}_w$, are

$$\overrightarrow{E_1} = \hat{x}A_1(z,r)\exp\left[-i\left(\omega_1 t-\vec{k}_1 z\right)\right], \tag{4.1(a)}$$

$$\vec{B}_1 = \frac{c\vec{k}_1\times\vec{E}_1}{\omega_1} \tag{4.1(b)}$$

$$\vec{B}_w = \hat{y}B_0\exp(ik_0 z) \tag{4.1(c)}$$

where $\overrightarrow{k_1}$ being the wave number of basic laser pulse, ω_1 be the natural frequency, $\overrightarrow{B_1}$ represents laser field, c is the speed of light, k_0 is the wiggler wave number and $A(z,r)$ being the amplitude of Gaussian wave given as,

$$A(z) = A_{10}(z, r)\,\text{Exp}\left[-ikS(r, z)\right] \tag{4.2}$$

Where A_{10} and S are two real functions of the radial distance r and the axial position z, A_{10} represents the unvarying amplitude of the fundamental laser pulse and is defined as follows,

$$A_{10}^2 = \frac{E_0^2}{f^2(z)}\,\text{Exp}\left[\frac{b^2}{2}\right]\left\{\text{Exp}\left[-2\left(\frac{r}{r_0 f(z)} + \frac{b}{2}\right)^2\right] + \text{Exp}\left[-2\left(\frac{r}{r_0 f(z)} - \frac{b}{2}\right)^2\right] + 2\,\text{Exp}\left[-\left(\frac{2r^2}{r_0^2 f^2(z)} + \frac{b^2}{2}\right)\right]\right\} \tag{4.3}$$

Electrons encounter the ponderomotive force and achieve oscillatory velocity which is given as

$$\vec{V}_1 = e\frac{\vec{E}_1}{mi(\omega_1 + iv)} \tag{4.4}$$

Electrons undergo oscillatory velocity at $2\omega_1$ due to ponderomotive force from an incident beam. This combined with a density ripple, results in a density perturbation at $2\omega_1$, resulting in the third harmonic current density $\vec{J}_3 = \vec{J}_3^L + \vec{J}_3^{NL}$ [25], where current density in linear and nonlinear form are given as under.

$$\vec{J}_3^L = \frac{n_0 e^2 \vec{E}_3}{3m_0 \gamma i \omega_1} \tag{4.5}$$

$$\vec{J}_3^{NL} = \frac{-n_0 e^5 B_w k_1 \vec{E}_1^3}{16 c i m_0^4 \omega_1^4 (\omega_1 + iv)}\left[\frac{5k_1}{18\omega_1} + \frac{k_1 + k_0}{\omega_1 + iv}\right]\hat{x} \tag{4.6}$$

Wave equation governing third harmonic field is given as

$$\nabla^2 \vec{E}_3 = \left[\frac{\varepsilon_0 + \varphi(E_1 E_1^*)}{c^2}\right]\frac{\partial^2 \vec{E}_3}{\partial t^2} + \frac{4\pi}{c^2}\frac{\partial \vec{J}_3^{NL}}{\partial t} + \frac{4\pi}{c^2}\frac{\partial \vec{J}_3^L}{\partial t} \tag{4.7}$$

Also $\varepsilon = \varepsilon_0 + \varphi(E_1 E_1^*)$ (4.8)

where $\varphi(E_1 E_1^*) = \frac{\omega_p^2}{\omega_1^2}\left[1 - \exp\left(-\frac{3m_0}{4M}\alpha E_0^2\right)\right]$ (4.9)

Using Eqs. (4.5), (4.6), (4.7) and (4.9) we have obtained a new equation as under

$$\nabla^2\vec{E}_3 + \left[\left(9\omega_1^2 - \frac{10\omega_p^2}{c^2}\right) + \frac{9\omega_1^2\phi\left(\overrightarrow{E_1}\overrightarrow{E_1^*}\right)}{c^2}\right]\vec{E}_3 = \frac{4\pi}{c^2}\frac{\partial\vec{J}_3^{NL}}{\partial t} \tag{4.10}$$

Beam width parameter equation according to Nanda et al.[28] is given as

$$\frac{\partial^2 f(z)}{\partial\xi^2} = \left[4\text{-}4\,b^2 - \frac{6\alpha E_0^2 m_0}{M}\left(\frac{\omega_1^2 r_0^2}{c^2}\right)\left(\frac{\omega_p^2}{\omega_1^2}\right)\mathrm{Exp}\left[\frac{b^2}{2}\right]\frac{1}{f^3(z)}\right] \tag{4.11}$$

b is the decentred beam parameter and ξ is the normalised distance.

The solution of Eq. (4.7) gives the particular integral

$$\vec{E}_3 = A_3^{'}(z,t)\exp\left[-i\left(3\omega_1 t - k_3 Z\right)\right] \tag{4.12}$$

$$A_3^{'} = A_{30}^{'}(\psi_3) \tag{4.13}$$

$$\frac{\partial E_3}{\partial z} = \exp\left[-i\left\{3\omega_1 t - (3k_1 + k_0)z\right\}\right]\left[\frac{\partial A_3^{'}}{\partial z} + i(3k_1 + k_0)A_3^{'}\right] \tag{4.14}$$

$$\frac{\partial^2 E_3}{\partial z^2} = \exp\left[-i\left\{3\omega_1 t - (3\,k_1 + k_0)z\right\}\right]\left[\frac{\partial^2 A_3^{'}}{\partial z^2} + 2i(3\,k_1 + k_0)\frac{\partial A_3^{'}}{\partial z} + [i(3k_1 + k_0)]^2 A_3^{'}\right] \tag{4.15}$$

neglecting term containing $\frac{\partial^2 A_3^{'}}{\partial z^2}$ as it is very small so we get

$$\frac{\partial^2 E_3}{\partial z^2} = 2i(3\,k_1 + k_0)A_3^{'}\exp\left[-i\left\{3\omega_1 t - (3\,k_1 + k_0)z\right\}\right]\frac{\partial A_3^{'}}{\partial z} + [i(3k_1 + k_0)]^{2A_3^{'}}\exp\left[-i\left\{3\omega_1 t - (3\,k_1 + k_0)z\right\}\right] \tag{4.16}$$

$$\frac{\partial A_3^{'}}{\partial z} = \frac{\partial A_{30}^{'}}{\partial z}\left\{\mathrm{Exp}\left[-6\left(\frac{r}{r_0 f(z)} + \frac{b}{2}\right)^2\right] + \mathrm{Exp}\left[-6\left(\frac{r}{r_0 f(z)} - \frac{b}{2}\right)^2\right] + 2\mathrm{Exp}\left[-3\left(\frac{2r^2}{r_0^2 f^2(z)} + \frac{b^2}{2}\right)\right]\right\}^{\frac{1}{2}}\exp(-iks) +$$

$$A_{30}^{'}\frac{\partial f}{\partial z}\left(\frac{1}{2}\right)\gamma^{-\frac{1}{2}}\left\{\mathrm{Exp}\left[-6\left(\frac{r}{r_0 f(z)} +\right.\right.\right.$$

$$\left.\left.\frac{b}{2}\right)^2\right]\left[\left(\frac{-6r^2}{r_0^2f^2(z)}\right)\left(\frac{-2}{f}\right)\left(\frac{\partial f}{\partial z}\right)-\left(\frac{6br}{r_0f(z)}\right)\left(\frac{-1}{f}\right)\left(\frac{\partial f}{\partial z}\right)-6\left(\frac{r}{r_0f(z)}-\frac{b}{2}\right)^2\right]\left(\frac{-6r^2}{r_0^2f^2(z)}\right)\left(\frac{-2}{f}\right)\left(\frac{\partial f}{\partial z}\right)+$$

$$\left.\left(\frac{6br}{r_0f(z)}\right)\left(\frac{-1}{f}\right)\left(\frac{\partial f}{\partial z}\right)+2\mathrm{Exp}\left[-3\left(\frac{2r^2}{r_0^2f^2(z)}+\frac{b^2}{2}\right)\right]\left(\frac{-6r^2}{r_0^2f^2(z)}\right)\left(\frac{-2}{f}\right)\left(\frac{\partial f}{\partial z}\right)\right]\Bigg\}\exp(-iks) \qquad (4.17)$$

$$\frac{\partial^2E_3}{\partial z^2}=$$
$$2i(3k_1+$$
$$k_0)\exp[-i\{3\omega_1t-(3k_1+$$
$$k_0)z\}]\frac{E_0}{f(z)}\mathrm{Exp}\left[\frac{b^2}{4}\right]\frac{\partial A_{30}}{\partial z}\gamma^{\frac{1}{2}}\exp(-iks)-A'_{30}\frac{E_0}{f^2(z)}\mathrm{Exp}\left[\frac{b^2}{4}\right]\frac{\partial f}{\partial z}\gamma^{\frac{1}{2}}\exp(-iks)+[i(3k_1+$$
$$k_0)]^2A'_3\exp[-i\{3\omega_1t-(3k_1+k_0)z\}]\exp(-iks),$$

$$\frac{\partial^2E_3}{\partial z^2}=$$
$$2i(3k_1+k_0)A'_3\exp[-i\{3\omega_1t-(3k_1+k_0)z\}]\psi_3\frac{\partial A'_{30}}{\partial z}+$$
$$[i(3k_1+k_0)]^2A'_{30}\psi_3\exp[-i\{3\omega_1t-(3k_1+k_0)z\}]$$
$$(4.18)$$

$$\int r\psi_3^*\psi_3dr=\int r\left\{\mathrm{Exp}\left[-6\left(\frac{r}{r_0f(z)}+\frac{b}{2}\right)^2\right]\right\}+\mathrm{Exp}\left[-6\left(\frac{r}{r_0f(z)}-\frac{b}{2}\right)^2\right]+2\mathrm{Exp}\left[-3\left(\frac{2r^2}{r_0^2f^2(z)}+\right.\right.$$
$$\left.\left.\frac{b^2}{2}\right)\right]dr\,,$$

$$\int r\psi_3^*\psi_3dr=\int r\left\{4-24\frac{r^2}{r_0^2f^2(z)}-6b^2\right\}dr, \qquad (4.19)$$

$$\int r\psi_3^*\psi_3dr=\int\left\{4r-24\frac{r^3}{r_0^2f^2(z)}-6rb^2\right\}dr, \qquad (4.20)$$

$$\int r\psi_3^*\psi_3dr=\left\{2r^2-6\frac{r^4}{r_0^2f^2(z)}-r^2b^2\right\}, \qquad (4.21)$$

$$\text{where }\psi_3=\left\{\begin{matrix}\mathrm{Exp}\left[-6\left(\frac{r}{r_0f(z)}+\frac{b}{2}\right)^2\right]+\mathrm{Exp}\left[-6\left(\frac{r}{r_0f(z)}-\frac{b}{2}\right)^2\right]\\+2\mathrm{Exp}\left[-3\left(\frac{2r^2}{r_0^2f^2(z)}+\frac{b^2}{2}\right)\right]\end{matrix}\right\}^{\frac{1}{2}}\exp(-3ik_3S) \qquad (4.22)$$

Using Eqs. (4.12) and (4.13) into Eq. (4.10) we obtain

$$\frac{\partial A_{30}''}{\partial \xi}\left\{2-b^2\right\}+\left[\begin{array}{c} -\left(\frac{9\omega_1^2 r_0^2}{c^2}\right)\left(1-\frac{\omega_p^2}{9\omega_1^2}\right)^2\left\{2-b^2\right\}+A_{30}'\left\{-\frac{24}{r_0^2 f^2(z)}\right\} \\ +\left[\begin{array}{c}\frac{36b^2}{2f^2(z)}+\frac{18b^2}{f^2(z)}-\frac{27b^4}{f^2(z)}-\frac{24}{2f^2(z)} \\ -\frac{9b^2}{2f^2(z)}\exp(-2)\end{array}\right] \\ -\left[\frac{10\omega_p^2}{c^2}\frac{-9\omega_1^2}{c^2}-\frac{9\omega_1^2\phi\left(\vec{E}_1\vec{E}_1^*\right)}{c^2}r_0^2\left\{2-b^2\right\}\right.\end{array}\right]A_{30}''= \tag{4.23}$$

Multiplying Eq .(4.12)by $r\psi_3^*$ and integrating with respect to r and substituting the value of $\phi\left(\vec{E}_1\vec{E}_1^*\right)=\frac{\omega_p^2}{\omega_1^2}\left[1-\exp\left(-\frac{3m_0}{4M}\alpha E_0^2\right)\right]$ we obtained the equation below .

$$2i\frac{\partial A_{30}''}{\partial \xi}\left\{2-b^2\right\}+\left[\begin{array}{c} -\left(\frac{9\omega_1^2 r_0^2}{c^2}\right)\left(1-\frac{\omega_p^2}{9\omega_1^2}\right)^2\left\{2-b^2\right\}+A_{30}'\left\{-\frac{24}{r_0^2 f^2(z)}\right\} \\ -\frac{36b^2}{2f^2(z)}+\frac{18b^2}{f^2(z)}-\frac{27b^4}{f^2(z)}-\frac{24}{2f^2(z)}\exp(-2) \\ -\left[\frac{10\omega_p^2}{c^2}\frac{-9\omega_1^2}{c^2}-\frac{\omega_p^2}{\omega_1^2}\left[1-\exp\left(-\frac{3m_0}{4M}\alpha E_0^2\right)\right]r_0^2\left\{2-b^2\right\}\right.\end{array}\right]A_{30}''=$$
$$\frac{3}{16}\left(\frac{\omega_p^2}{\omega_1^2}\right)\left(\frac{\omega_1^2 r_0^2}{c^2}\right)\left(1-\frac{\omega_p^2}{\omega_1^2}\right)^{\frac{1}{2}}\left(\frac{e^2A_{10}^2}{m^2\omega_1^2c^2}\right)\left(\frac{eB_w}{m\omega_1 c}\right)\left[\begin{array}{c}+3\left(1-\frac{\omega_p^2}{9\omega_1^2}\right)^{\frac{1}{2}} \\ -\frac{31}{18}\left(1-\frac{\omega_p^2}{\omega_1^2}\right)^{\frac{1}{2}}\end{array}\right]\left\{2-3b^2\right\} \tag{4.24}$$

where $A_{30}''=A_{30}'/A_{10}$ is the normalise third harmonic amplitude.

4.3 Results and discussion

The linked equations for the beam width parameter f and the normalised amplitude A_{30}'/A_{10} of third harmonic pulse are represented by equations (4.11) and (4.15) .We have taken into account an incoming laser with the following parameters $I = 1.024\times10^{18}\,\mathrm{W/cm^2}$, $\omega_1 = 1.2\times10^{14}\,\mathrm{rad/s}$, beam width of incident laser 46 μm and wiggler magnetic field is 20 T. The equations for f and A_{30}'/A_{10} has been numerically optimized at different parameter's $\omega_1 r_0/c = 24$, $\varepsilon_3 A_{10}^2/\varepsilon_0 = 1$, $eA_{10}/m_1c = 5$, $eB_w/m\omega_1 c = 3$ and $\omega_p/\omega_1 = 0.8$, The results have been illustrated through graphs. In Fig. 1, the alteration of the third harmonic pulse's normalized amplitude with ξ for diverse values of $eA_{10}/m\omega_1 c = 1$,3 and 5 is shown. The findings show that the normalized amplitude of the third harmonic pulse increases significantly when the incident laser's normalized intensity is at its highest. which is clearly from the graph that at high value of normalised intensity that is $eA_{10}/m\omega_1 c = 5$, the amplitude is 0.38 which is at its peak .As the pondermotive force becomes vigorous and it forces the electrons far away from the axial zone, therefore making refractive index maximum. Due to this gain in efficiency of THG is substantial. Sharma et al.[29], in their study revealed that a cosh Gaussian laser beam enhances SHG efficiency by adding momentum to second harmonic photons in the wiggler magnetic field. This efficiency is enhanced with increased laser intensity, wiggler field strength, and plasma density.

The normalised amplitude of the third harmonic pulse is shown graphically in Figure .2 at various values of the normalised wiggler field, $eB_w/m\omega_1 c = 1, 2,$ and 3, with the other parameters staying the same as in Figure 1. The cyclotron frequency is maintained by the wiggler magnetic field, which confines the electrons in the plasma zone and increases THG efficiency. It is noticed that A'_{30}/A_{10} tends to increases from 0.10 to 0.38 on increasing $eB_w/m\omega_1 c = 1, 2$ and 3. Figure .3 shows variation the normalized amplitude of Third harmonic pulse with ξ, at contrasting values of normalized density of the plasma $\omega_p/\omega_1 = 0.4, 0.6$ and 0.8, where rest of the parameters being same as mentioned in Fig. 1. Our results illustrate substantial increase in third harmonic amplitude, at higher values of ω_p/ω_1, due to rise in density of plasma, the value of A'_{30}/A_{10} shows a rise from 0.02 to 0.37 on enhancing ω_p/ω_1 from 0.4 to 0.8. Therefore, the efficacy of THG shows notable increase in the basic lasers focus area with plasma frequency as shown in Fig.4. The effectiveness of THG is also affected by the decentred parameter, as shown in Fig. 3. The decentred parameter is ascertained to be highly sensitive to THG, since the normalised amplitude of THG increases dramatically with a slight change in the decentred parameter's value. This demonstrates the decentred parameter's sensitivity. A little change in b from 0.54 to 0.58 causes the normalised amplitude to vary from 0.2 to 0.36.

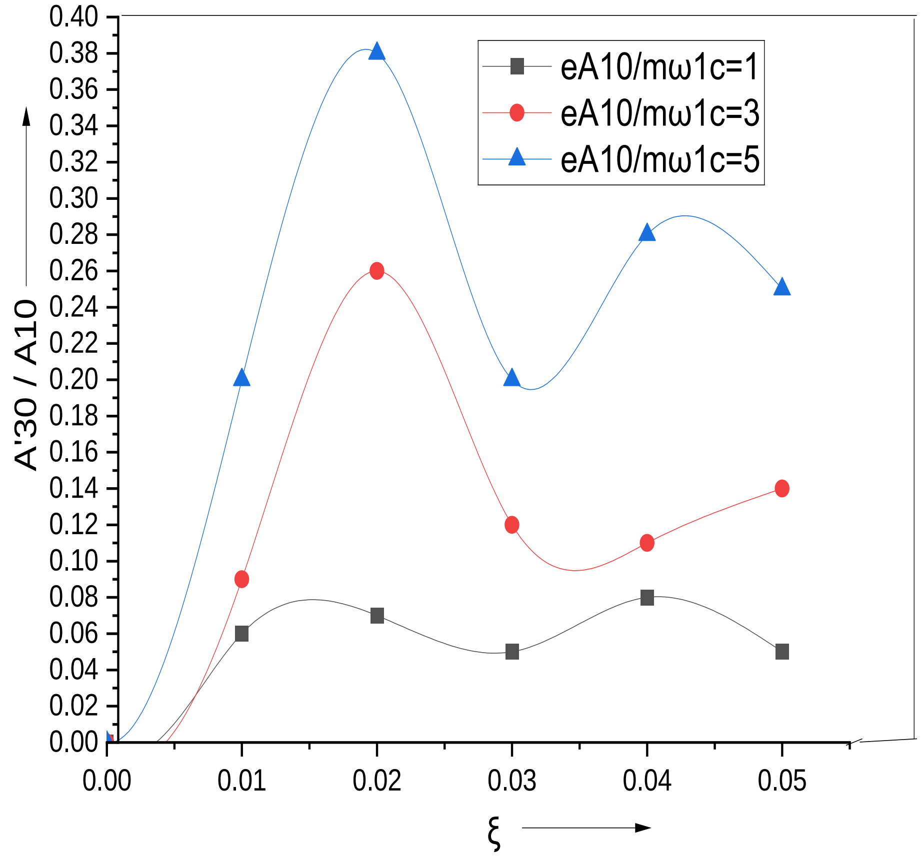

Fig .4.1 The variation of the normalised third harmonic amplitude A'_{30}/A_{10} with ξ for various $eA_{10}/m\omega_1 c$ values of 1, 3, and 5. Other parameters are $\omega_1 r_0/c$=24, $\varepsilon_2 A_{10}^2/\varepsilon_0 = 1$, $eA_{10}/m\omega_1 c = 5$, $eB_w/m\omega_1 c = 3$, $\omega_p/\omega_p = 0.8$.

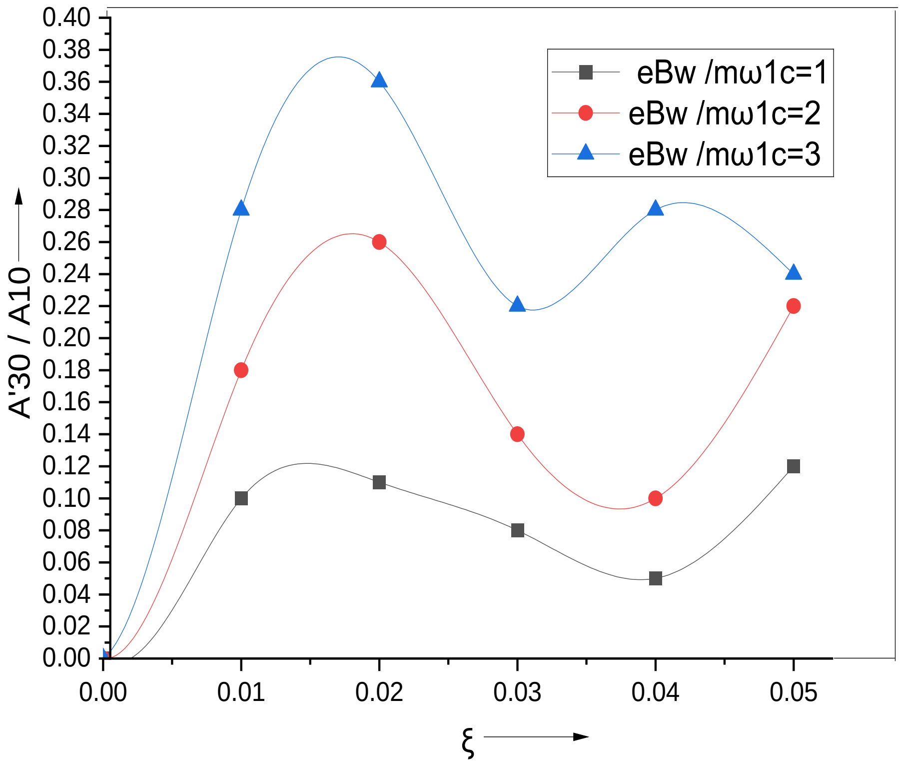

Fig 4.2 The variation of the normalised third harmonic amplitude A'_{30}/A_{10} with ξ for various $eB_w/m\omega_1 c$ values like 1, 2, and 3. Other parameters are $\omega_1 r_0/c$=24, $\varepsilon_2 A_{10}^2/\varepsilon_0 = 1$, $eA_{10}/m\omega_1 c = 5$, $eB_w/m\omega_1 c = 3$.

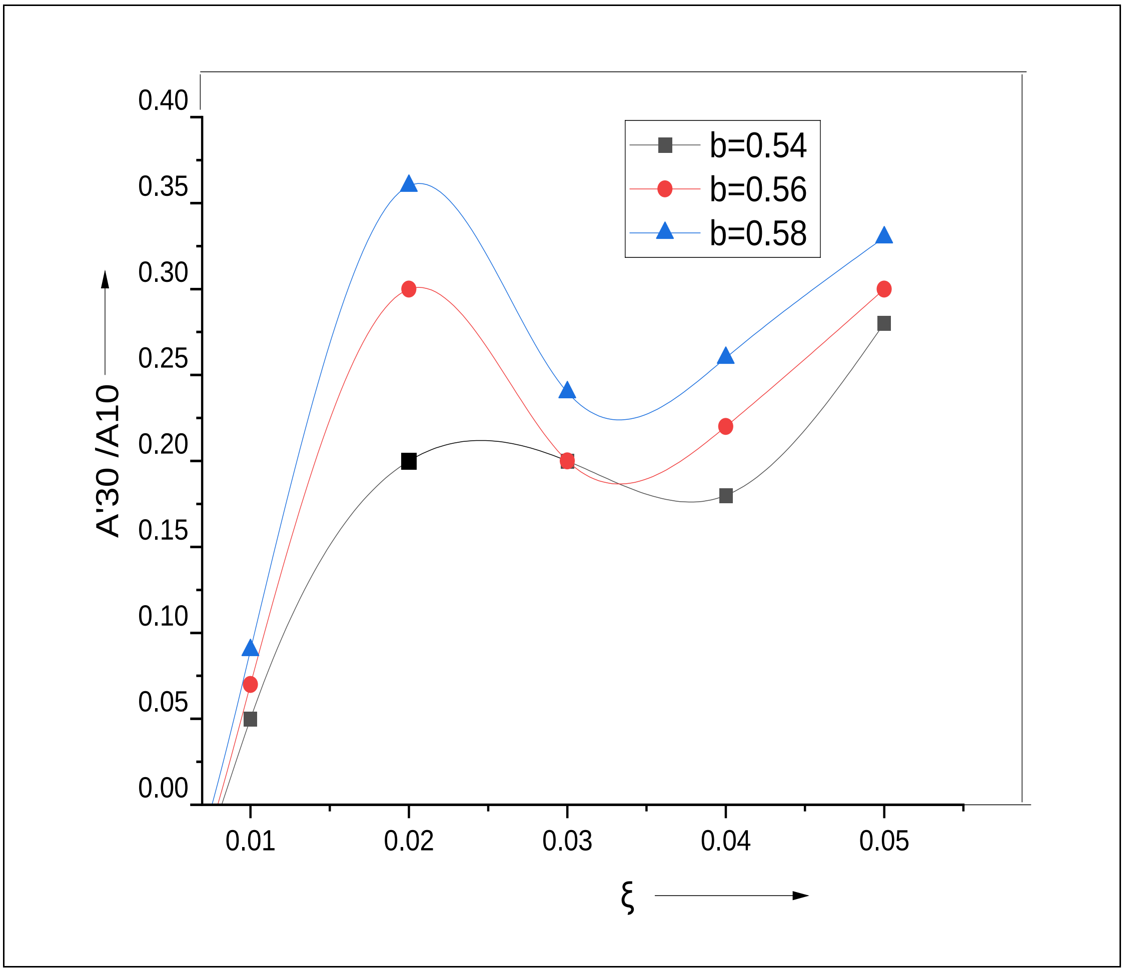

Fig .4.3 The variation of the normalised third harmonic amplitude A'_{30}/A_{10} with ξ for various b, values 0.72, 0.76, 0.78. Other parameters are $\omega_1 r_0/c$=24, $\varepsilon_2 A_{10}^2/\varepsilon_0 = 1$, $eA_{10}/m\omega_1 c = 5$, $eB_w/m\omega_1 c = 3$, $\omega_p/\omega_1 = 0.8$.

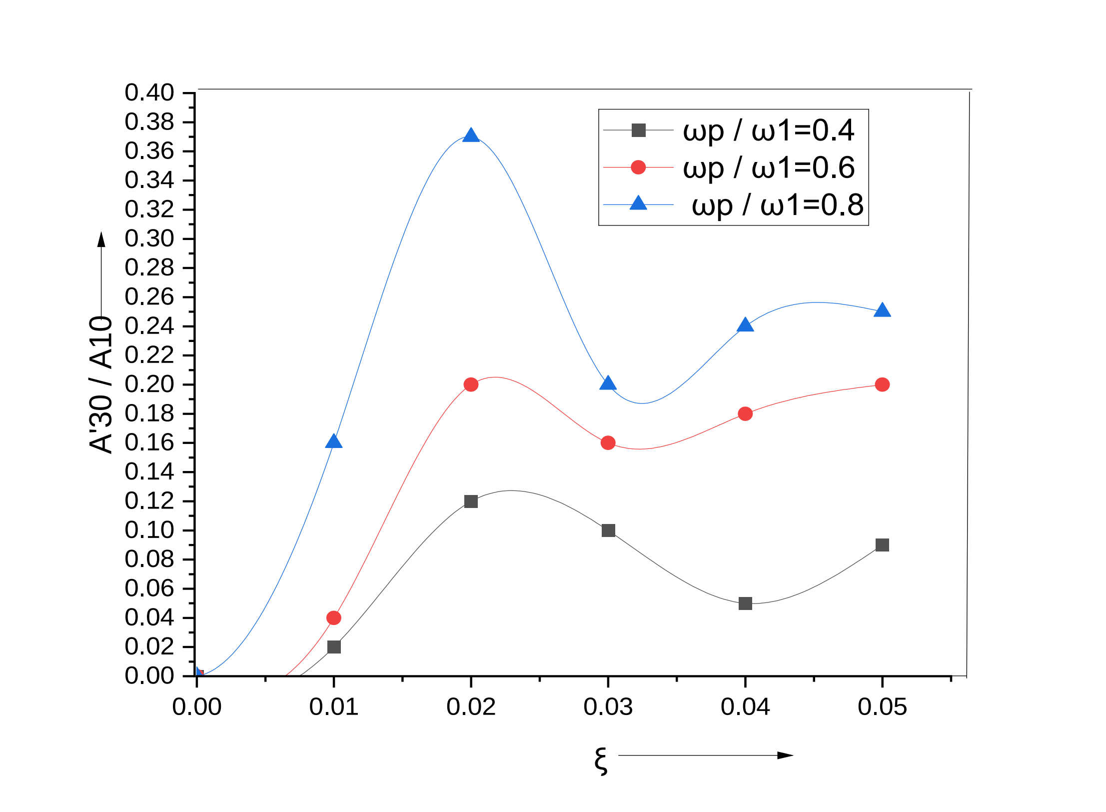

Fig 4.4 The variation of the normalised third harmonic amplitude A'_{30}/A_{10} with ξ for various $\omega_p/\omega_1 = 0.4, 0.6, 0.8$. Other parameters are $\omega_1 r_0/c$=24, $\varepsilon_2 A_{10}^2/\varepsilon_0 = 1$, $eA_{10}/m\omega_1 c = 5$, $eB_w/m\omega_1 c = 3$, $\omega_p/\omega_1 = 0.8$.

4.4 Conclusion

In this paper, third harmonic generation of a cosh-Gaussian laser in magnetized plasma is considered. The wiggler magnetic field was found to enhance THG efficiency by ensuring phase matching and sustaining the cyclotron frequency. Maximizing $eA_{10}/m\omega_1 c = 5$ (incident field strength) and $eB_w/m\omega_1 c = 3$(wiggler field strength) yields the greatest output i.e 0.39 and 0.37. The numerical results indicated that THG efficiency increased with increasing intensity of an incident laser, with an increase in strength of a wiggler field, and an increase in plasma density. From these results, it has been revealed that optimization of these parameters is quite essential for efficient third harmonic generation in magnetized plasma.

References

[1] X. Chen, O. Nadiarynkh, S. Plotnikov, P.J. Campagnola, Second harmonic generation microscopy for quantitative analysis of collagen fibrillar structure, Nature Protocols. **7**, 654–669 (2012).

[2] K. Tilbury, P.J. Campagnola, Applications of second-harmonic generation imaging microscopy in ovarian and breast cancer, Perspectives in Medicinal Chemistry. **7** , PMC-S13214 (2015).

[3] R. Ganeev, J. Chakera, M. Raghuramaiah, A. Sharma, P. Naik, P. Gupta, Experimental study of harmonic generation from solid surfaces irradiated by multipicosecond laser pulses, Physical Review E. **63**, 026402 (2001).

[4] R. Cicchi, F.S. Pavone, Probing collagen organization: practical guide for second-harmonic generation (SHG) imaging, Fibrosis: Methods and Protocols. 409–425 (2017).

[5] K. Brixius, A. Beyer, G. Mette, J. Güdde, M. Dürr, W. Stolz, K. Volz, U. Höfer, Second-harmonic generation as a probe for structural and electronic properties of buried GaP/Si (0 0 1) interfaces, Journal of Physics: Condensed Matter **30** ,484001 (2018).

[6] P. Campagnola, Second harmonic generation imaging microscopy: applications to diseases diagnostics, Analytical Chemistry. **83** ,3224–3231 (2011).

[7] R.A. Natal, J. Vassallo, G.R. Paiva, V.B. Pelegati, G.O. Barbosa, G.R. Mendonça, C. Bondarik, S.F. Derchain, H.F. Carvalho, C.S. Lima, others, Collagen analysis by second-harmonic generation microscopy predicts outcome of luminal breast cancer, Tumor Biology. **40**, 1010428318770953 (2018).

[8] X.-T. Gan, C.-Y. Zhao, S.-Q. Hu, T. Wang, Y. Song, J. Li, Q.-H. Zhao, W.-Q. Jie, J.-L. Zhao, Microwatts continuous-wave pumped second harmonic generation in few-and mono-layer GaSe, Light: Science & Applications. **7**, 17126–17126 (2018).

[9] S. Le Blanc, M. Downer, R. Wagner, S.-Y. Chen, A. Maksimchuk, G. Mourou, D. Umstadter, Temporal characterization of a self-modulated laser wakefield, in: AIP Conference Proceedings, American Institute of Physics. pp, 651–663 (1997).

[10] L. Marrucci, D. Paparo, G. Cerrone, C. de Lisio, E. Santamato, S. Solimeno, S. Ardizzone, P. Quagliotto, Probing interfacial properties by optical second-harmonic generation, Optics and Lasers in Engineering .**37**, 601–610 (2002).

[11] V. Sharma, V. Thakur, N. Kant, Third harmonic generation of a relativistic self-focusing laser in plasma in the presence of wiggler magnetic field, High Energy Density Physics .**32**, 51–55 (2019).

[12] S. Banerjee, A. Valenzuela, R. Shah, A. Maksimchuk, D. Umstadter, High harmonic generation in relativistic laser–plasma interaction, Physics of Plasmas 9 (2002) 2393–2398.

[13] S.M. Hooker, Developments in laser-driven plasma accelerators, Nature Photonics. **7,** 775–782 (2013).

[14] C. Liu, V. Tripathi, Third harmonic generation of a short pulse laser in a plasma density ripple created by a machining beam, Physics of Plasmas. **15** (2008).

[15] H.R. ASKARI, M. NOROOZI, Effect of a wiggler magnetic field and the ponderomotive force on the second harmonic generation in laser-plasma interactions, Turkish Journal of Physics. **33**, 299–311 (2009).

[16] S. Shibu, V. Tripathi, Phase-matched third harmonic generation of laser radiation in a plasma channel: nonlocal effects, Physics Letters A. **239**, 99–102 (1998).

[17] M. Abedi-Varaki, S. Jafari, Second-harmonic generation of a linearly polarized laser pulse propagating through magnetized plasma in the presence of a planar magnetostatic wiggler, The European Physical Journal Plus. **133**, 1–7 (2018).

[18] G. Purohit, P. Rawat, R. Gauniyal, Second harmonic generation by self-focusing of intense hollow Gaussian laser beam in collisionless plasma, Physics of Plasmas 23 (2016).

[19] K. Singh, V. Gupta, V. Tripathi, Relativistic laser harmonic generation from plasmas with density ripple, Optics Communications. **226** ,377–386 (2003).

[20] P. Jha, R.K. Mishra, G. Raj, A.K. Upadhyay, Second harmonic generation in laser magnetized–plasma interaction, Physics of Plasmas **14** (2007).

[21] M. Trippenbach, M. Matuszewski, E. Infeld, C.L. Van, R. Tasgal, Y. Band, Enhancement of third harmonic generation by wave vector mismatch to counter phase-modulation, Optics Communications. **229** ,391–395 (2004).

[22] V. Thakur, N. Kant, Effect of pulse slippage on density transition-based resonant third-harmonic generation of short-pulse laser in plasma, Frontiers of Physics. **11** ,1–8 (2016).

[23] V. Sharma, V. Thakur, A. Singh, N. Kant, Second harmonic generation of a self-focused Hermite-Gaussian laser in plasma, Chinese Journal of Physics. **71** ,312–318 (2021).

[24] A. Sharma, Third harmonic generation efficiency at higher powers in a collisional plasma, Journal of Applied Physics. **55 ,** 690–692 (1984).

[25] J. Rajput, N. Kant, H. Singh, V. Nanda, Resonant third harmonic generation of a short pulse laser in plasma by applying a wiggler magnetic field, Optics Communications. **282** ,4614–4617 (2009).

[26] J. Wadhwa, A. Singh, Generation of second harmonics of intense Hermite–Gaussian laser beam in relativistic plasma, Laser and Particle Beams. **37** ,79–85 (2019).

[27] D. Nazir, V. Sharma, V. Thakur, Magnetically enhanced third harmonic generation using q-Gaussian laser beam in plasma, Journal of Optics. (2023) 1–7.

Chapter - 5

Second Harmonic Generation of Circularly Polarized Hermite-cosh Gaussian laser beam in Magnetized plasma

5.1 Introduction

Nonlinear optical phenomena in plasmas, including second harmonic generation, have become crucial for ultrafast laser-matter interactions and compact radiation sources in quantum technologies [1]. The second harmonic generation (SHG) is particularly significant among the several harmonic generations because of its wide range of applications, like magnetic resonance imaging (MRI) [2,3], in medical science [4], in optoelectronics [5]. Unlike traditional nonlinear crystals, plasmas offer damage-free media capable of sustaining extreme laser intensities, enabling efficient harmonic generation through relativistic electron mass variations, ponderomotive forces, and density modulations [6]. Recent advancements in structured light beams, such as Laguerre-Gaussian, Bessel, and Airy modes, have revolutionised nonlinear optics by introducing spatially tailored intensity and phase profiles that enhance momentum transfer and nonlinear coupling efficiencies [7–9]. Among these, Hermite-cosh-Gaussian (HChG) beams stand out due to their hybrid transverse structure, combining the mode selectivity of Hermite polynomials with asymmetric intensity enhancement via hyperbolic cosine (cosh) modulation [10]. This unique profile enables precise control over electron dynamics in plasmas, making HChG beams ideal for studying high-order harmonic generation (HHG) and parametric instabilities [11,12].

Circularly polarised lasers, in contrast to linearly polarised counterparts, drive azimuthally symmetric electron motion in plasmas, suppressing deleterious effects like filamentation and Raman scattering while enhancing phase-matched nonlinear interactions [13,14]. Such polarisation-dependent dynamics are critical for SHG, where the rotational component of the electron quiver velocity generates coherent currents at twice the incident laser frequency. Despite extensive studies on SHG with

Gaussian and Laguerre-Gaussian beams [15]. The interplay between HChG beams, circular polarisation, and relativistic plasma Nonlinearities remain underexplored. This gap hinders the optimisation of structured light-plasma systems for applications in attosecond science, terahertz radiation, and plasma-based photonic devices [16,17]. HchG laser beam self-focusing in magnetically confined plasma with a density ramp profile was investigated by [18] they demonstrated that when $\mathrm{b} = 0$, where b being decentred beam parameter, the diffraction becomes the primary factor of nonlinear component for $\mathrm{m} = 0, 1,$ and 2.

Our results reveal how structured beams enable mode-selective SHG with spatially tunable profiles, offering advantages over conventional Gaussian beams. This study focuses on next generation photonic systems, providing insights into the design of plasma-based frequency converters and diagnostic tools for laser-driven fusion experiments [19,20]. Structured Light-Plasma Coupling they demonstrated that for HChG beam's transverse mode structure increases SHG efficiency through asymmetric ponderomotive gradients, a feature absent in standard Hermite-Gaussian beams [21]. By leveraging the azimuthal symmetry of circular polarization, we achieve phase-matched SHG with minimal parasitic instabilities, outperforming linear polarization schemes [22]. The derived scaling laws for SHG intensity versus beam parameters and plasma density provide actionable guidelines for experimentalists designing plasma-based optical devices [23].

Previous studies have explored SHG in plasmas using Gaussian and Laguerre-Gaussian beams, focusing on axial symmetry and orbital angular momentum effects. However, the HChG beam's hybrid profile introduces transverse mode mixing and localized intensity hotspots, which amplify nonlinear currents at specific spatial regions [24]. [25], In their investigation of the decentred parameter's impact on the relativistic self-focusing of the HchG laser beam in plasma, found that $\mathrm{m} = 2$ resulted in increased self-focusing [26], Stronger HchG beam focussing was demonstrated by [27] ,who also examined how the beam width parameter behaved at various decentred parameter and incoming laser beam frequency values.

Our work unifies these aspects, offering a comprehensive framework for SHG optimization in structured light-plasma systems.

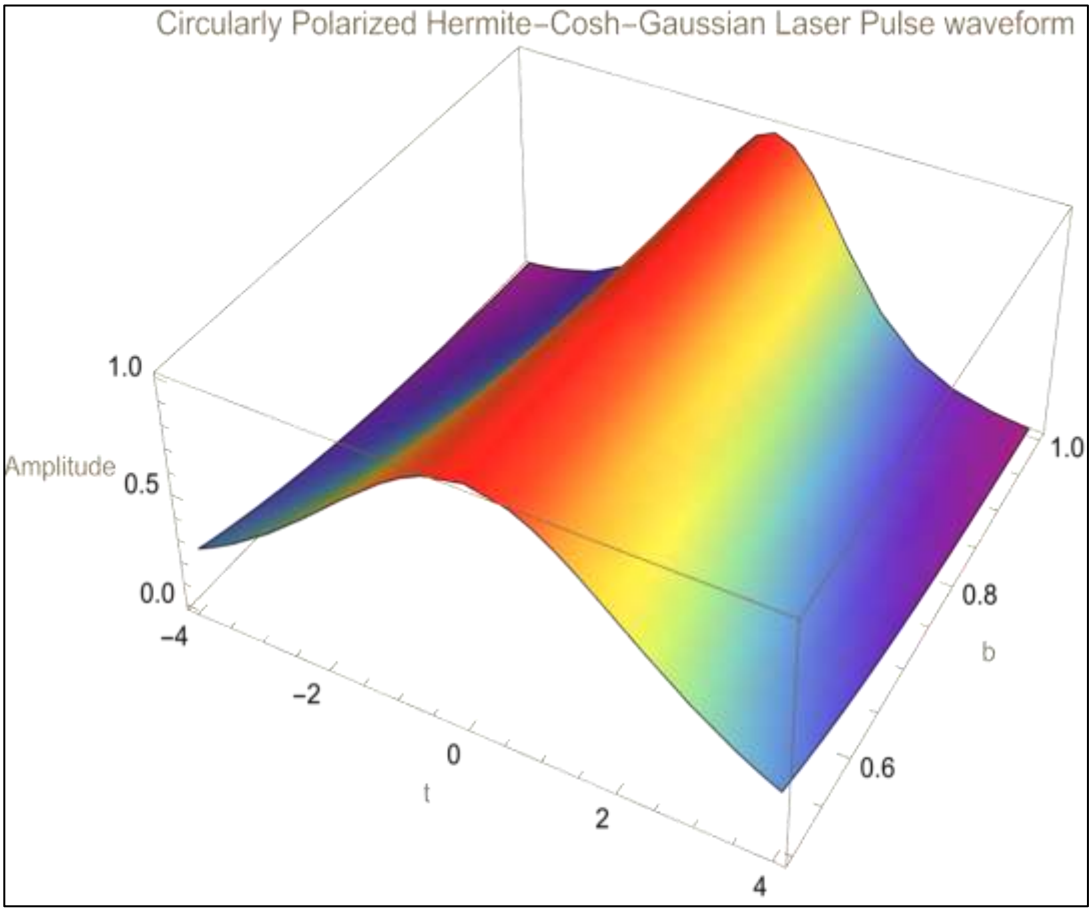

Fig. 5.1: The pulse wave shape of a Hermite cosh-Gaussian laser for decentered parameters $b = 0.5$ and 0.1

The decentred parameter b changes the form of the Circularly Polarised Hermite–Cosh–Gaussian (HCG) Laser Pulse waveform by changing the symmetry and peak location of the pulse. The waveform becomes more asymmetrical as b increases, with the peak moving away from the centre. In nonlinear optics and plasma physics usage, it entails that the pulse energy distribution will not be around the time axis, hence impinging upon laser interaction with a medium. This circular rotation of electric field components allows circular polarisation of the beam to provide greater energy transfer and interaction of matter. The hyperbolic cosine function yields an asymmetric distribution of intensities, which can be used to form the beam under controlled conditions. Because of their nonlinear propagation nature, HCG beams find applications in high-intensity laser applications as well. Their self-healing nature, which allows them to recover even after they have been affected in some way, makes them even more resilient for applications in optical systems. These beams' ability to undergo shape transformation through parameter modifications are most suitable for uses such as laser machining, optical trapping, and studies in complex plasma physics.

The manuscript follows a sectional format where in Section II, we calculated the normalised amplitude expressions. We then used the beam width parameter expressions that other colleagues had found to solve these equations numerically. The findings of results and discussions are presented visually in Section III. Conclusion of the findings is provided in Section IV.

5.2 Theoretical Framework

We have taken into consideration the strong Hermite cosh-Gaussian laser beam that strikes the plasma when there is wiggler field present. The electric field $\overrightarrow{E_1}$of the incoming laser and the wiggler field $\vec{B}_w$ are as follows

$$\overrightarrow{E_1}(r,t) = A\, H_m(x)\, H_m(y) \cosh\left(\frac{br}{r_0}\right) \cosh\left(\frac{br}{r_0}\right) \exp\left(\frac{-x^2+y^2}{r_0(z)^2}\right) \exp\left(i\left(kz-\omega t+\phi\right)\right)$$

(5.1)

$$\vec{B}_1 = \frac{c\vec{k}_1 \times \vec{E}_1}{\omega_1} \tag{5.2}$$

$$\vec{B}_w = \hat{y} B_0 \exp(ik_0 z) \tag{5.3}$$

Where $A = A_0(r,z)\exp{-ikS}$, (5.4)

$$A_0^2 = \frac{E_{20}^2}{f^2(z)}\left[H_m\left(\frac{\sqrt{2}r}{r_0 f(z)}\right)\right]^2 e^{\left(\frac{b^2}{2}\right)} + 2\exp\left[-\left(\frac{2r^2}{r_0^2 f(z)^2}+\frac{b^2}{2}\right)\right] \tag{5.5}$$

where A_0 and S being real functions of 'r' and 'z'. A_0 is maximum amplitude of incident laser, k being wave vector of fundamental laser $\vec{k}_0$ is wiggler wave number A is varying amplitude of incident pulse. The Hermite function is denoted by H_m while b signifies the decentered parameter.

Because of the incoming laser's electromagnetic field, electrons achieve oscillatory velocity, which is as under

$$\vec{v}_1 = e\frac{\vec{E}_1(r,t)}{mi(\omega_1+iv)} \tag{5.6}$$

In order to generate second harmonic current density $\vec{J}_2$ density perturbation beats with velocity $\vec{v}$. The beam spatial extent for each mode of Hermite cosh Gaussian beam is given as [27].

For $m = 0$

$$\frac{\partial^2 f(z)}{\partial \xi^2} = \left[4\text{-}4\,b^2\text{-}\frac{6\alpha E_0^2 m_0}{M\gamma}\left(\frac{\omega_1^2 r_0^2}{c^2}\right)\left(\frac{\omega_p^2}{\omega_1^2}\right)\text{Exp}\left[\frac{b^2}{2}\right]\,\right]\frac{1}{f^3(z)} \tag{5.7}$$

For $m = 1$

$$\frac{\partial^2 f(z)}{\partial \xi^2} = \left[4\text{-}4\,b^2\text{-}\frac{12\alpha E_0^2 m_0}{M\gamma}\left(\frac{\omega_1^2 r_0^2}{c^2}\right)\left(\frac{\omega_p^2}{\omega_1^2}\right)\text{Exp}\left[\frac{b^2}{2}\right]\left(b^2\text{-}2\right)\,\right]\frac{1}{f^3(z)} \tag{5.8}$$

For $m = 2$

$$\frac{\partial^2 f(z)}{\partial \xi^2} = \left[\text{-}8\,b^2\text{-}\frac{24\alpha E_0^2 m_0}{M\gamma}\left(\frac{\omega_1^2 r_0^2}{c^2}\right)\left(\frac{\omega_p^2}{\omega_1^2}\right)\text{Exp}\left[\frac{b^2}{2}\right]\left(5\text{-}2b^2\right)\right]\frac{1}{f^3(z)} \tag{5.9}$$

The second harmonic field's wave equation may be shown as follows

$$\nabla^2\vec{E}_2 = \epsilon_0 + \frac{\phi\left(E_1\,E^*\right)}{c^2}\frac{\partial^2\vec{E}_2}{\partial t^2}\,\frac{4\pi}{c^2}\frac{\partial\vec{J}_2^{NL}}{\partial t} + \frac{1}{c^2}\frac{\partial^2\vec{J}_2^{L}}{\partial t^2}, \tag{5.10}$$

This equation can be further written as

$$\nabla^2\vec{E}_2 + \left[\left(\frac{4\omega_1^2\text{-}5\omega_p^2}{c^2}\right) + \frac{4\omega_1^2\varphi\left(\vec{E_1}\,\vec{E_1^*}\right)}{c^2}\right]\vec{E}_2 = \frac{4\pi}{c^2}\frac{\partial\vec{J}_2^{NL}}{\partial t} \tag{5.11}$$

Where $\vec{J}_2 = \vec{J}_2^L + \vec{J}_2^{NL}$, and $\vec{J}_2^L$ and $\vec{J}_2^{NL}$ are linear and nonlinear current densities.

Now particular integral of Eq. (5.10) would be

$$\vec{E}_2 = A'_2 \mathrm{Exp}[-i\{2\omega_1 t - k_2 z\}] \tag{5.12}$$

$$A'_2 = A'_{20}(Z)\psi_2 \tag{5.13}$$

$$\psi_2 = \left\{\mathrm{Exp}\left[-4\left(\frac{r}{r_0 f(z)} + \frac{b}{2}\right)^2\right] + \mathrm{Exp}\left[-4\left(\frac{r}{r_0 f(z)} - \frac{b}{2}\right)^2\right] + 2\mathrm{Exp}\left[-2\left(\frac{2r^2}{r_0^2 f^2(z)} + \frac{b^2}{2}\right)\right]\right\}^{\frac{1}{2}} \exp(-ik_2 S) \tag{5.14}$$

Using Eqs. (5.12) & (5.14) into Eq. (5.10) we obtained

$$-2i(2k_1 + k_0)\left[\psi_2 \frac{\partial A'_{20}}{\partial z} + +A'_{20}\frac{1}{2}\psi_2\left(\frac{8r^2}{r_0^2 f^3(z)}\right)\left(\frac{\partial f}{\partial z}\right) + A'_{20}\frac{1}{2}\gamma^{-\frac{1}{2}}\left(\frac{2br}{r_0 f^2(z)}\right)\left(\frac{\partial f}{\partial z}\right)\left\{\mathrm{Exp}\left[-4\left(\frac{r}{r_0 f(z)} + \frac{b}{2}\right)^2\right] - \mathrm{Exp}\left[-4\left(\frac{r}{r_0 f(z)} - \frac{b}{2}\right)^2\right]\right\}\right] + A'_{20}\left(-i(2k_1 + k_0)\right)^2 +$$

$$A'_{20}\left\{\begin{array}{c}\left(-\frac{4}{r_0^2 f^2(z)}\right)\psi_2 + \left(\frac{16r^2}{r_0^4 f^4(z)}\right)\psi_2 + \left(\frac{8br}{r_0^3 f^3(z)}\right)\gamma^{-\frac{1}{2}} + \\ \frac{1}{2}\left(-\frac{8r}{r_0^2 f^2(z)}\right)\psi_2 + \frac{1}{2}\left(\frac{-4b}{r_0 f(z)}\right)\gamma^{-\frac{1}{2}}\left\{\mathrm{Exp}\left[-4\left(\frac{r}{r_0 f(z)} + \frac{b}{2}\right)^2\right] - \mathrm{Exp}\left[-4\left(\frac{r}{r_0 f(z)} - \frac{b}{2}\right)^2\right]\right\}\end{array}\right\} +$$

$$\left[\left(\frac{4\omega_1^2 - 5\omega_p^2}{c^2}\right) + \frac{4\omega_1^2 \varphi(\vec{E}_1 \vec{E}_1^*)}{c^2}\right] A'_{20}\psi_2 = \frac{4\pi\, \partial \vec{J}_2^{NL}}{\exp[-i\{2\omega_1 t - (2k_1 + k_0)z\}] c^2\, \partial t} \tag{5.15}$$

Multiplying Eq. (5.15) by $r\psi_2^*$ so then integrating with respect to r we obtained

$$-4i\left[\frac{\partial A''_{20}}{\partial \xi}\{1-b^2\}\cosh^2\left(\frac{br}{r_0}\right)\right] +$$

$$\left\{\begin{array}{l}-\frac{8r_0^2\omega_1^2}{c^2}\left(1-\frac{\omega_p^2}{4\omega_1^2}\right)\{1-b^2\} + \left\{\left(-\frac{16}{f^2(z)}\right)\{1-b^2\} + \left\{\left(\frac{24b^2}{f^2(z)}\right)\{1-b^2\}\right\}\right\} \\ -\left(\frac{2b^2}{f^2(z)}\right)\Big)\exp(-2)\cosh^2\left(\frac{br}{r_0}\right) + \frac{\omega_1^2 r_0^2}{c^2}\left[\left(4-\frac{5\omega_p^2}{\omega_1^2}\right) + 4\phi(E_1 E_1^*)\right]2\{1-b^2\}\cosh^2\left(\frac{br}{r_0}\right)\end{array}\right\} =$$

$$\frac{r_0^2\omega_p^2 n_0}{c^2\gamma}\left(\frac{eB_W}{m\omega_1 c}\right)\left(\frac{eA_{10}}{m\omega_1 c}\right)\left(+2\left(1-\frac{\omega_p^2}{4\omega_1^2}\right)^{\frac{1}{2}} - \frac{1}{4}\left(1-\frac{\omega_p^2}{\omega_1^2}\right)^{\frac{1}{2}}\right)\{1-b^2\}\cosh^2\left(\frac{br}{r_0}\right) \tag{5.16}$$

$$\phi(E_1 E_1^*) = \frac{\omega_p^2}{\omega_1^2}\left[1 - \exp\left(-\frac{3m_0}{4M}\alpha E_0^2\right)\right] \tag{5.17}$$

putting the above value of $\phi\left(E_1 E_1^{*}\right)$ in equation 5.16 we got the final equation as

$$-4i\left[\frac{\partial A''_{20}}{\partial \xi}\left\{1\text{-}b^2\right\}\cosh^2\left(\frac{br}{r_0}\right)\right]+$$

$$\left\{\begin{array}{l} -\frac{8r_0^2\omega_1^2}{c^2}\left(1\text{-}\frac{\omega_p^2}{4\omega_1^2}\right)\left\{1\text{-}b^2\right\}+\left\{\left(-\frac{16}{f^2(z)}\right)\left\{1\text{-}b^2\right\}+\left\{\left(\frac{24b^2}{f^2(z)}\right)\left\{1\text{-}b^2\right\}\right\}\right\} \\ -\left(\frac{2b^2}{f^2(z)}\right)\Bigg)\exp(-2)\ \cosh^2\left(\frac{br}{r_0}\right)+\frac{\omega_1^2 r_0^2}{c^2}\left[\left(4\text{-}\frac{5\omega_p^2}{\omega_1^2}\right)+\right. \\ \qquad 4\frac{\omega_p^2}{\omega_1^2}\left[1\text{-}\exp\left(-\frac{3m_0}{4M}\alpha E_0^2\right)\right]\Big]2\left\{1\text{-}b^2\right\}\cosh^2\left(\frac{br}{r_0}\right) \end{array}\right\} A''_{20} =$$

$$\frac{r_0^2\omega_p^2 n_0}{c^2}\gamma\left(\frac{eB_W}{m\omega_1 c}\right)\left(\frac{eA_{10}}{m\omega_1 c}\right)\left(+2\left(1\text{-}\frac{\omega_p^2}{4\omega_1^2}\right)^{\frac{1}{2}}-\frac{1}{4}\left(1\text{-}\frac{\omega_p^2}{\omega_1^2}\right)^{\frac{1}{2}}\right)\left\{1\text{-}b^2\right\}\cosh^2\left(\frac{br}{r_0}\right) \tag{5.18}$$

Where $A''_{20} = A'_{20}/A_{10}$ is the normalised amplitude for second harmonic pulse.

5.3 Results and discussion

Eqs. (5.7), (5.8), (5.9) and (5.18) these equations are solved through numerical computation at optimal values of various laser parameters we have taken into consideration intensity of laser $I = 1.024 \times 10^{22}\,\mathrm{W/cm^2}$, $\omega_1 = 1.2 \times 10^{16}\mathrm{rad/s}$ width of the incoming laser beam $50\mu\mathrm{m}$ and wiggler field strength is $20\,\mathrm{T}$, $\omega_1 r_0/c = 18$, $\varepsilon_2 A_{10}^2/\varepsilon_0 = 1$, $eA_{10}/m\omega_1 c = 3$, $eB_w/m\omega_1 c = 3$, and $\omega_p/\omega_1 = 0.9$ and obtained results are represented graphically.

The width of the pumping laser varies with normalised distance of propagation because to decentred beam characteristics, self-focusing, and diffraction. The intensity peak is pushed off-axis by a decentred beam, which causes asymmetric development during transmission. The beam stability and energy distribution are impacted by the non-uniform focussing or divergence that results from this. For effective laser-plasma interaction, beam width fluctuation must be managed by appropriately adjusting the decentred beam parameter.

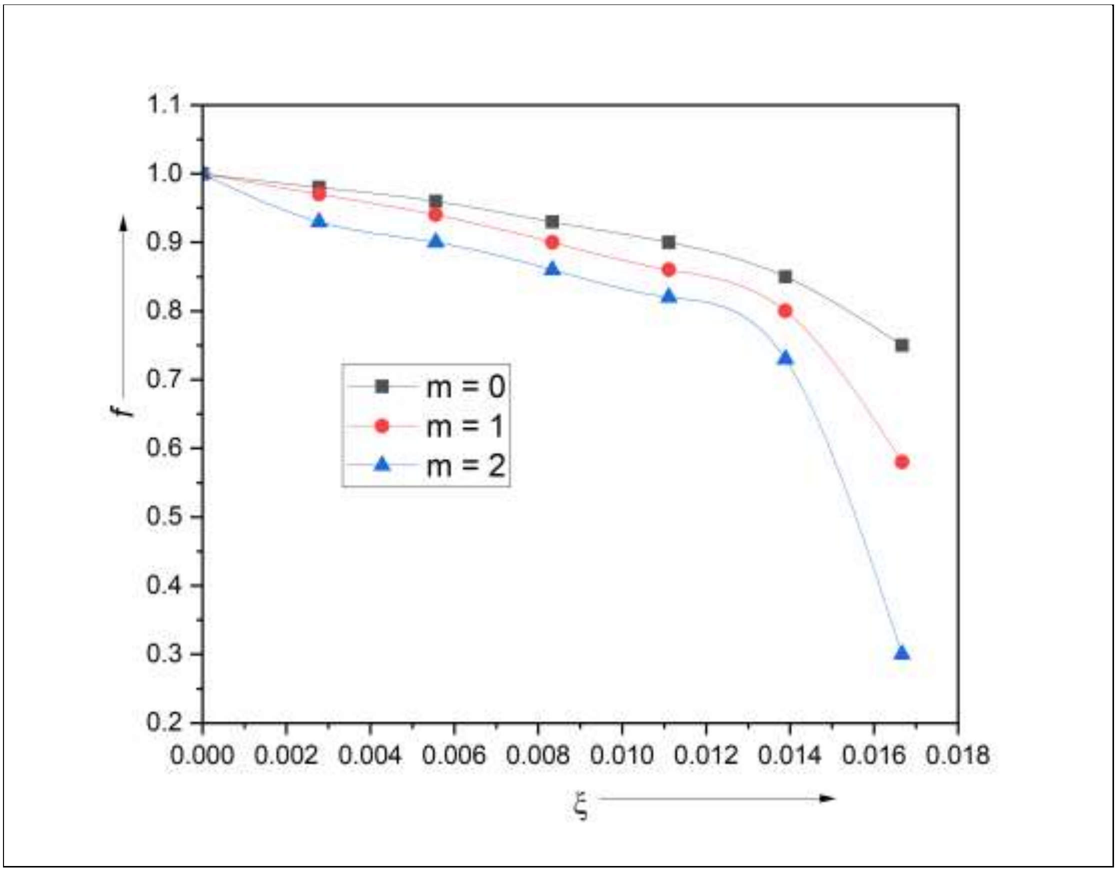

Fig. 5.2. For $m = 0, 1, and\ 2$, how (f) varies with ξ is evaluated for the primary laser.

(i) Effect of intensity on amplitude of second harmonic pulse

The pulse's amplitude is greatly affected with the power of a fundamental laser pulse because of the enhanced nonlinear interactions in the plasma. More second harmonics are produced when nonlinear polarisation is encouraged by higher intensity. However, phase matching may be disrupted by relativistic effects and plasma instabilities beyond a certain threshold, which would reduce the efficiency of harmonic conversion. The optimal intensity range is required to get maximum second harmonic amplification. The fluctuation of normalized second harmonic field versus ξ at varying values of incident laser pulse $eA_{10}/m\omega_1 c = 1,2,3$ being plotted in Fig.3. Similar findings were reported by [28], for the second harmonic production of a cosh Gaussian laser beam. They demonstrated that increased self-focusing causes the normalised amplitude of the second harmonic pulse to grow as laser power increases.

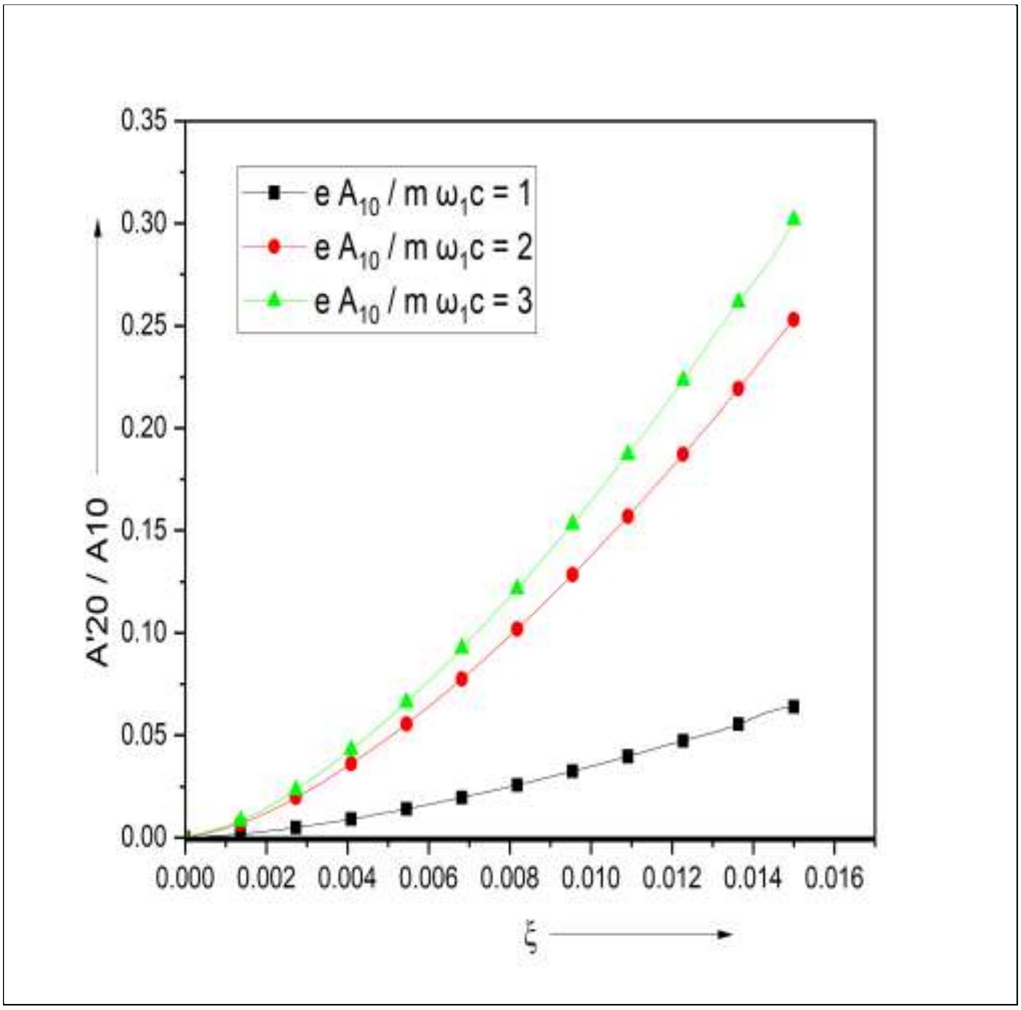

Fig. 5.3 The behaviour of normalised amplitude with distance ξ is analyzed for the various values of normalised intensity $eA_{10}/m\omega_1 c$ like 1,2 and 3.

(ii) Response of Wiggler magnetic field towards amplitude of second harmonic pulse

The second harmonic pulse's amplitude is greatly affected by the wiggler magnetic field, which modifies the electron pathways in the laser-plasma interaction. Electrons oscillate more transversely in stronger wiggler fields, which raises the nonlinear current density and encourages the creation of second harmonics. However, the efficiency of harmonic amplification may be diminished by phase mismatches caused by extremely strong fields. Fig.4 shows the variation of amplitude of pulse of circularly polarized beam with normalised distance ξ, at values of normalised wiggler magnetic field $eB_w/m\omega_1 c = 1,2$ &3 the values of normalised amplitude of second harmonic pulse 0.04 , 0.26 and 0.36 respectively. We deduced that the second harmonic pulse's amplitude increases dramatically at larger normalised wiggler magnetic field levels because the wiggler field satisfies the resonance criterion. It was shown by [29], that the third harmonic production of a Gaussian laser due to wiggler magnetic field exhibits a notable increase at higher wiggler field levels. Their peak for the normalised third harmonic amplitude was 0.132 while as in this present work maximum the value for a circularly polarized HcG beam is 0.36 so it means that the gain is more prominent when we have used circularly polarized Hermite cosh Gaussian beam.

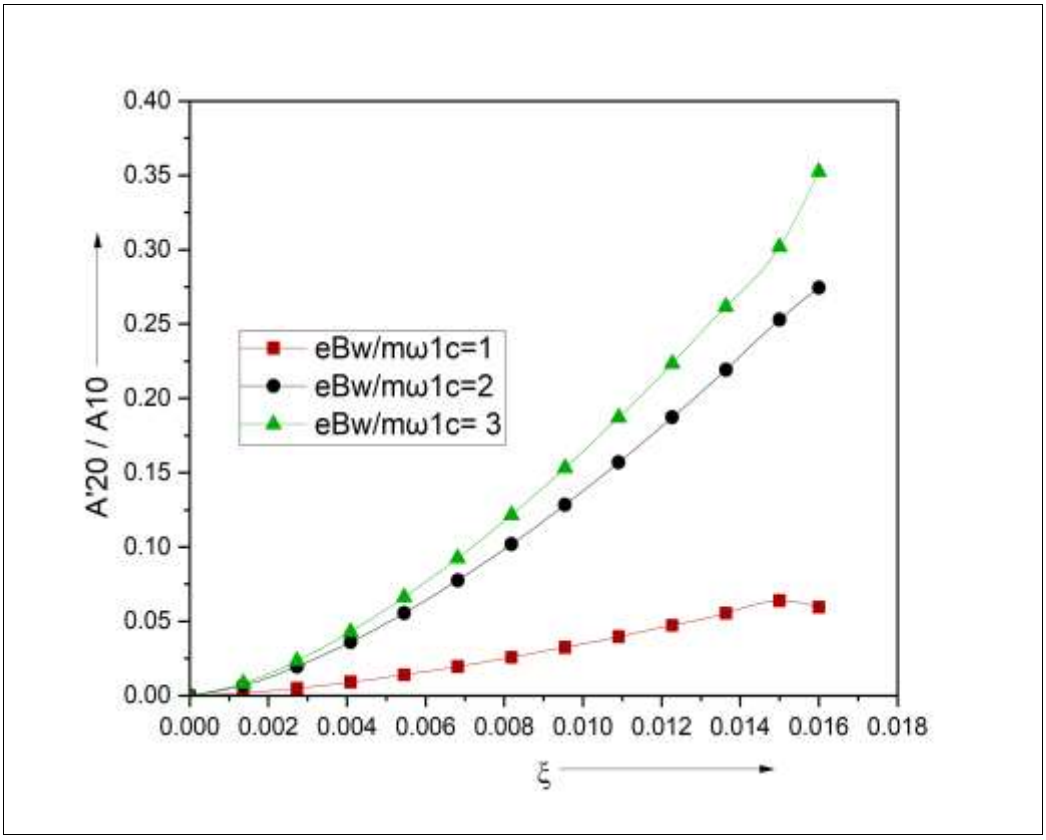

Fig. 5.4 The behaviour of the dimensionless second order amplitude A'_{20}/A_{10} with propagation distance ξ is analyzed for the various values of normalised wiggler magnetic field $eB_w/m\omega_1 c = 1,2$ and 3.

(iii) Effect of density on amplitude

The magnitude of the second order pulse to be greatly impacted by phase matching and nonlinear current generation, which are influenced by the plasma density. Because of the poor nonlinear response at low densities, fewer harmonics are produced. The amplitude shows a upward rise with density owing to the intensification of nonlinear coupling. However, dephasing effects and plasma absorption can reduce harmonic output at very high densities; for optimal efficiency, density optimisation is essential. Fig.5, depicts the alteration of normalised amplitude of second order frequency multiplied pulse, with respect to normalised propagation distance ξ. As when the density of plasma increases the pulse experiences a reduction in phase velocity which results in the increase of refractive index so there is enhanced efficiency [28], in their study demonstrated that normalised amplitude of the pulse for a beam with normalised distance showed zenith value of 0.38 , although our findings indicate the highest value of 0.39 which is better than previous work.

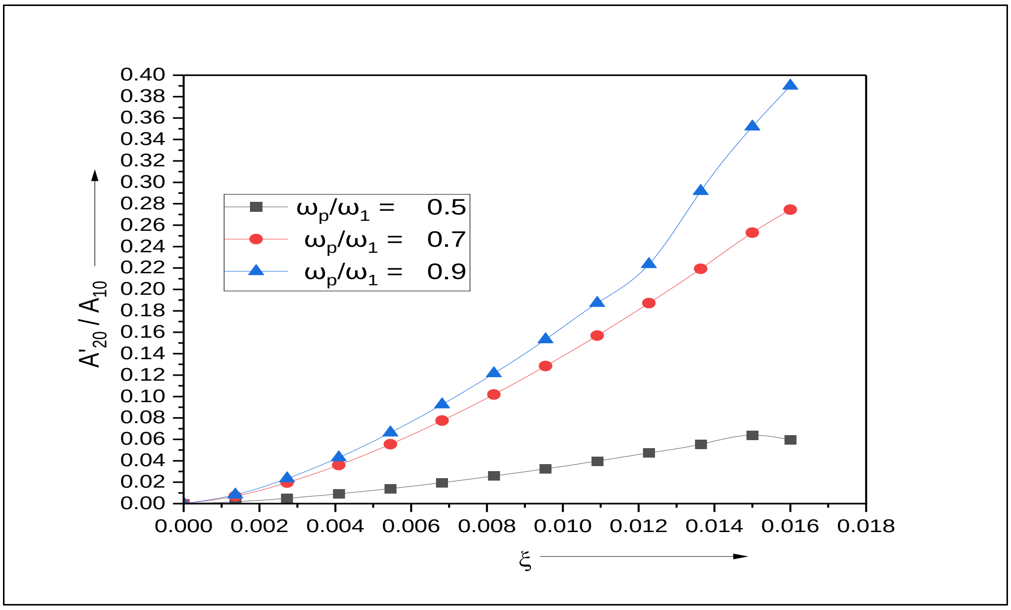

Fig. 5.5 For ω_p/ω_1 equal to $0.5, 0.7,$ and $0.9,$ the amplitude's dependence on ξ is investigated.

(iv) Effect of density on amplitude of second harmonic pulse

The normalised amplitude of second harmonic pulse varies with the normalised propagation for various decentred beam parameter values, which we have chosen to be $0.54, 0.56, 0.58$ as shown in Fig .6. It is observed that even a slight change in the beamwidth parameter causes the normalised pulse to vary thus showing the sensitivity of decentred beam parameter, as a minor variation in value of decentred beam parameter the normalised amplitude of circularly polarised Hermite cosh Gaussian beam increases rapidly. A minor variation in b from 0.54 to 0.58 amplitude varies from 0.45 to 0.58. [25], have presented similar study for Hermite cosh Gaussian beam in magnetic plasma and have discussed about the sensitivity of decentred beam width parameter with varying decentred parameter. In a recent study [30], showed that optimising laser intensity, wiggler magnetic field strength, and plasma density greatly increases third harmonic generation (THG) in magnetised plasma. Higher wiggler field strength and laser intensity caused the normalised amplitude to grow from 0.10 to 0.38, whereas changes in plasma density from 0.4 to 0.8 caused the amplitude to increase from 0.02 to 0.37. There was additional sensitivity to the decentred beam parameter, with minor changes impacting THG efficiency.

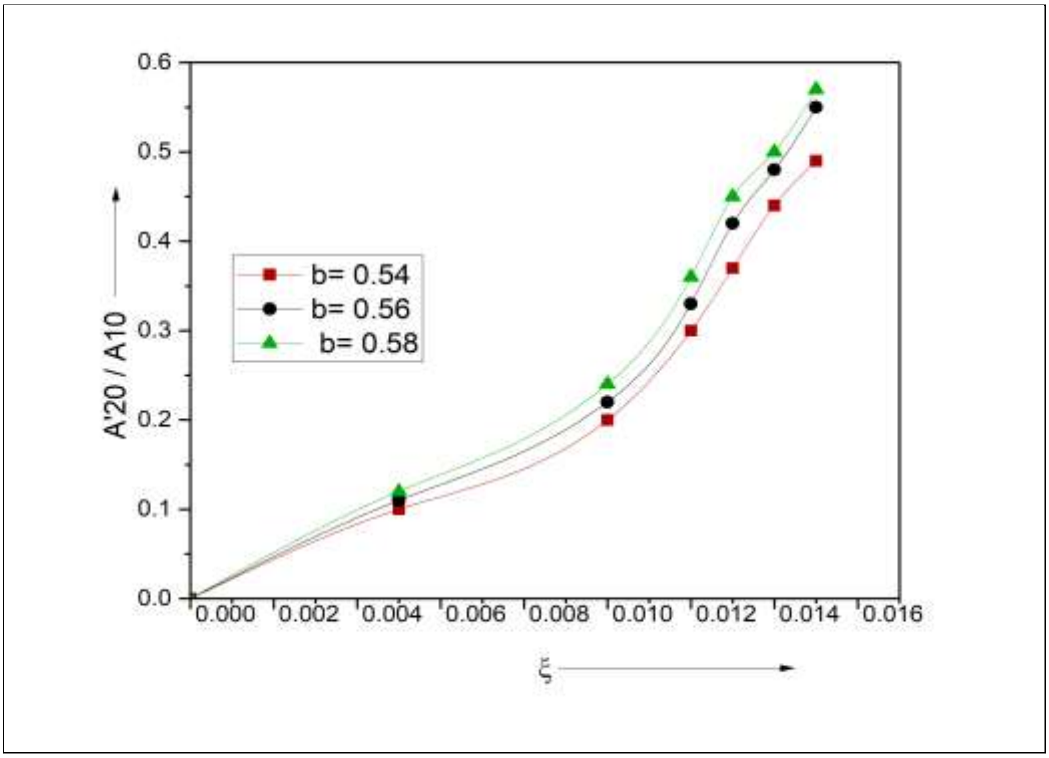

Fig. 5.6 Change in the normalized second harmonic amplitude A'_{20}/A_{10} with respect to the normalized propagation distance for different values of the decentring parameter $b = 0.54, 0.56 \& 0.58$.

5.4 Conclusion

The work demonstrates that structured light beams, especially HChG beams, significantly enhance SHG efficiency in magnetised plasmas. SHG performance is optimized by combining external magnetic fields, circular polarization, and structured beam profiles. The results demonstrate that SHG amplitude can be significantly enhanced by adjusting beam parameters, wiggler field strength $eB_w/m\omega_1 c = 3$, having amplitude value 0.36 and plasma density $\omega_p/\omega_1 = 0.9$, having amplitude value 0.39 making it highly relevant for high-intensity laser-plasma applications, such as terahertz radiation, attosecond research, and plasma-based photonic devices.

References

[1] Mourou G A, Tajima T and Bulanov S V , Optics in the relativistic regime *Reviews of modern physics,* **78** (2006) 309.

[2] Keikhosravi A, Bredfeldt J S, Sagar A K and Eliceiri K W , Second-harmonic generation imaging of cancer *Methods in cell biology* **123 (**2014**)** 531.

[3] Pavone F S and Campagnola P J , *Second harmonic generation imaging* (CRC Press Boca Raton) **56** (2014) 432

[4] Campagnola P J and Dong C-Y , Second harmonic generation microscopy: principles and applications to disease diagnosis *Laser & Photonics Reviews,* **5** (2011)13

[5] Xia C, Zhang H, Dong J, Xu W, Zhu G, Li Y, Gu B, Yang X, Shi Z, Xu C, and others, Visualizing Structural Defects at Hidden Interfaces of Micro-Optoelectronic Devices by Second Harmonic Generation Microscopy *ACS Applied Optical Materials,* **2 (**2024) 1566.

[6] Esarey E, Ting A, Sprangle P, Umstadter D and Liu X 1993 Nonlinear analysis of relativistic harmonic generation by intense lasers in plasmas *IEEE transactions on plasma science,* **21 (**1993**)** 95.

[7] Davis J, Mitry M, Bandres M and Cottrell D , Observation of accelerating parabolic beams *Optics Express,* **16** (2008) 12866

[8] Rubinsztein-Dunlop H, Forbes A, Berry M V, Dennis M R, Andrews D L, Mansuripur M, Denz C, Alpmann C, Banzer P, Bauer T, and others , Roadmap on structured light *Journal of Optics,* **19 (**2016) 013001

[9] Zhan Q , Cylindrical vector beams: from mathematical concepts to applications *Advances in Optics and Photonics* **1 (**2009) 57

[10] Kant N, Wani M A and Kumar A Self-focusing of Hermite–Gaussian laser beams in plasma under plasma density ramp *Optics Communications,* **285** (2012)4483

[11] Beier N and Dollar F Two-color high-harmonic generation from relativistic plasma mirrors *Physical Review E,* **108** (2023) 015201

[12] Sun W, Wang X and Zhang Y, Terahertz generation from laser-induced plasma *Opto-Electronic Science* **1** (2022) 220003

[13] Gleixner F and Kumar N Electronic parametric instabilities of an ultrarelativistic laser pulse in a plasma *Physical Review E,* **101** (2020) 033201

[14] Vodungbo B, Sardinha A B, Gautier J, Lambert G, Valentin C, Lozano M, Iaquaniello G, Delmotte F, Sebban S, Lüning J, and others ,Polarization control of high order harmonics in the EUV photon energy range *Optics express* **19** (2011)4346

[15] Bhatia A, Walia K and Singh A , Second-harmonic generation of intense Laguerre Gaussian Beam in collisional plasma: Effect of nonlinear absorption *Chinese Journal of Physics,* **81 (**2023) 206

[16] Kumar M, Tripathi V and Jeong Y U , Laser driven terahertz generation in hot plasma with step density profile *Physics of Plasmas* ,**22** (2015) 063106

[17] Rajpoot R and Takahashi E J , Systematic analysis of an attosecond pulse generation by a subcycle laser field *Phys. Rev. Res.* **7** (2025) 013047

[18] Nanda V, Kant N and Wani M A , Self-focusing of a Hermite-cosh Gaussian laser beam in a magnetoplasma with ramp density profile *Physics of Plasmas* ,**20** (2013) 47

[19] Danson C, Hillier D, Hopps N and Neely ,D Petawatt class lasers worldwide *High Power Laser Science and Engineering* **3** (2015) 3

[20] Rocca J J, Capeluto M G, Hollinger R C, Wang S, Wang Y, Kumar G R, Lad A D, Pukhov A and Shlyaptsev V N , Ultra-intense femtosecond laser interactions with aligned nanostructures *Optica*, **11** (2024)437

[21] Ali K, Kumar S, Mishra D, Kumar A and Varma A , Nonlinear absorption of Hermite cosh-Gaussian laser beam in an assembly of cylindrical carbon nanotubes embedded with static magnetic field *Optical and Quantum Electronics* **56 (**2024) 41

[22] Zhang Y X, Rykovanov S, Shi M, Zhong C L, He X T, Qiao B and Zepf M, Giant Isolated Attosecond Pulses from Two-Color Laser-Plasma Interactions *Phys. Rev. Lett.* **124** (2020) 114802

[23] Tan X, Song H, Ji Y, Tang H, Fang Y-Y, Xu X-Y, Li Y-Y, Li X-K, Zhu K-D and Jin X-M , Scalable and programmable three-dimensional photonic processor *Phys. Rev. Appl.* **20** (2023) 044041

[24] Baeva T, Gordienko S and Pukhov A ,Theory of high-order harmonic generation in relativistic laser interaction with Overdense plasma *Phys. Rev. E* **74** (2006) 046404

[25] Nanda V, Kant N and Wani M A , Sensitiveness of decentred parameter for relativistic self-focusing of Hermite-cosh-Gaussian laser beam in plasma *IEEE Transactions on Plasma Science* **41** (2013) 2251

[26] Patil S, Takale M, Navare S and Dongare M , Focusing of Hermite-cosh-Gaussian laser beams in collisionless magnetoplasma *Laser and Particle Beams* **28** (2010) 343

[27] Kant N and Nanda V , Stronger self-focusing of Hermite-Cosh-Gaussian (HChG) laser beam in plasma *Open Access Library Journal,* **1** (2014) 8

[28] Singh N, Gupta N and Singh A , Second harmonic generation of Cosh-Gaussian laser beam in collisional plasma with nonlinear absorption *Optics Communications* **381** (2016) 180

[29] Sharma H, Jaloree H and Parashar J , Magnetic wiggler-assisted third-harmonic generation of a Gaussian laser pulse in plasma *Turkish Journal of Physics* **37** (2013) 368

[30] Nazir D, Sharma V and Thakur V , Third Harmonic Generation of Cosh-Gaussian Laser Beam In Magnetized Plasma *Journal of Optics*, **1** (2025) 6

Chapter- 6

Optimized Third Harmonic Generation in Plasma Using a Cosh-Gaussian Beam with an Exponential Density Ramp

6.1 Introduction

High-intensity laser-plasma interactions have been a subject of great interest due to their wide range of applications in nonlinear optics, plasma diagnostics, and high-energy density physics [1–3]. One of the key nonlinear processes in such interactions is the generation of harmonics, wherein a fundamental laser beam undergoes frequency conversion due to plasma nonlinearities [4,5]. In particular, third harmonic generation (THG) has been extensively studied as a means to achieve high-frequency radiation sources and enhance laser energy deposition in plasma-based systems [6,7]. The efficiency of THG is highly dependent on plasma density gradients, which influence phase matching conditions and nonlinear susceptibility [8,9]. Among various beam profiles, the cosh-Gaussian beam has gained attention due to its unique intensity distribution, which provides enhanced confinement and self-focusing properties [10–12]. Unlike Gaussian or Hermite-Gaussian beams, the cosh-Gaussian beam exhibits a nontrivial transverse intensity modulation that affects its interaction with plasma waves, leading to modified nonlinear effects [13] . Laser-plasma interactions also exhibit strong nonlinear effects including self-focusing and phase modulation and relativistic nonlinearity, which significantly impact harmonic generation[14,15]. Additionally, ponderomotive force-driven plasma wave excitation plays a vital role in accessing the nonlinear current responsible for harmonic generation [16]. In plasma with density variation [17], the phase matching criteria for harmonic generation are significantly altered. The gradient of the density ramp influences the phase velocity of plasma waves, leading to either constructive or destructive interference in the harmonic signal. Proper tuning of the density ramp can optimize phase matching and maximize harmonic conversion efficiency. Several studies have shown that tailored plasma density profiles can improve nonlinear wave interactions, leading to more efficient harmonic generation and energy transfer.

Furthermore, the cosh-Gaussian beam structure itself introduces extra parameters of variability in shaping the laser-plasma interaction. Due to its localized intensity enhancement along the transverse direction, it allows better confinement of energy, reducing diffraction losses and enhancing nonlinear interactions. Such effects make cosh-Gaussian beams particularly suitable for plasma-based frequency conversion applications, including the generation of coherent extreme ultraviolet (EUV) and X-ray radiation [18]. In this current work, we analyse the third harmonic generation of a cosh-Gaussian laser beam traversing through an undersense plasma having exponential density ramp. We derive the governing equations for normalised amplitude third harmonic amplitude. Taking into account the modified susceptibility due to the density gradient. Using analytical approximations and numerical simulations, we explore modulation introduced by density ramp in the efficiency of the THG process. Our results provide new insights into optimizing frequency conversion in plasma-based nonlinear optical systems.

The paper is structured as follows: Section II presents the theoretical framework, including the laser field representation and wiggler field. Section III contains results and discussions. Section IV and V contains conclusions and references.

6.2 Theoretical framework

Consider an intense cosh –Gaussian laser beam propagating through plasma with electric and magnetic field as under

$$\vec{E}_1 = \hat{x}A_1(z,t)\exp\left[-i\left(\omega_1 t - k_1 z\right)\right], \quad (6.1)$$

$$\vec{B}_1 = \frac{c\vec{k}_1 \times \vec{E}_1}{\omega_1}, \quad (6.2)$$

$$\vec{B}_w = B_0 \exp(ik_0 z), \quad (6.3)$$

here $\overrightarrow{k_1}$ is unit vector repersenting number of waves of the fundamental laser, ω_1 represents its angular frequency, $\overrightarrow{B_1}$ corresponds to the associated laser magnetic field. The parameter c refers to the speed of light, k_0 indicates the wave number of the wiggler field and $A(z,r)$ stands for the amplitude profile of Gaussian beam expressed as,

$$A(z) = A_{10}(r,z)\text{Exp}[\text{-}ikS(r,z)] \tag{6.4}$$

In this context A_{10} and S be real valued functions the term A_{10} characterizes the unvarying amplitude of the fundamental laser pulse and is shown by the following expression,

$$A_{10}^2 = \frac{E_0^2}{f^2(z)}\text{Exp}\left[\frac{b^2}{2}\right]\left\{+2\,\text{Exp}\left[\text{-}\left(\frac{2r^2}{r_0^2 f^2(z)} + \frac{b^2}{2}\right)\right]\right\} \tag{6.5}$$

The ponderomotive force causes electrons to oscillate with a velocity expressed as

$$\vec{V}_1 = e\frac{\vec{E}_1}{mi(\omega_1 + iv)} \tag{6.6}$$

Driven by the ponderomotive force of an incident beam, electrons exhibit an oscillatory velocity at a certain frequency $2\omega_1$. The interaction of this velocity with a density ripple leads to a density perturbation at $2\omega_1$, ultimately producing a third harmonic current density. $\vec{J}_3 = \vec{J}_3^L + \vec{J}_3^{NL}$ [19], The subsequent linear and nonlinear expressions for current density are provided.

$$\vec{J}_3^L = \frac{n_0 e^2 \vec{E}_3}{3m_0\gamma i\omega_1} \tag{6.7}$$

$$\vec{J}_3^{NL} = \frac{\text{-}n_0 e^5 B_w k_1 \vec{E}_1^3}{16cim_0^4\gamma^4\omega_1^4(\omega_1 + iv)}\left[\frac{5k_1}{18\omega_1} + \frac{k_1 + k_0}{\omega_1 + iv}\right]\hat{x} \tag{6.8}$$

The third harmonic field is governed by the wave equation presented below,

$$\nabla^2\vec{E}_3 = \left[\frac{\varepsilon_0 + \varphi(E_1 E_1{}^*)}{c^2}\right]\frac{\partial^2\vec{E}_3}{\partial t^2} + \frac{4\pi}{c^2}\frac{\partial\vec{J}_3^{NL}}{\partial t} + \frac{4\pi}{c^2}\frac{\partial\vec{J}_3^L}{\partial t} \tag{6.9}$$

Also $\varepsilon = \varepsilon_0 + \varphi(E_1 E_1{}^*)$ (6.10)

where $\varphi(E_1 E_1{}^*) = \frac{\omega_p^2}{\omega_1^2}\left[1\text{-}\exp\left(\text{-}\frac{3m_0}{4M}\alpha E_0^2\right)\right]$ (6.11)

$k_1 = \omega_1/c\,(1\text{-}\omega_p^2/\omega_1^2)^{1/2}$, $\omega_p = (4\pi n_0 e^2/m_0\gamma)\exp(z/dR_d)$, $\omega_{p0}^2 = (4\pi n_0 e^2/m_0)$
therefore $k_1 = \omega_1/c(1\text{-}\omega_{p0}^2/\gamma\,\exp(z/dR_d))^{1/2}$

Using Eqs. (6.5), (6.6), (6.7) and (6.9) we have obtained a new equation as under

$$\nabla^2\vec{E}_3 + \left[\left(9\omega_1^2\text{-}\frac{10\omega_p^2}{c^2}\right) + \frac{9\omega_1^2\phi\left(\vec{E}_1\vec{E}_1^*\right)}{c^2}\right]\vec{E}_3 = \frac{4\pi}{c^2}\frac{\partial\vec{J}_3^{NL}}{\partial t} \tag{6.12}$$

The equation for the beam width parameter as proposed by Nanda et al.[20], is shown as

$$\frac{\partial^2 f(z)}{\partial\xi^2} = \left[4\text{-}4\,b^2\text{-}\frac{6\alpha E_0^2 m_0}{M}\left(\frac{\omega_1^2 r_0^2}{c^2}\right)\left(\frac{\omega_p^2}{\omega_1^2}\right)\text{Exp}\left[\frac{b^2}{2}\right]\frac{1}{f^3(z)}\right] \tag{6.13}$$

Here, b represents the off-centre beam parameter, and ξ denotes the normalized propagation distance."

The further solution of Eq. (6.9) gives us a particular integral

$$\vec{E}_3 = A_3'(z,t)\exp[\text{-}i(3\omega_1 t\text{-}k_3 Z)] \tag{6.14}$$

$$A_3' = A_{30}'(\psi_3) \tag{6.15}$$

$$\text{where } \psi_3 = \left\{\begin{matrix}\text{Exp}(\xi/d)\left[\text{-}6\left(\frac{r}{r_0 f(z)}+\frac{b}{2}\right)^2\right] + \text{Exp}(\xi/d)\left[\text{-}6\left(\frac{r}{r_0 f(z)}\text{-}\frac{b}{2}\right)^2\right] \\ +2\text{Exp}(\xi/d)\left[\text{-}3\left(\frac{2r^2}{r_0^2 f^2(z)}+\frac{b^2}{2}\right)\right]\end{matrix}\right\}^{\frac{1}{2}} \tag{6.16}$$

with the help of equations 6.11, 6.12 and 6.13 we got

$$
\begin{aligned}
&\Bigg\{\Bigg[\Bigg[\frac{\omega_1}{c}\left(1-\frac{1}{\omega_1^2}\left(\frac{4\pi n_0 e^2}{m_0\gamma}\right)\exp\left(\frac{z}{dR_d}\right)\right)^{1/2} - z\frac{\omega_{p0}^2\exp(z/dR_d)}{2c\gamma dR_d\omega_1\left(1-\frac{\omega_{p0}^2}{\gamma\omega_1^2}\exp(z/dR_d)\right)^{1/2}}\Bigg] \\
&\qquad\Bigg\{-\left(\frac{1}{f}\frac{\partial f}{\partial z}\frac{r^2}{2}+\phi(z)\right)\frac{\omega_{p0}^2\exp(z/dR_d)}{2c\gamma dR_d\omega_1\left(1-\frac{\omega_{p0}^2}{\gamma\omega_1^2}\exp(z/dR_d)\right)^{1/2}} \\
&\qquad+\frac{\omega_1}{c}\left(1-\frac{1}{\omega_1^2}\left(\frac{4\pi n_0 e^2}{m_0\gamma}\right)\exp\left(\frac{z}{dR_d}\right)\right)^{1/2}\left(\frac{r^2}{2}\left(\frac{1}{f}\frac{\partial^2 f}{\partial z^2}\right)+\frac{\partial\phi}{\partial z}\right)\Bigg\} \\
&-\hat{x}A_{10}\Bigg[\Bigg[\frac{\omega_1}{c}\left(1-\frac{1}{\omega_1^2}\left(\frac{4\pi n_0 e^2}{m_0\gamma}\right)\exp\left(\frac{z}{dR_d}\right)\right)^{\frac{1}{2}} - z\frac{\omega_{p0}^2\exp\left(\frac{z}{dR_d}\right)}{2c\gamma dR_d\omega_1\left(1-\frac{\omega_{p0}^2}{\gamma\omega_1^2}\exp\left(\frac{z}{dR_d}\right)\right)^{\frac{1}{2}}}\Bigg]\Bigg]^2 + \\
&\qquad\hat{x}(z,t)\left[\left(\frac{A_{10}r^2}{r_0^4 f^5}-\frac{A_{10}}{r_0^2 f^3}\right)-A_{10}k_1^2\left(r\frac{1}{f}\frac{\partial f}{\partial z}\right)^2\right]+\hat{x}(z,t)\frac{1}{r}\left[\frac{-A_{10}r}{r_0^2 f^3}\right] \\
&\qquad-\left[\frac{10\omega_p^2-9\omega^2}{c^2}-\frac{9\omega^2}{c^2}\frac{\omega_p^2}{\omega_1^2}\left[1-\exp\left(-\frac{3m_0}{4M}\alpha E_0^2\right)\right]\right]A_{10} = 0\Bigg]\Bigg\}
\end{aligned}
$$

(6.17)

Equating coefficient of $r^2 = 0$ we got

$$
\begin{aligned}
&2i\{2-b^2\}\Bigg(-\frac{\xi\exp(\xi/d)}{6\gamma d\left(1-\frac{\omega_{p0}^2}{\gamma 9\omega_1^2}\exp(\xi/d)\right)^{\frac{1}{2}}}\left(\frac{\omega_{p0}^2}{\omega_1^2}\right)+ \\
&\left[\left(1-\left(\frac{1}{9\gamma}\right)\left(\frac{\omega_{p0}^2}{\omega_1^2}\right)\exp(\xi/d)\right)^{\frac{1}{2}}\right]\left\{\frac{\partial A_{30}^*}{\left(1-\frac{\omega_p^2}{\omega_1^2}\right)^{\frac{1}{2}}\partial\xi}\left(\frac{f_1^2}{3}\right)\right\}-\frac{i\xi}{\gamma d}\left[\begin{matrix}-\frac{1}{6\gamma d(1-\frac{\omega_{p0}^2}{\gamma 9\omega_1^2}\exp(\xi/d))^{\frac{1}{2}}}\\ +[(1-(\frac{1}{9\gamma})\exp(\xi/d))^{\frac{1}{2}}]\end{matrix}\right]\left\{\frac{A_{30}f_1^4}{\left(1-\frac{\omega_p^2}{\omega_1^2}\right)}\left(i\frac{\partial f_1}{f_1\,\partial\xi}\frac{1}{4}\right)\left(\frac{\omega_{p0}^2}{\omega_1^2}\right)^2\left[\frac{(\exp(\xi/d))^2}{\left(1-\left(\frac{1}{\gamma}\right)\left(\frac{\omega_{p0}^2}{\omega_1^2}\right)\exp(\xi/d)\right)^{1/2}}\right]\right\}+ \\
&i\frac{A_{30}''}{\left(1-\frac{\omega_p^2}{\omega_1^2}\right)^{\frac{1}{2}}}\left(\frac{\omega_{p0}^2}{\omega_1^2}\right)\left[-\frac{3\xi\omega_{p0}^2\exp(\xi/d)}{2\gamma d^2 9\omega_1^2\left(1-\frac{\omega_{p0}^2}{\gamma 9\omega_1^2}\exp(\xi/d)\right)^{\frac{1}{2}}}-\frac{3f_1^2\xi(\exp(\xi/d))^2}{4(\gamma d 9)^2\left(1-\frac{\omega_{p0}^2}{\gamma 9\omega_1^2}\exp(\xi/d)\right)^{\frac{3}{2}}}\left(\frac{\omega_{p0}^2}{\omega_1^2}\right)-\frac{f_1^2\exp(\xi/d)}{3\gamma d\left(1-\frac{\omega_{p0}^2}{\gamma 9\omega_1^2}\exp(\xi/d)\right)^{\frac{1}{2}}}\right]\left(\frac{-1}{6}\right)i^2 A_{30}''R\Bigg(-\frac{\xi\exp(\xi/d)}{6\gamma d\left(1-\frac{\omega_{p0}^2}{\gamma 9\omega_1^2}\exp(\xi/d)\right)^{\frac{1}{2}}}\left(\frac{\omega_{p0}^2}{\omega_1^2}\right)^2+ \\
&9\left(1-\left(\frac{\omega_{p0}^2}{9\omega_1^2\gamma}\right)\exp(\xi/d)\right)^{\frac{1}{2}}\Bigg]^2\left(-\frac{r_0^2\omega_1 f_1^2}{c^2 6}\right)+A_{30}''(z)+A_{30}'(z)-\left[\frac{10\omega_p^2}{\omega_1^2}-9\frac{\omega_p^2}{\omega_1^2}\left[1-\exp\left(-\frac{3m_0}{4M}\alpha E_0^2\right)\right]\right]\{2-b^2\}A_{30}''(z)\left(-\frac{f_1^2}{6}\right)\left(\frac{r_0^2\omega_1^2}{c^2}\right)= \\
&-\frac{1}{16\gamma^4}\left(\frac{\omega_p^2}{\omega_1^2}\right)\left(\frac{r_0^2\omega_1^2}{c^2}\right)\left(1-\frac{\omega_p^2}{\omega_1^2}\right)^{1/2}\left(\frac{e^2A_{10}^2}{m^2c^2\omega_1^2}\right)\left(\frac{eB_w}{mc\omega_1}\right)\left[3\left(1-\frac{\omega_p^2}{9\omega_1^2}\right)^{1/2}-31\left(1-\frac{\omega_p^2}{\omega_1^2}\right)^{1/2}\right]\{2-3b^2\}
\end{aligned}
$$

(6.18)

The equation (6.18) is the final equation of the amplitude.

6.3 Results and Discussion

To evaluate the effectiveness of third -order harmonic generation, we numerically solve the coupled wave equations considering the nonlinear polarization induced by the cosh-Gaussian laser in plasma .The results highlight the role of density gradients, phase matching conditions, and beam self-focusing on THG efficiency.

(i) Dependence of (f) on (ξ).

In a plasma medium, the optical density is influenced the local electron density. When an exponential density ramp is introduced, the electron density gradually increases along the direction of laser propagation. This spatial variation reduces the refractive index progressively, creating an inhomogeneous optical environment for the beam.

Fig.1 demonstrates that how f varies with propagation distance ξ. It is observed that f has its minimum value 0.43 at $\xi = 1.45$ and in presence of a gradual density variation minimum value of f at $\xi = 1.45$ is 0.13, which depicts that with increase in plasma density, the nonlinear refractive index increases result stronger self-focusing. Due to ponderomotive force electrons expelled from low plasma density region and due to highly intense beam the mass variation takes place. Due to this relativistic nonlinearity arises results stronger self-focusing. On introducing the density ramp plasma density further increases results decrease in refractive index and self- focusing becomes stronger and f decreases significantly. So, the laser beam experiences a stronger refractive gradient, which acts like a negative lens. This increased divergence leads to a faster reduction in f, as observed in the red dashed curve. The ramped density disrupts the balance between diffraction and any self-focusing effects, causing the beam to spread more rapidly. Valkunde et al.[21] reported comparable findings for a q-Gaussian laser pulse propagating through both uniform and exponentially varying plasma densities, demonstrating that self-focusing effects are significantly enhanced in the presence of an exponential density ramp. Gupta et al.[22] observed that f exhibits oscillatory behaviour under uniform plasma conditions, while the introduction of a density ramp allows f to retain its minimum value over an extended propagation distance.

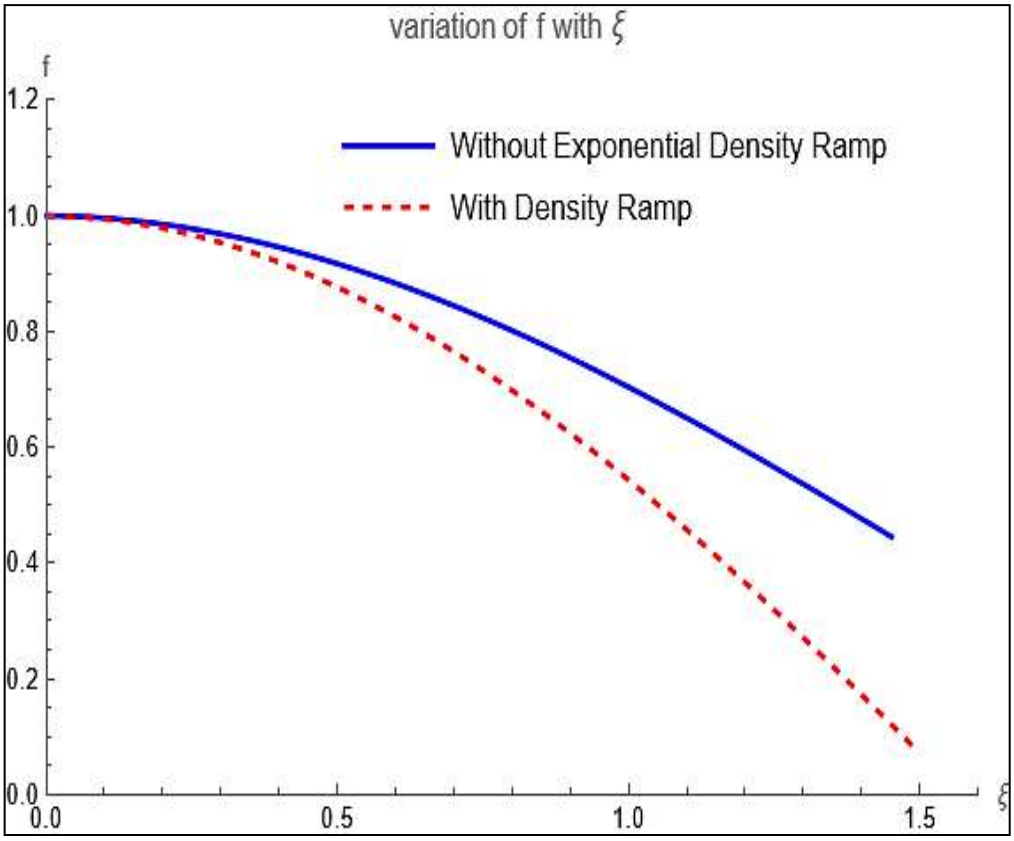

Fig. 6.1 Variation of beam width f parameter with normalised propagation distance ξ with and without density ramp.

(ii) Variation in laser power directly influences the strength of the resulting wave oscillations.

As depicted in the graph, an increase in the normalized laser amplitude $eA_{10}/m\omega_1 c$ leads to a significant enhancement in the normalized third harmonic amplitude A'_{30}/A_{10} with propagation distance ξ. However, as the laser intensity increases, relativistic and ponderomotive effects become more prominent, leading to stronger electron oscillations and enhanced nonlinear currents at 3ω. These effects collectively amplify the third harmonic signal over the course of propagation. Consequently, higher input intensities as a result more efficient energy conversion from the fundamental to the third harmonic, making laser intensity a critical parameter in optimizing third harmonic generation in plasma.

Figure 2 demonstrates how A'_{30}/A_{10} varies with distance ξ at values of $eA_{10}/m\omega_1 c = 1,3$ &5 corresponding values of $A'_{30}/A_{10} = 0.05,0.26$ &0.43 respectively at value of $\xi = 1.6$ gaining the peak value and so after that defocusing comes into play. Thakur and Kant have also studied that there is gain in the amplitude for different $eA_{10}/m\omega_1 c$ values under the influence of plasma density ramp.[23]

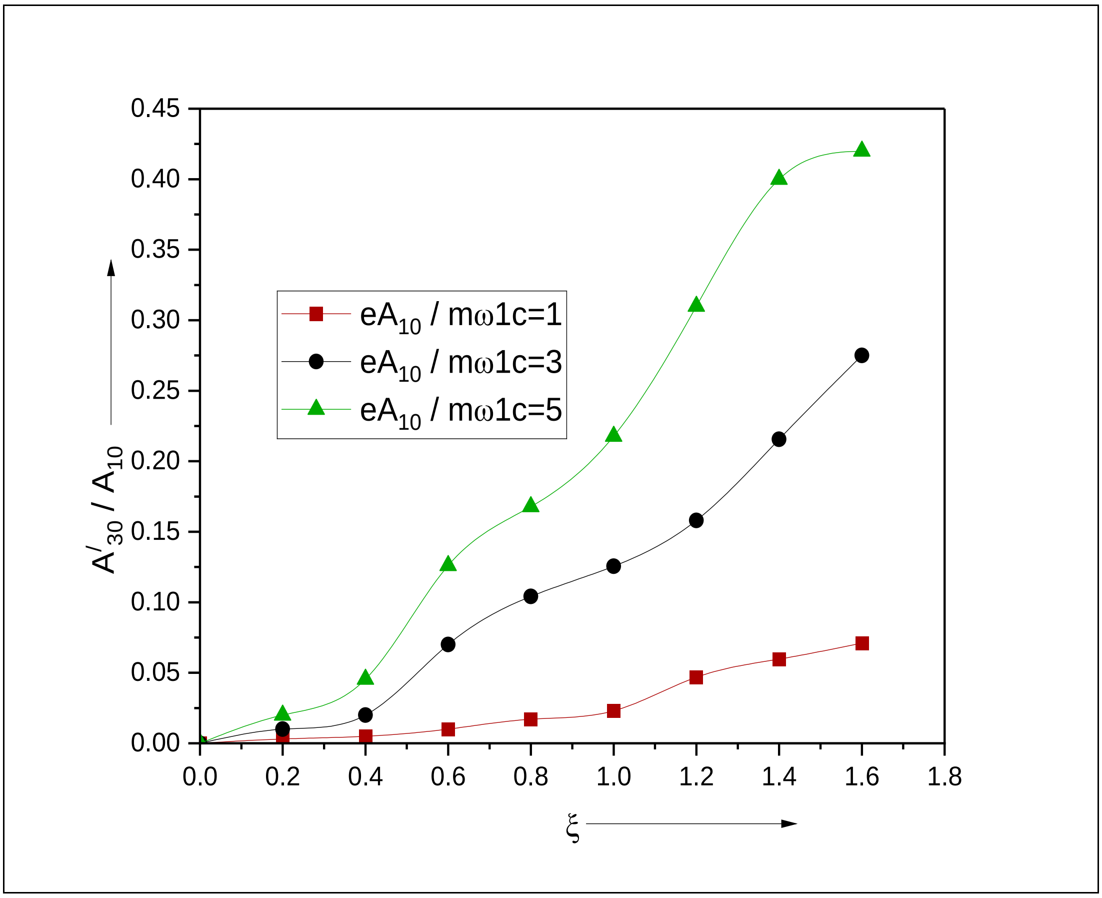

Fig. 6.2 Evolution of amplitude with ξ for various values of normalised intensity $eA_{10}/m\omega_1 c$ like 1,3 and 5.

(iii) Amplitude modulation under influence of wiggler field

The externally applied transverse magnetic field induces additional oscillatory motion of electrons by exerting a electromagnetic force, causing them to follow helical trajectories. As a result, the electron quiver motion becomes more intense, even at moderate laser intensities, leading to an increase in the strength of current sources which led to third harmonic generation. This enhancement in nonlinear currents amplifies the third harmonics. Additionally, wiggler field breaks symmetry of the interaction system, which favours the generation of odd harmonics such as the third harmonic, even under conditions where they would otherwise be suppressed. In certain configurations, the magnetic field can also resonantly couple with the laser driven motion, further boosting harmonic generation efficiency. When field strength rises, the nonlinear coupling also increases thus the wiggler magnetic field acts as an effective control parameter, significantly enhancing third harmonics in magnetized plasma. Figure 3 shows variation of A''_{30}/A_{10} with distance of propagation ξ for the multiple values of $eB_w/mc\omega_1 = 0.001, 0.003$ &0.005. It is seen that $A''_{30}/A_{10} =$ 0.05,0.17 &0.23 at the value of $\xi = 1.6$. Vaziri et al. investigated (SHG) for varying strengths of the wiggler field and found that the normalized SHG amplitude increases as the magnetic field intensity rises.[24]

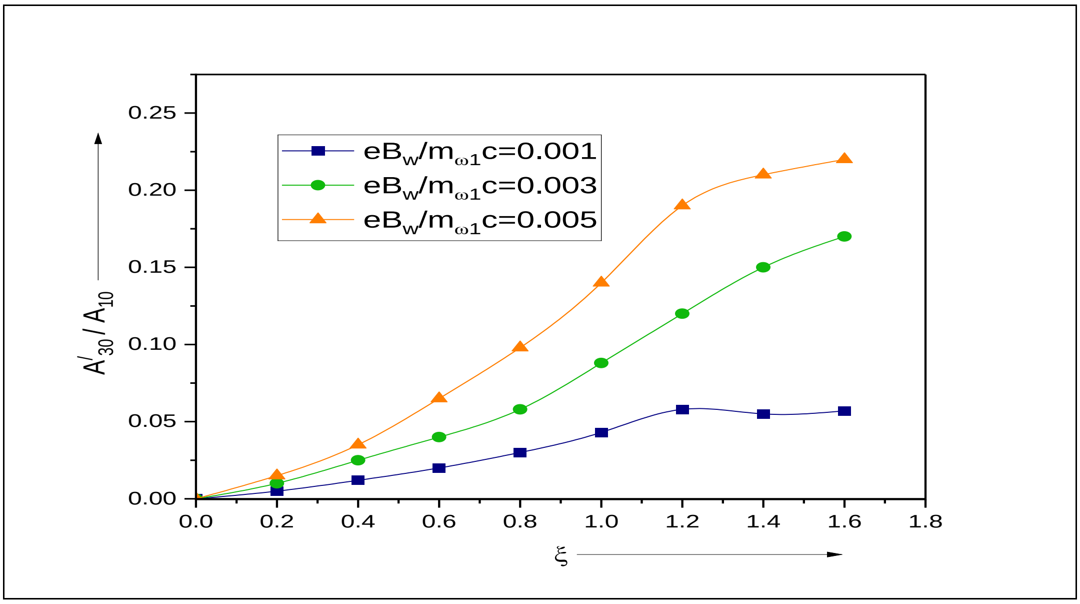

Fig. 6.3 Variation of normalized third harmonic amplitude A'_{30}/A_{10} with normalized propagation distance ξ for the values of normalised wiggler magnetic field $eB_w/m\omega_1 c = 0.001$,0.003 and 0.00 5.

(iv) Impact of electron density on the amplitude

Plasma density is a critical factor that significantly influences the amplitude . However, if the density becomes too high (approaching or exceeding the critical density), the laser experiences reflection and absorption, limiting its penetration and thereby reducing its effeciency. Moreover, the third harmonic wave itself must propagate through the plasma; higher densities can introduce dispersion and damping, which may attenuate the harmonic signal. An optimal density range exists where the fundamental laser can propagate while maintaining strong nonlinear interactions to efficiently generate and transmit the third harmonic pulse. Therefore, controlling plasma density is essential for maximizing third harmonic amplitude, as both under and over dense regimes can limit the generation and propagation of harmonics.

Figure 4 shows the variation of A'_{30}/A_{10} with propagation distance ξ the peak value is noted at the value of $\omega_p/\omega_1 = 0.8$ which is 0.15. This indicates that at higher ω_p/ω_1ratios, stronger plasma frequencies enhance gain. The intense ponderomotive force drives electron expulsion, causing density variations that introduce nonlinearity and lead to harmonic generation. Kant et al.[17] conducted a similar study on SHG and observed that introducing a density ramp which tends to a significant increase in the normalized amplitude at higher wiggler magnetic field strengths.

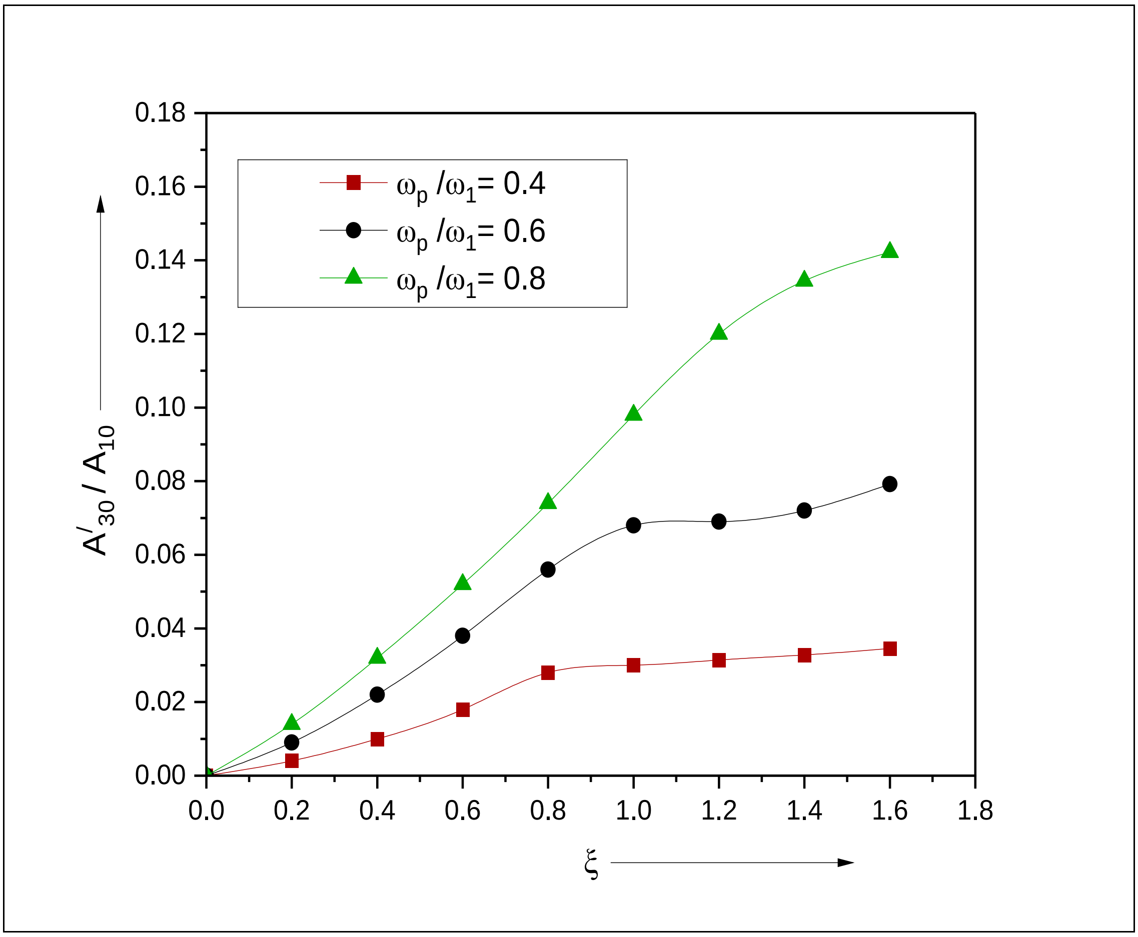

Fig. 6.4 Variation of normalized third harmonic amplitude A'_{30}/A_{10} with normalized propagation distance ξ.

(v) Effect of decentred beam parameter on amplitude of third harmonic pulse

The decentred beam parameter plays a viatl role in shaping the spatial intensity distribution of the laser beam . When a beam is decentred i.e., its peak intensity is shifted away from the propagation axis the symmetry of the beam is broken, resulting in an asymmetric interaction with plasma electrons. This asymmetry enhances the nonlinear current components, particularly those responsible for generating odd harmonics like the third harmonic. A moderate decentred parameter can significantly increase the amplitude of the third harmonic by intensifying localized field gradients and enhancing nonlinear source terms.. Therefore, there exists an optimal range of decentred beam values where third harmonic generation is maximized. Overall, the decentred beam parameter serves as a tunable factor that can be exploited to control and enhance the efficiency of THG in plasma-based nonlinear optical systems.

In Figure 6 It is observed that even a slight change in the beam width parameter causes the normalised THG amplitude to vary thus showing the sensitivity of decentred beam parameter. A minor variation in b from 0.52 to 0.56 amplitude varies from 0.16 to 0.24. Similar results were shown by Nazir et al.[15] in their recent study that minor variation in b leads to abrupt increase in the amplitude of harmonic pulse.

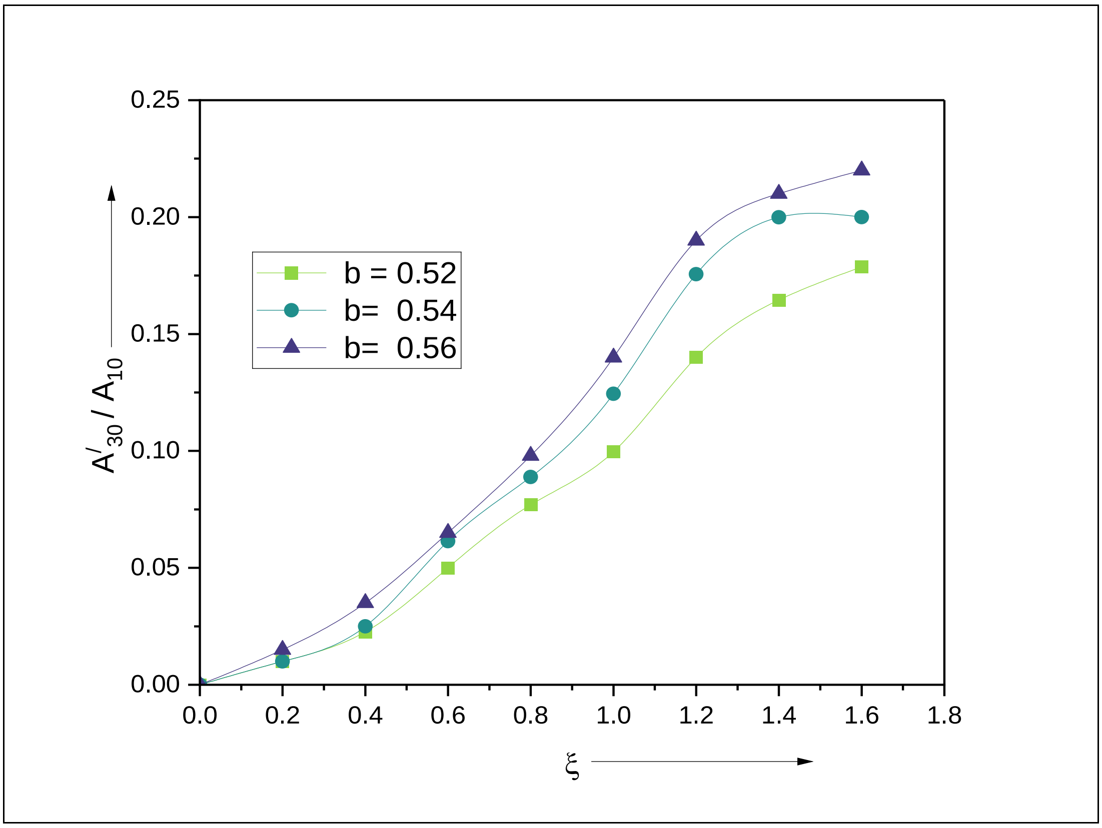

Fig. 6.5 Variation of normalized third harmonic amplitude A'_{30}/A_{10} with normalized propagation distance for different values of decentered parameter $b = 0.52, 0.54 \& 0.56$.

6.4 Conclusion

The relative increase in the intensity of the laser produces greater effects of relativity and ponderomotive forces making the non-linear current increase and the efficiency of the THG to improve, the intensity value $eA_{10}/m\omega_1 c = 5$, has maximum amplitude value i.e 0.44.

The addition of the wiggler magnetic field involves some extra circular motion by the electrons which helps improve the transfer of angular momentum and, in turn, the third harmonic amplitude. The results show the dependence the plasma density have on the efficiency of THG in the sense that there are optimal ranges of density which offer strong nonlinear coupling with low absorbing regions. Furthermore, the asymmetry of the intensity distribution created by the decentred beam parameter reduces the counteractive effects of nonlinear interactions and assists in augmenting localized field gradients necessary for third harmonic generation. The interaction of the shaping of the beam, designed plasma profiles, and the outer magnetic fields is a powerful method for controlling the generation of harmonics which is important for the development of plasma based frequency converters.

References

[1] G.A. Mourou, T. Tajima, S.V. Bulanov, Optics in the relativistic regime, *Reviews of Modern Physics*, **78** (2006) 309.

[2] P. Sprangle, E. Esarey, A. Ting, Nonlinear theory of intense laser-plasma interactions, *Physical Review Letters,* **64** (2011) 1990.

[3] C. Joshi, Plasma accelerators, *Scientific American*, **294** (2006) 40.

[4] H. Milchberg, C. Durfee Iii, T. McIlrath, High-order frequency conversion in the plasma waveguide, *Physical Review Letters,* **75** (1995)2494.

[5] A. Pukhov, J. Meyer-ter-Vehn, Laser wake field acceleration: the highly non-linear broken-wave regime, *Applied Physics B,* **74** (2002) 355.

[6] T.Y. Tsang, Optical third-harmonic generation at interfaces, *Physical Review A,* **52** (1995) 4116.

[7] J. Vieira, R.M. Trines, E.P. Alves, R. Fonseca, J. Mendonça, R. Bingham, P. Norreys, L. Silva, High orbital angular momentum harmonic generation, *Physical Review Letters,* **117** (2016) 265001.

[8] E. Esarey, P. Sprangle, J. Krall, Laser acceleration of electrons in vacuum, *Physical Review E,* **52** (1995) 5443.

[9] S. Wilks, W. Kruer, M. Tabak, A. Langdon, Absorption of ultra-intense laser pulses, *Physical Review Letters,* **69** (1992) 1383.

[10] T.S. Gill, R. Mahajan, R. Kaur, Self-focusing of cosh-Gaussian laser beam in a plasma with weakly relativistic and ponderomotive regime, *Physics of Plasmas,* **18** (2011) 23.

[11] A.A. Butt, N. Kant, V. Thakur, Self-focusing of a q-gaussian laser beam under the influence of an exponential plasma density ramp in plasma, *Physica Scripta,* **98** (2023) 045621.

[12] A.A. Butt, D. Nazir, N. Kant, V. Sharma, V. Thakur, The effect of density ramp on self-focusing of q-Gaussian laser beam in magnetized plasma, *Journal of Optics* , **1** (2023) 9.

[13] V. Thakur, M.A. Wani, N. Kant, Relativistic self-focusing of Hermite-cosine-Gaussian laser beam in collisionless plasma with exponential density transition, *Communications in Theoretical Physics,* **71**(2019) 736 .

[14] D. Nazir, V. Sharma, V. Thakur, Magnetically enhanced third harmonic generation using q-Gaussian laser beam in plasma, *Journal of Optics* , **1** (2023) 7.

[15] D. Nazir, V. Sharma, V. Thakur, Third Harmonic Generation Of Cosh-Gaussian Laser Beam In Magnetized Plasma, *Journal of Optics* , **1** (2025) 6.

[16] T. Baeva, High harmonic generation from relativistic plasma, PhD Thesis, *Ph. D. thesis,* **33** (2008) 2313.

[17] V. Thakur, N. Kant, Resonant second harmonic generation in plasma under exponential density ramp profile, *Optik*, **168** (2018) 159.

[18] A. Belafhal, M. Ibnchaikh, Propagation properties of Hermite-cosh-Gaussian laser beams, *Optics Communications,* **186** (2000) 269.

[19] J. Rajput, N. Kant, H. Singh, V. Nanda, Resonant third harmonic generation of a short pulse laser in plasma by applying a wiggler magnetic field, *Optics Communication,s* **282** (2009) 4614.

[20] V. Nanda, N. Kant, M.A. Wani, Sensitiveness of decentered parameter for relativistic self-focusing of Hermite-cosh-Gaussian laser beam in plasma, *IEEE Transactions on Plasma Science,* **41** (2013) 2251.

[21] A.T. Valkunde, B.D. Vhanmore, T.U. Urunkar, K.M. Gavade, S.D. Patil, M.V. Takale, Effect of exponential density transition on self-focusing of q-Gaussian laser beam in collisionless plasma, in: *AIP Conference Proceedings, AIP Publishing*, **23** (2018) 410234.

[22] D.N. Gupta, M.S. Hur, I. Hwang, H. Suk, A.K. Sharma, Plasma density ramp for relativistic self-focusing of an intense laser, *JOSA B,* **24** (2007)1155.

[23] V. Thakur, N. Kant, Exponential density transition-based enhanced second harmonic generation in plasma, *Laser and Particle Beams,* **36** (2018) 363.

[24] M. Vaziri, S. Sohailya, A. Bahrampour, Resonant second harmonic generation in plasma by self-focused twisted beam, *Optics Communications,* **341** (2015) 295.

Chapter- 7

Summary and Future Scope

This study offers a comprehensive theoretical analysis of second harmonic generation (SHG) and third harmonic generation (THG) in high-intensity laser beams interacting with plasma, focusing on the influence of various laser beam profiles. SHG and THG are essential nonlinear optical processes that occur when a high-power laser pulse interacts with plasma, generating harmonic components that are significantly enhanced through nonlinear effects. These effects include the ponderomotive force, which expels electrons from regions of high intensity, and relativistic mass variations that alter the plasma frequency, enhancing the refractive index and facilitating phase matching.

The study specifically investigates the impact of different laser beam profiles such as q-Gaussian, cosh-Gaussian (chG), and Hermite-cosh-Gaussian (HchG) beams on the efficiency of SHG and THG. The interaction of intense laser pulses with plasma results in density perturbations that lead to the formation of a transverse nonlinear current, which couple with the fundamental frequency to produce SHG and THG. Initially, these harmonics are of low amplitude, but their intensity increases substantially due to the combined effects of density ripples, relativistic corrections, and enhanced laser intensity. In particular, the q-parameter associated with the q-Gaussian beam plays a crucial role in controlling the transverse intensity distribution of the laser pulse. By varying the q-parameter, the beam profile can be continuously tuned from a conventional Gaussian shape $(q = 1)$ to flatter or more sharply localized intensity distributions for $q \neq 1$ .This tunability allows effective control over the spatial localization of laser energy and the resulting ponderomotive force acting on plasma electrons. Since harmonic generation is highly sensitive to local field intensity and electron density modulation, variation of the q-parameter directly influences the strength of the nonlinear current responsible for SHG and THG.

The study examines the role of the wiggler magnetic field, which can further boost harmonic generation. The wiggler field maintains the cyclotron motion of electrons, thereby confining them and facilitating momentum transfer. This interaction significantly amplifies the harmonic components, especially in high-intensity laser regimes, with the HchG beam demonstrating the highest efficiency in harmonic generation under similar laser conditions. The HchG beam's hybrid structure combining the cosh-Gaussian envelope with Hermite modulation results in tighter spatial confinement of the laser energy, which promotes stronger plasma interactions and increases harmonic yield. This is particularly evident at higher laser intensities, where the HchG beam outperforms other profiles such as Gaussian and q-Gaussian beams. Moreover, the chG and HchG beams exhibit stronger oscillatory behaviour in the generated harmonics, offering unique advantages in controlling phase and spatial distribution of the harmonics.

This research has broad implications for several applications in science and technology. The enhanced harmonic generation observed in this study can be applied to microscopic imaging for cellular diagnostics, where nonlinear optical contrast mechanisms improve imaging resolution, and in surface and interface analysis in condensed matter and materials science. It can also improve plasma diagnostics through nonlinear reflection and Doppler-shifted measurements.

Additionally, high-order harmonic generation, particularly in the THG process, can generate terahertz radiation, which has potential applications in ultrafast signal processing, terahertz imaging, and fibre-optic communications. The study also demonstrates that the THG process, when driven by high-power lasers, can be tuned across a wide spectral range (from approximately 1300 nm to 1650 nm), covering the fibre telecommunications window at 1550 nm, making it highly relevant for integrated photonics and quantum communication technologies.

The findings of this research also pave the way for future advancements in nanophotonics, quantum optics, and nonlinear metamaterials, especially in the context of high-power laser sources and engineered plasma media. The combined effects of beam shaping, external magnetic control, and relativistic dynamics present new possibilities for controlling light-matter interactions at extreme intensities, opening the door to more efficient nonlinear optical devices. Furthermore, the study provides valuable insights into the underlying mechanisms of SHG and THG, which can inform the design of future experiments and practical applications in various fields, including sensing, imaging, and telecommunications. This research lays the foundation for developing compact, high-performance optical systems, where efficient harmonic generation plays a key role in optimizing device performance.

In conclusion, this study contributes significantly to our understanding of laser-plasma interactions, providing theoretical insights that will aid in the development of next-generation nonlinear optical devices and photonic technologies, while also suggesting new experimental avenues for further exploration. The outcomes of this research would hold significant promise for a range of applications in diverse fields, including high-energy physics, material science, and medical imaging. Additionally, the research would also highlighten the importance of precise control over the laser parameters, plasma properties, and geometric configurations for optimizing the harmonic generation process.